Republic of Iraq
Ministry of Higher Education
& Scientific Research
University of Babylon
College of Education for Pure Sciences
Department of Physics

Study of Solar Cells Efficiency Changes with Coated by Polymeric Mixtures of Plants Dyes

A Thesis

Submitted to the Council of the College of Education for Pure Sciences University of Babylon in Partial Fulfillment of the Requirement for the Degree doctor of philosophy in Education/ Physics

By

Ameen Alwan Mohaimeed Malooh

B. in Education/ Physics
University of Babylon (2004)
M. Education/ Physics

University of Babylon (2017)

Supervised by

Prof. Dr. Bahaa H. Rabee

2023 A.D **1444 A.H**

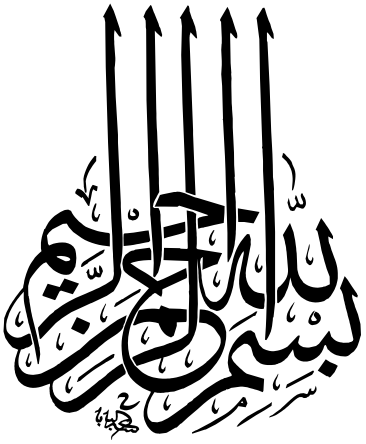

﴿ وَالشَّمْسِ وَضُحَاهَا ۞ وَالْقَمَرِ
إِذَا تَلَاهَا ۞ وَالنَّهَارِ إِذَا
جَلَّاهَا ﴾

الشيخ العلامة السعدي رحمه الله

سورة الشمس مدنية (1-3)

Dedication

I dedicate this effort

TO

Al-Hujjah Ibn Al-Hassan (peace be upon him)

The soul of My father,

My mother,

My wife,

My brothers and My sisters

My son (Sadiq)and

My daughters (Fatima, Rafraf)

Ameen✍

Acknowledgments

Praise be to Allah lord of the world, and best prayers and peace be unto his best messenger Mohammed, and his pure descendants.

I would like to express my deep gratitude and appreciation to my supervisor, **Prof. Dr. Bahaa H. Rabee** for his guidance, suggestions, and encouragement throughout the research work, without him this thesis work would have been impossible.

I would like to thank the staff of Department of Physics in College of Education for Pure Sciences in university of Babylon for their kind attention and encouragement.

I am very grateful to Dr.Khalid Haneen and Dr.Ahmed Hashim and my friend Mohanad Hassan for their efforts to finish this work.

Finally, I would like to thank my family for their help and encouragement and everyone who helped me during the preparation of this thesis.

Ameen

Abstract

In this study, PVA/TiO_2 films with various titanium dioxide concentrations (0, 1, 2, and 3 wt%) were prepared using the spin coating process. Then four thin films of PVA/TiO_2(3 wt.%) were prepared with four different proportions of 1,2,3 and 4 ml of berry, crocus and pomegranate dyes, with spin coater 700 rpm for 10 sec to 774±3nm thickness of films.

The results of the optical microscope showed the construction of a net of TiO_2 NPs inside polymer that increased the movement of electrons. The Fourier transformation-infrared spectroscopy(FTIR) recorded vibrational peak for nanocomposites concentrations, but when added (TiO_2 3wt.%) decreases the FT-IR spectra. The peak of IR-rad transmittance denotes a shift in peak locations and the creation of a new peak, which is due to the interaction of PVA and dye. Conjugated bonds appeared for the anthocyanin, anthocyanid and carotenoid core chains observed in berry, pomegranate and crocus respectively. The morphology of PVA/TiO_2 agglomerates, as seen by FE-SEM, demonstrates porous irregular cauliflower-like characteristics, while the morphology of TiO_2 shows the creation of tiny clusters of spherical shape particles. It was discovered that nanocomposites had spherical shape and grain sizes of 47.01 nm. From the images it can be remarked seen that the increase in particle size because increase concentration of TiO_2.

The (PVA/TiO_2/berry, crocus and pomegranate dyes) nanocomposites show that the absorbance is increasing with increasing concentration of natural dyes. Absorbance increases with increasing concentration of natural dyes from(1-4)ml. These films absorb visible light according to their wavelengths and can be used as a photosensor in solar cells. The transmittance decrease with increase concentration of TiO_2, and recorded highest peak at 81.9% in crocus dye. The absorption coefficient has high values ($\alpha>10^4 cm^{-1}$), indicating that the direct transition has a high value. The energy gap decreases(3.64-3,58)eV with increase concentration TiO_2, also the lowest possible energy gap was recorded for Pomegranate dye (3.32-3.26)eV. The optical constants increase with increase concentration of TiO_2, also increase with increase concentration berry crocus and pomegranate dyes.

The electrical conductivity($\sigma_{d.c}$) at a concentration of 2% was reached (4.81×10^{-6}, 4.9×10^{-6} and 6.4×10^{-6}) $(ohm.cm)^{-1}$ for berry, crocus and pomegranate dyes, respectively. The electrical conductivity of (PVA/TiO_2 berry, crocus and pomegranate dyes) nanocomposites increase with increasing temperature. It also shows a high values in correlation with the content of natural dyes. The decrease in electrical resistivity may be attributed to the homogeneity of (PVA/TiO_2) nanocomposites (the lack of defects), and this leads to an increase in the concentration of free electrons and thus a decrease in the resistance. The activation energy show decrease(0.60-0.29) eV with increasing TiO_2 nanoparticle concentrations. Also the lowest possible activation energy was recorded for pomegranate dye (0.54-0.19) eV, when the concentration was increased from (1-4)ml.

The I-V curves of the SnO_2/p-Si heterojunction under both dark and light circumstances showed. The photocurrent increases as the bias voltage rises. After covering it with (PVA/TiO_2/berry, crocus, and pomegranate dyes) nanocomposites on the surface SnO_2/p-Si, the efficiency of the solar cell increase. The efficiency(η) increase from (4.3-4.75%) was recorded after being coated with(PVA/TiO_2/pomegranate dye) nanocomposite. Therefore, this film can be used as a covering for solar cells.

Table of Contents

List of figures

List of Tables

List of Symbols and Abbreviations

Symbol	Physical Meanings
λ	Wavelength
n	Refractive index
$k_\circ$	Extinction coefficient
A	Absorption
I_o	Incident intensity of light
I_A	Absorbed intensity of light
T	Transmittance
I_T	Intensity of transmitted
k	Wave vector
α	Absorption coefficient
t	Thickness of film
h	Planck constant
υ	Photon frequency
$E_g^{opt.}$	Optical energy gap
B	Constant depend on the type of transitions
r	Value determines the type of electronic transitions
E_{ph}	Energy phonon
c	Velocity of light
N	Complex refractive index
ε'	Dielectric constant
ε	Complex dielectric constant
ε_r	Real dielectric constant

ε_i	Imaginary dielectric constant
σ_{op}	Optical Conductivity
E_{act}	Activation energy
K_B	Boltzmann constant
$\sigma_{d.c}$	D.C Electrical conductivity
R_{dc}	Electrical resistance
L, b	Length, breadth
ρ_{dc}	Resistivity
(I-V)	Current-voltage
V_{oc}	Open circuit potential
Isc	Short circuit current
F.F	Fill factor
P_{out}	Power output
P_{in}	Power input
η	Efficiency
I_{max}	Current output
V_{max}	Voltage output
I_{ph}	Photo current
I_t	the current in the lit environment
I_d	the current in the dark
Abbreviations	
TiO_2	Titanium dioxide
PVA	Polyvinyl Alcohol
p-type	Positive electric conductivity
n-type	Negative electric conductivity
C.B	Conduction band
RT	Room Temperature

FT-IR	Infrared Spectroscopy Testing using Fourier Transforms
FE-SEM	Scanning Electron Microscopy
LSL	Light scattering layer
DSSC	Dye-sensitized solar cell
PCE	power conversion efficiency
PSCs	perovskite solar atoms
ETL	Electron transport layer
TTIP	Titanium tetraisopropoxide
CMC	Carboxymethyl cellulose
DEG	diethylene glycol
UV-Vis	Ultra violet visible
D.C	Direct current
emf	Electromotive force
PVAc	Poly(vinyl Acetate)
LCD	Liquid crystal display
ANI	Aniline

Chapter One
Introduction

1.1Introduction

The sun is the essential factor that aids life and its continuation on Earth, and it is an endless source of energy. many people expect it participate significantly in the future production of energy for human activity[1].Solar energy, which is the renewable energy on earth and is growing, is used to generate electric power all round the world because of its environmental, economic, and strategic advantages[2]. In order to harness the sun's power, photovoltaic solar cells PV are important due to their ability to directly transform solar radiation into usable electricity. It is almost completely pollution-free and has the potential to supply power around the clock. There has been an uptick in the production of inexpensive flat-panel solar panels thanks to recent advances in technology [3]. When an object is exposed to light, a voltage is produced at the junction created between an electrode and an electrolyte, as discovered by Becquerel in 1839. The main issue for solar cells and the efficiency of their power conversion is the photovoltaic impact of significant voltage, which was originally observed by Ohi on a silicon p-n junction in 1940 [4]. Plants, vegetables, fruits, flowers, and leaves all contain pigments that can be used to create natural colours. Successful use of natural pigments such as betalains, carotenoids, chlorophyll, and flavonoids as photosensitizer in the photovoltaic solar cell [5].

Large molecules with a complicated structure make up organic dyes, which exhibit a broad absorption and fluorescence spectrum in the visible and ultraviolet parts of the electromagnetic spectrum [6]. Anthocyanin, the component of natural dye, is a type of colour pigment found in many plants. In addition to providing plants with their characteristic hues, anthocyanin molecules also act as light sponges, soaking up rays in the visible spectrum[7].

Fillers with nanometer-scale dimensions are used to strengthen the polymer matrix in a material class called polymer nanocomposites. These composites are made by mixing a nanofiller with a polymer to create a material with the same or better physical and mechanical qualities as their traditionally filled equivalents, but with lower loadings of fillers [8]. Composites are made up of at least Both chemical and physical distinct stages divided by a sharp boundary[9]. Metal oxide or polymer-metal nanocomposite is a novel material class that combines the benefits of

both polymers and semiconductor oxides. Polymers can be combined with other in the form composites to achieve unique physical, chemical, optical, and electrical characteristics not found in component materials, and have received a lot of interest for a variety of device applications[10]. Composite materials are heterogeneous in composition and mechanically anisotropic[11].Reinforcing material is frequently incorporated in a continuous phase, also known as the matrix or binder, in composites. Incorporating dispersed phases into the matrix, which might be an engineered material such as ceramic, metal, or polymer, is a common way to boost strength and improve overall qualities[12].

There are three characteristics on which the composite depends, the matrix, the reinforcement, and the matrix-to-reinforcement adhesion[13]. The term "composites" has been around long before humans. Wood is a composite substance found in nature, made up of a resinous matrix of another polymer, the polysaccharide lignin, and a type of polymer, cellulose, with great strength and stiffness[6,7]. 3D net of inorganic atoms are typically created on the polymer backbone composite materials made from polymers and inorganic particles as a result of the stronger contact greater than that between the inorganic particles and the matrix polymer [14-16]. Fundamental idea underlying nanocomposites is to expose the polymer matrix to extensive interaction with nanoscale construction components [17].Polymers (natural and manufactured) and nanomaterials (materials with a nanoscale topography or made up of nanoscale building components) make up nanocomposites[18].

Nanocomposites materials have emerged as viable alternatives to microcomposites and homogenitic, but they come with their own set of hurdles in terms of elements composition and stoichiometry control in the nanocluster phase[19]. The properties of nanocomposite materials are dependent not only on the characteristics of their constituent components but also on the morphology and interfacial characteristics of the composite itself [20]. Biological implant materials, electrical packaging, and automobile or aircraft components are all possible applications. While certain attributes will be shared throughout the applications, others will be highly distinct. To dissipate charge from lightning strikes, a digital bundle polymer composites must be non-conductive, however some aviation parts may require it[21].

1.2-Classification of Polymers

Polymers are commonly classified as thermoplastics or thermosets, depending on whether they can be melted and reformed using heat and pressure. While thermoset polymers and thermoplastics may both be recycled, due to their malleability under heat and pressure, thermoplastics make for more convenient recycling[22]. The following are the several types of polymers [23].

1-Polymers are divided into three types based on their structure: linear, branched, and network polymers.

2- Polymerization mode-based classification.

3-Classification based on molecular forces[23].

1.3- Classification Polymers Based on Their Homogeneity

Different types of polymers are classified according to the homogeneity of repeating units:

1- Homopolymers

Homopolymers are materials that are formed from the same monomer[24].

2- Copolymers

Copolymers are made up of at least two monomer units with differing chemical compositions.

3-Composite Polymers.

Polymer composites are made by combining a thermoplastic or thermoset polymer matrix with paper, mineral pigments, short fibres, long fibres, continuous fibres, and textiles as organic or inorganic fillers to increase mechanical strength., physical, and chemical characteristics for specific applications[12].

1.4 Classification Based on Sources Polymers

Polymers come from two basic sources.:

1- Natural Polymers

Biocompatibility, biodegradability, and low toxicity are some of the features that this type of polymer may give. Its constituents are derived from plants and animals, including wood, cotton, wool, and silk. Starch, protein, and cellulose are natural polymers that are found in food[25]

2- Synthetic Polymers

Other qualities of synthetic polymers include mechanical and physical properties, as well as heat stability. Plastics, synthetic leather, and several other colors are examples of polymers, which are made from simple chemical components[26].

Polymer Structure

In the polymerization process, several small molecules of different sorts are joined together to form chains or networks, yielding a large molecule with hundreds or thousands of atoms [26].

Polymers are divided into three classes based on their structure.:

A. Polymers with a linear structure:

These polymers have molecular series of a certain length as their basic structural unit, coupled in a linear manner; there are no branches other than twisted totals included in the monomer itself. As a fig. 1.1-a .

B. Branched Polymers:

Polyfunctional molecules react to produce structural units that can be connected together to construct nonlinear structures. In other situations, each polymer chain's side growth is stopped before it has a chance to connect up with another chain. Branched polymer molecules are the consequence of this process[27]. As a figure (1.1-b).

C. Cross-Linked Polymers:

In other circumstances, expanding polymer chains become chemically connected, resulting in a cross-linked structure. Bakelite and melamine formaldehyde are two popular polymers that form with Cross Linked structures. As a figure (1.1-c)[15,20].

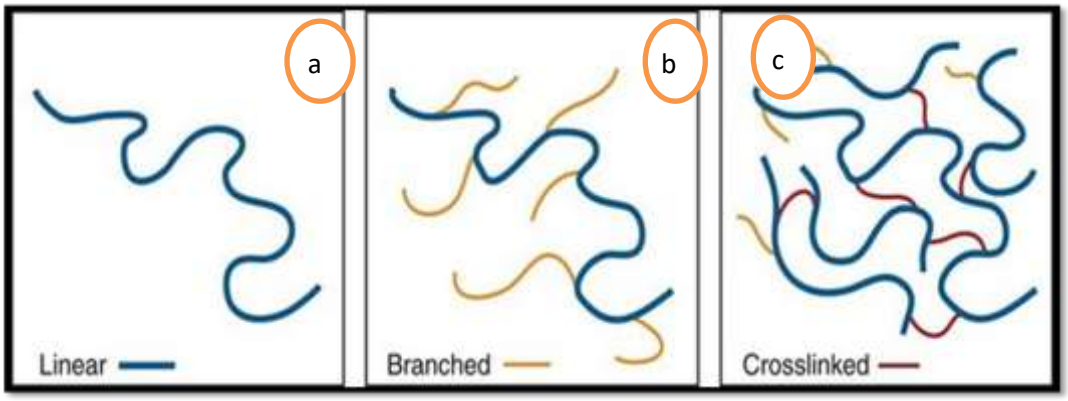

Figure -1.1: All the various polymeric chains [28]**: a. a linear b. Branch c. Cross-linked**

1.5- Nanomaterial

One of the most important technologies of the present and future involves nanoparticles[29]. The essence of nanotechnology is the production of microscopic materials, but nanotechnology is a vital aspect of science and technology because it allows scientists to manipulate atoms and molecules in materials with sizes ranging from 1 to 100 nanometers. Small pieces, including as optical and electrical devices, sensors, and other devices, can be used to create gadgets and products with this technology. At present, there is a lot of research and initiatives focused at creating this technology. Many other fields can benefit from this technique, the manufacture of materials with magnetic and optical characteristics[18]. Because of their size, form, and chemical structure, these materials frequently exhibit unique features[30].The characteristics of nanomaterial differ greatly from those of other materials due to two main factors: Quantum effects and increasing relative surface area[31].

1.6-Polyvinyl Alcohol (PVA)

PVA (polyvinyl alcohol) is a water-soluble transparent polymer that is widely used in industry due to its outstanding chemical and physical qualities, as well as its non-toxicity and chemical resilience[32]. PVA is an interesting material because it possesses a high dielectric strength, a powerful charge storage capacity, and electrical and optical properties that change depending on the dopant. Carbon, methane, and hydroxyl groups are all linked together over the length of the chain. These hydroxyl groups (OH) might be used as a hydrogen bonding resource,

which is an essential component in the construction of polymer blends [33].

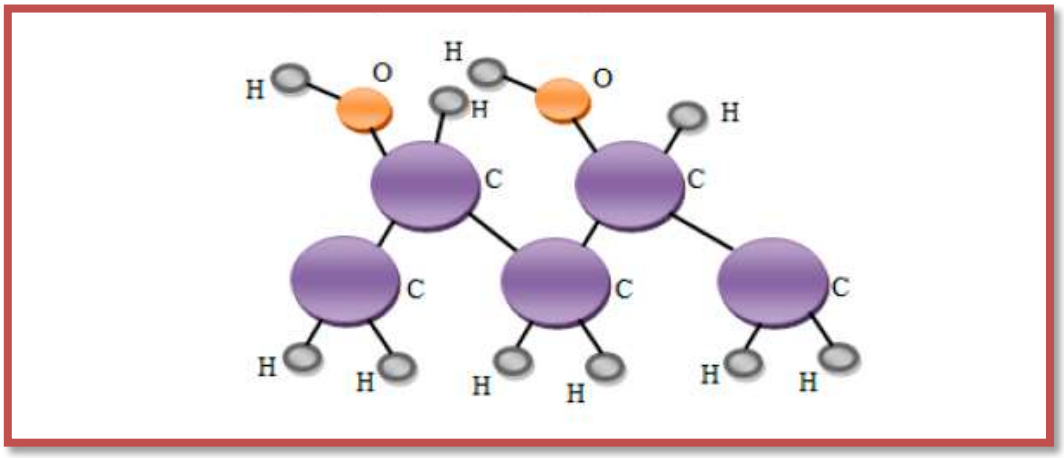

Figure (1.2): The structure of PVA synthesized by the hydrolysis of polyvinyl acetate[33].

Polyvinyl alcohol, with the formula $(C_2H_4O)_n$, is commonly utilized in an array of different contexts, with semiconductors being one of the most common. Due to the creation of hydrogen bonds with hydroxyl groups during the polymerization process, in addition to possessing chemical and physical properties as shown in Table (1.1). polyvinyl alcohol with polar bond shows flexible side groups when the bond rotates, resulting in a chemical composition shift of the polymer repeating unit. PVA is utilised in many different fields, including as the commercial, food, medical, and manufacturing sectors. It has been utilised in the production of surgical threads, paper products, and materials for the packaging of food. PVA has gotten a lot of attention because of its appealing film-forming properties, as well as its processability and biocompatibility. PVA polymers can be utilised in photovoltaic and optoelectronic devices as a consequence of this conclusion [34].

The polymerization of vinyl acetate to polyvinyl acetate (PVAc)polyvinyl alcohol is produced with change of PVAc by hydrolysis process[35], as shown in figure (1.2). PVA is a visible light polarizing material, allowing it to be utilized as a raw material for polarizer film used in LCD panels, lenses, and optical filters[36].

Table(1.1):Physical and chemical properties of polyvinyl alcohol [37].

Property	**Value**

Exterior	Small, granular, and white to off-white
Formula for molecules	$(C_2H_4O)_n$
Density g/cm^3	1.19 - 1.39
Specific gravity	1.27-1.31
Solution PH	5 - 6.5
Specific heat J/kg . K	1.67
Refractive index	1.55
Melting temperature (T_m) ^oC	Fully hydrolyzed grades have a ph of 230, whereas partially hydrolyzed grades have a ph of 180-190.
Thermodynamic Stability	Color changes gradually over 100 °C; darkens quickly above 150 °C; decomposes quickly at 200 °C.
Thermodynamic conductivity W/(m.K)	0.2
Thermodynamics of the glass transition (T_g) ^oC	85
Resistivity to electrical current Ω.cm	(3.1 - 3.8) x 10^7
Stability during storage (solid)	unlimited so long as it is kept away from moisture

1.7 Titanium Dioxide- TiO_2

TiO_2 has the chemical formula TiO_2 and occurs in nature as titanium oxide [38]. Dye White 6 and Pigment White, also known as CI 77891, are two names for titanium white. When assigned the E number E171, The versatility of this substance is exemplified by the fact that it may be used for a variety of purposes, such as those of paint, sunscreen, and food colouring. As seen in the figure (1-3), rutile and ilmenite are two examples of minerals that contain titanium dioxide in their crystalline form, anatase, and brookite,. Ries crater in Bavaria has produced monoclinic baddeleyite as well as orthorhombic high-pressure forms, were discovered. Rutile is the most frequent and stable form of the mineral. Rutile may be produced by heating either anatase or brookite. The titanium in rutile, anatase, and brookite is distributed across six atomic positions. Because of its high refractive index (n=2.7), titanium dioxide is the white pigment. It has a greater refractive index than all but

a select few other materials. Dyes of TiO_2 use exceeds 4 million tons annually over the world [39].

Each phase's optical characteristics are similar, however there are some minor differences. Band gaps in rutile (3.06 eV), anatase (3.29 eV), and brookite (2.20 eV) were measured. The Fermi level of the anatase form is just a hair higher than that of the rutile (0.1eV), and a little widening of the band gap. In thin films, the charge carrier mobility of the anatase structure is found to be higher than that of the rutile structure[40]. Anatase is the preferred structure for photocatalytic actions, even though it has been established that all three are photocatalytic. Small changes in electrical structure between brookite and anatase result from the crystal's immediate surroundings [30-31]. TiO_2's excellent sensitivity and, more importantly, its extraordinary stability in hard settings make it a popular choice for use in gas sensing applications. TiO_2 exists as three different polymorph phases: the stable rutile (tetragonal), the intermediate brookite (orthorhombic), and the unstable anatase (tetragonal)[41].The physical and chemical characteristics of the three TiO_2structures are shown in Table (1.2). The photocatalytic, photo electrochemical, and gas sensor uses of anatase, rutile, and brookite have all been investigated. Different pressures and temps exerted by rock formations in the Earth are responsible for the differences in these three crystal forms[29,32].

Both the anatase and brookite phases may be produced by heating the material to very high temperatures around 700°C and 750 °C, respectively, both anatase and brookite lose their stability and transform into more brittle phases, both will return to the rutile phase[39].

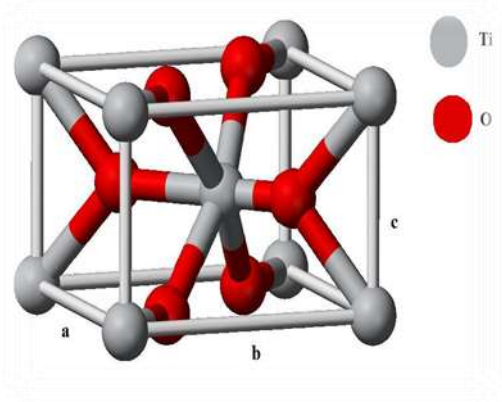

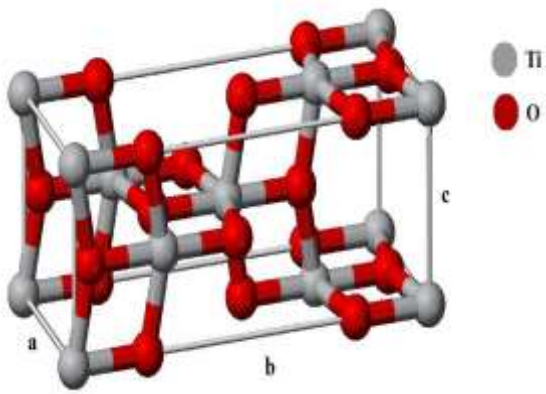

A **B**

C

Figure -1.3: Forms that crystalline TiO_2 [41]**.**

A. Rutile B. Anatase C. Brookite

Table -1.2 Comparison of the three TiO_2 structures in terms of their physical and chemical characteristics [42].

Properties	Rutile	Anatase	Brookite
Formula for molecules	TiO_2	TiO_2	TiO_2
Molary mass(g/mol)	79.866	79.866	79.866
Crystalline Structure	Tetragonal	Tetragonal	Orthorhombic
Energy gap (eV)	3.06	3.29	3.33
Color	White solid	White solid	White solid
Density (g/cm^3)	4.27	3.90	4.13
Melting point (°C)	1855	Transformed into rutile	Transformed into rutile
Boiling point	2972		

Refractive index (n_D)	2.609	2.488	2.583
Dielectric constant (ε)	110~117	48	78
Hardness (Mohs scale)	7.0~7.5	5.5~5.6	5.5~5.6

1.8 The natural dyes

Several organic dyes have been utilized to create output that is as good as inorganic dyes, however the results tend to waver and fall short of the inorganic dyes maximum[43].DSSCs can utilize natural dyes taken from flowers, fruits, and leaves. Natural dye-sensitized solar cells have piqued scientists' interest due to its low cost, biodegradability, and environmental friendliness. The maximal absorption wavelength of a suitable sensitizer should be in the visible light spectrum. The dye extraction media is one of several parameters that influences dye light absorption[44].

A. Berry dye

The blackberry is a historically farmed fruit, and its benefits to human health from vitamins, minerals, and antioxidants, as well as its importance in industry and medicines, all contribute to the creation of new jobs. In addition, the extracted red berry dye has become the focus of researchers' interest because it has a high absorption of light in the visible region, it is a photosensitizer and contains anthocyanin, which has a chemical composition shown in Figure(1-4). Anthocyanidins are common plant pigments that are the sugar-free equivalents of anthocyanins. The most important characteristic of the anthocyanin dye.

1- Attract insects and birds to facilitate pollination and fertilization
2- play an important role in the resistance of plant diseases.
3- Aesthetic and attractive aspects of botanical flowers [45].

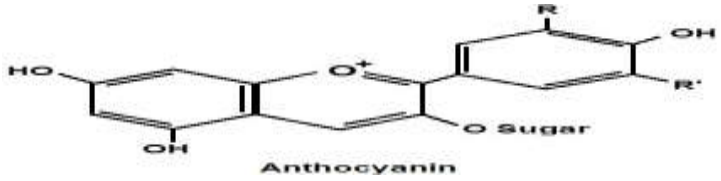

Figure (1-4) : Anthocyanin dye[45]

B. Crocus dye

Harvesting the pollen-bearing structures, or stigmas, of the autumn crocus (Crocus sativus), which are aromatic and golden in colour, results in the production of a spice as well as a dye. The bittersweet, exotic aroma and flavour of saffron make it a popular spice for cooking and decorating. The primary producers of saffron are Iran and some parts of India. Each flower has three stigmas that are picked, set out platters, in order to be used as a culinary spice and colouring after being dried over charcoal fires. Seventy-five thousand saffron flowers are needed to produce one pound of the spice (0.45 kilogram). Saffron essential oil consists mostly of picrocrocin, with a concentration of between 0.5 and 1%. Dyeing occurs using crocin[46]. Solar cell sensitization using saffron flower extract[47].

The most important uses of saffron dye.

1-Saffron is one of the medicinal plants used in medicine

2- Saffron extract is used in the perfume industry[46].

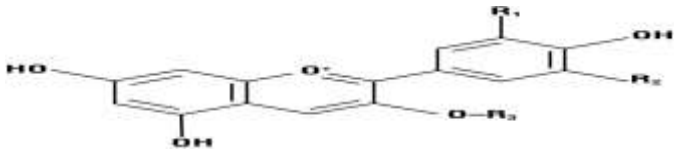

Figure (1-5): Crocin dye[46]

C. Pomegranate dye

It is known in the scientific community by its botanical name, Punica Granatum. In addition to those regions, the Indian subcontinent and North Africa are also major producers of these shrubs. Pomegranates are classified as berries and have a flower-shaped stem. Some of its selling points are its eye-catching crimson hue and tangy flavour. Pomegranates have a sweet and sour flavour due to their pH level, which is around 4.4 [48].The major component of pomegranate coloring is cyanin. Pomegranate dye absorption was discovered in the visible area at the 555 nm peak. So it will act as a light sensitizer[49].

1.9 Solar Cell

One of the most promising industries for the future is the solar cell sector thin membrane applications, having received remarkable attention over

the past years due to the low cost of preparation and the possibility of manufacturing large areas of it[50]**.** Becquerel was the first to identify the photovoltaic effect in 1939, when he noticed the creation of an electric current when light fell on one of two poles submerged in an electronic solution, and discovered that the current was proportional to the intensity of the falling light. Chapin and his team developed the first solar cell connection (p-n) in 1954, which converted around 6% of monocrystal silicon into electric power[3]. Heterojunction solar cells combine two different technologies into one cell: a crystalline silicon cell sandwiched between two layers of amorphous "thin-film" silicon. This allows an increase in the efficiency of the panels and more energy to be harvested easily when compared to conventional silicon solar panels. The most common type of solar panels is made with crystalline silicon - either monocrystalline or polycrystalline. Amorphous silicon is thin-film silicon unlike crystalline silicon, amorphous silicon does not have a regular crystalline structure. Instead, the silicon atoms are randomly ordered. As a result, manufacturing this type of solar cell is less expensive[50]. Heterojunction solar technology takes advantage of this by building a solar panel out of three different layers of photovoltaic material. The top and the bottom layer are made up of thin-film amorphous solar cells, the middle layer is a crystalline solar cell. The thin-film silicon on top captures some sunlight before it hits the crystalline layer, and it also grabs some sunlight that reflects off the layers below. It's very thin, so much of the sunlight passes right through and the sunlight that passes through the middle i.e the crystalline layer is absorbed by the thin amorphous layer that is below[3].

Tin oxide (SnO_2) is an n-type metal oxide that may be made from a pre-dispersed nanoparticles (NPs) dispersion that has been annealed at temperatures below 150°C. It has been extensively investigated as a material for electron transport layers in dye-sensitized and perovskite solar cells. SnO_2 is a high-potential photovoltaic material[51]. When compared to other transparent conductive oxides, In comparison to p-Si, it has a higher work function, better contact, more thermal stability, greater mechanical durability, lower chemical stability, and lower toxicity. When it comes to electron transport layers, SnO_2 is remarkable because it possesses a wide band gap, excellent mobility, remarkable optical and chemical stability, high conduction and valence band depth,

and high transparency. These are only some of the many desirable qualities that it possesses, its simple, low - temperature preparation [49-50].Because of its broad band gap and low reflecting index of 2, SnO_2 was chosen to make a solar cell using n-type SnO_2 layer and p-type silicon wafers[52].

1.10 A p-n Heterojunction

Heterojunction It is a volumetric connection in which two or more semiconducting materials differ in energy gap, electronic affinity, work function, and dielectric constant. When manufacturing junctions, it must be taken into account that the mismatch does not exceed 1%, as well as the convergence of the thermal expansion coefficient to the extent of avoiding dislocations at the separating surface[45,51]. Because they consistently stay, to a very fair approximation, charge neutral even when the device is biassed, the n and p regions outside the depletion region are known as quasi-neutral regions. All reliable conductors often possess this charge-neutral feature. Significant charge concentrations cannot exist inside good conductors because if they did, they would produce drift currents that would neutralise the charge density by creating electric fields. Good conductors are charge neutral on scales longer than the screening length and longer than the dielectric relaxation time[51].

assumed that the applied potential falls completely across the depletion region (i.e. across the junction) and not across the conductive n or p regions (quasi-neutral regions) or across the metal contacts. The effect of the applied voltage is taken into account by changing the electrostatic potential across the depletion region when $V < 0$ (reverse bias). Consider the case $V > 0$ (forward bias). that the applied potential falls completely across the depletion region (i.e. across the junction) and not across the conductive n or p regions (quasi-neutral regions) or across the metal contacts. The effect of the applied voltage is taken into account by changing the electrostatic potential across the depletion region[15]. as a fig. (1-6).

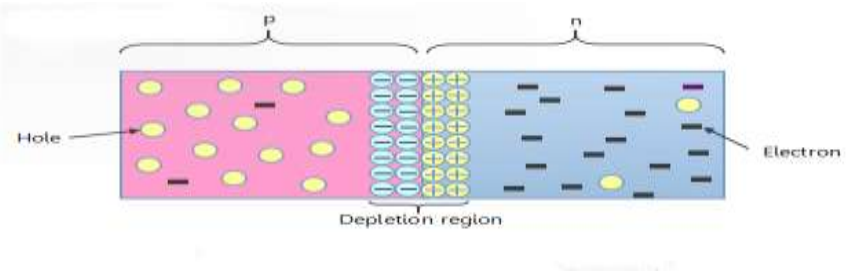

Fig (1-6): A p-n junction[15].

1.11 A p-Si semiconductor

A particular kind of semiconductor is a p-type one. It is referred to as a p-type semiconductor when a trivalent impurity (such as boron, aluminium, etc.) is added to an intrinsic or pure semiconductor (silicon or germanium). Acceptor impurities include trivalent impurities such as boron (B), gallium (Ga), indium (In), aluminium (Al), and others. Ordinary semiconductors are composed of materials that don't conduct electricity well but aren't particularly resistive to it either. They occupy the middle ground between insulators and conductors. When electrons flow through a material, an electric current is created. The substance must have an electron hole for the electron to enter in order for it to move. More holes than electrons are present in p-type semiconductors. As a result, the current can only travel in one direction as it moves along the material from hole to hole[4].

Silicon is most frequently used to make semiconductors. An element called silicon has four electrons in its outer shell. Additional components, like as boron or aluminium, are combined with silicon to create a p-type semiconductor. The outer shell of these materials only contains three electrons. Where the fourth electron would have been if the semiconductor were made entirely of silicon is left empty when the extra material partially substitutes some of the silicon[7].

The bulk of solar cells on the market today are silicon-based. Research on organic and quantum dot solar cells, as well as other types of next-generation solar cells [3]. By combining n-type and p-type semiconductor materials, p-n junctions are created. Electrons diffuse from the n-type side

to the p-type side because the n-type region has a high electron concentration and the p-type region has a high hole concentration. Similar to how electrons move from one form of matter to another, holes move by diffusion[15].

If the electrons and holes were not charged, this diffusion process would go on until there was an equal distribution of electrons and holes on both sides, just as there is when two gases come in contact. In contrast, when the electrons and holes travel to the other side of the junction in a p-n junction. In the p-type region, the dominant carrier, holes, have a far larger concentration than the minority carrier, electrons[49].Compared to the majority, the injected minority carrier density is low. Since the depletion zone is uncharged, neither generation nor recombination can take place. [51].

Depending on the polarity and magnitude of the applied potential, the depletion area may be reduced or increased. Heterojunction (P-Si/N-Ge) diodes are semiconductor devices made of various types of semiconductor materials. One of the most basic semiconductor devices available is a PN Junction Diode, which only allows current to flow in one way. Additionally, the semiconductor's p-side, or positive side, has an excess of holes, whereas the n-side, or negative side, has an excess of electrons [50].

1.12 Literature survey

Hossein *et al.* 2014[53] prepared the red-BS dye doped polyvinyl alcohol (PVA) thin films are examined as a function of dye concentration. On a glass substrate, three thin film samples with varying concentrations of red-BS dye were produced using the spin-coating process. The optical properties of films, including indices of refraction, absorption rates, and dielectric properties, are retrieved using their transmission and reflection spectrum, and the influence of dye impurity on these parameters is investigated. Band gap energies may be calculated using the Tauc method. By raising a concentration of dye impurity in PVA films, the band gap energy of samples is reduced.

Al-Omair *et al.* 2014[54] prepared the dye-sensitized ZnO photoelectrode solar cells' photovoltaic properties were studied in relation

to photosensitivity can be increased by using organic dyes like Orange IV and Eosin Y. (DSSCs). At-home ZnO nanoparticle synthesis allowed for the development of ZnO. ZnO nanostructures were studied utilising tools including XRD, SEM, and BET. In all assays, the Orange IV outperformed the Eosin Y-sensitized cell. Therefore, this occurred because orange IV has the largest molar extinction coefficient. the I-V curves of the DSSCs with various types of organic dyes under illumination. It was found that the cell sensitized with Orange IV dye showed the largest area of the current-density curve, indicating that this cell generated the highest output power. Meanwhile, the cell utilizing the Eosin Y dye showed the smallest area of the current-density curve, generating the lowest power.

Vanja Gilja *et al.* 2017[55] studied the Aniline (An) was oxidised on-site in the presence of TiO2 particles to produce polyaniline/titania (PANI/TiO2) composite photocatalysts. This motivated the creation and analysis of photocatalysts with various concentrations of PANI polymer. In order to determine the conductivity of the synthesised PANI polymer, FT-IR spectroscopy and thermogravimetric analysis were used. In order to show how the aggregation process changed depending on the amount of aniline employed, micrographs of the composites were acquired combined TEM/FE-SEM. Due to the homogenization of PANI during its development, the photocatalysts containing 15% PANI (15PANI/TiO_2) showed the lowest aggregate size.

Vanja Gilja *et al.* 2018[56] prepared the Aniline (ANI) was chemically oxidised in situ in existence of varying concentrations of diethylene glycol to yield polyaniline/zinc oxide (PANI/ZnO) composite photocatalysts that can be used in neutral conditions (DEG). It was determined that PANI/ZnO composite photocatalysts would be the most effective at removing organic pigment from the model effluent. they are interested in learning more that we can create low-cost varied catalysts with excellent catalytic action and durability, they have developed PANI/ZnO composite photocatalysts for effective removal of organic pigment from wastewater. Using the PANI polymer, a conductive polymer, which absorbs Vis irradiation, into the composite photocatalysts broadened their applicability beyond that of ZnO, which is selectively

active in the UV spectrum. The composite photocatalysts were characterised using a wide variety of techniques.

Muhammad *et al.* 2019[57] studied the light scattering layer is accomplished with a coating of TiO_2 NPs, (PVA/TiO_2) nan fibers (LSL). photoanode. Since employing PVA/TiO2 nanofibers as LSL decreases radiation loss and boosts electron excitation, TiO_2 NPs adorned with polyvinyl alcohol (PVA) and titanium dioxide (TiO_2) nanofibers had a high power conversion efficiency (PCE). is 4.06 percent, which is 33 percent greater than TiO_2 nanoparticles without LSL, resulting in a high PCE. In comparison to TiO_2 nanoparticles without LSL, including PVA/TiO_2 nanofbers as LSL enhances electron life duration and charge collecting efficiency.

Gerrit Boschloo 2019[58] prepared the during the last three decades, dye-sensitized solar cells have been extensively studied. However, there are still numerous factors to investigate in order to increase their effectiveness. Dye molecules can be tweaked indefinitely to improve performance. Steric groups, for example, can be used to slow down recombination events and prevent undesirable aggregation. To boost light absorption and create a stronger blocking effect, more ideal dye packing on the mesoporous TiO_2 surface is required.

Mahsen, *et al.* 2019 [59] syntheses the natural sensitizers produced from plants such as teak, tamarind, and eucalyptus are utilised in dye-sensitized solar cells that are based on TiO_2 technology. Besides considerable adsorption on the semiconductor (TiO_2) surface, The dyes were very absorbent in the sun's visible spectrum (400-700 nm). These extracted dyes were put to use in the construction of DSSCs. There was a wide variety of incident photon to current efficiencies (IPCEs; often abbreviated as "efficiency"), from 12% to 37%. Of the four colours tested, the teak extract's photosensitization effects on cell output were the most impressive.

Onyekachi and Onuegbu2019[60] studied four different extraction procedures were used to extract dye from the dried fruit of Rothmannia whitfieldii. A colourless supernatant solution was obtained after 45 minutes of heating in a solvent and an acid. Under the identical conditions for extraction, The supernatant solution obtained by the alkali

process was dark brown, whereas that obtained through the aqueous process was black. After analysing FTIR spectroscopy was used to analyse the colored solutions, the researchers concluded that only the alkali procedure was successful in removing the possible dye, which contained tannins. Based on these findings, the supernatant solution of an aqueous extraction of Rothmannia whitfieldii fruit contains functional groups are identical to those present in the dry pulverised fruit. Due of this, the aqueous technique yielded no discernible colour.

Amone *et al.* 2020[61] studied the types of dyes used to gather photons have a significant impact on the manufacturing costs and energy conversion efficiency of DSSCs. Natural dyes derived from various sources have emerged as viable alternatives to synthetic photosensitizers due to their advantageous qualities such as low cost, full biodegradability, availability, and low environmental impact. Researchers have used mixing of different dyes, copigmentation of dyes, acidifying of dyes, and other ways to increase the energy conversion efficiency of natural photosensitizers, resulting in noteworthy performance. This research examines the parameters that influence anthocyanin pigment stability as well as the solvents required for efficient anthocyanin extraction. Furthermore, the possible use of anthocyanin dyes as photosensitizers for DSSC is discussed, as well as previous research.

Jin Kim *et al.* 2020[62] manufactured cells made of perovskite solar atoms (PSCs), As a successor to TiO_2 ETL, which is fast nearing the maximum power conversion efficiency, It has come to everyone's attention that SnO_2 ETL has a higher electron extraction rate and is more stable. That's why it's so important to create more effective PSCs by working out how to increase ETL speed. Consequently, SnO_2/MAPbI3 solar cells perform better than TiO_2/MAPbI3, in terms of efficiency. According to different orbital hybridization and dipole contact electron transfer mechanisms at the MAI- and PbI2-terminations, post-transition metallic (sp valence) oxide ETLs will perform better for PSCs than transition metallic (d valence) oxide ETLs.

Alesa *et al.* 2020[63] prepared the polyvinyl alcohol (PVA) thin films containing extract of natural pigment from a local flower were used to make solar cell thin films. Thin films were made from polyvinyl alcohol solutions of 0.1g/ml in water and plant pigments of varying

concentrations (0%, 15%, 25%, and 50%) for all four samples. The solutions were then used to make varying concentrations of dye in PVA: low, medium, and high. The UV-Vis scanner was used to pinpoint the spots where absorption was taking place (CECIL 2700). A number of optical properties were investigated using UV-Vis spectroscopy. The samples were run through an FTIR spectrophotometer for analysis. The use of a differential scanning calorimeter. Both the UV and FTIR absorption of a PVA thin film were improved when natural colours were used in the formulation.

Chapman *et al.* 2021[64] prepared the film thickness model based from a well-established equation of state, the spin-coating with toluene of extremely low-viscosity poly(methylmethacrylate) films. Spin-coating solutions' dynamic viscosity and density are studied in detail as a function of concentration. When the film drying rate for a given system was used to calibrate the film thickness model, it was found that this metric grows proportionally with the square root of spin speed. When it comes to managing film thickness, a three-dimensional design space may be generated with the help of process mapping. FTIR were measured on both the PMMA starting material and final dried film to verify that no chemical changes occurred, Highly similar thermal behavior is observed for both samples, which suggests that the bulk chemical properties of the polymer were not affected by the spin-coating process. The small differences associated with the spin-cast film can be attributed to loss of residual solvent.

Vishwas 2021[65] studied the sol-gel process is used to make titanium dioxide (TiO_2) thin films and nanoparticles utilizing titanium tetraisopropoxide (TTIP) as the precursor ingredient. The solution casting process is used to make poly (vinyl alcohol) (PVA) films. TiO_2 nanoparticles are doped into PVA films. UV/VIS spectrophotometers are used to investigate the optical characteristics of TiO_2 films. Very high transmittance in the visible spectrum and strong UV absorption are observed. By growing wavelength, refractive index dropped. The stretching and bending vibrational modes in TiO_2 films and PVA doped with TiO_2 nanoparticles are studied using an FTIR spectrum.

Khormali *et al*. 2021[66] examination the process for highly effective, ecologically friendly, and one-of-a-kind Dy_2O_3/ZnO-Au ternary

nanocomposites, the extract of pomegranate plant served as a covering and plummeting agent. In order to find the optimal combination, we put a number of different permutations of basic and plummeting agents, sonication intensity, and sonication time through their paces. FT-IR, XRD, FE-SEM, TEM, and DRS are only few of the methods that were used, were used to examine the manufacturing process. As revealed by XRD and TEM analysis, nanocomposites have a spherical shape with crystallites of 85–90 nm. The nanocatalyst was evaluated for its ability to degrade the anionic dye erythrosine (ES) and the cationic dye basic violet 10 using UV and visible light irradiation (BV10).

Askary *et al.* 2022[67] prepared the (CMC)/polyvinyl alcohol (PVA) blends was used to create nanocomposites comprising carboxymethyl cellulose with varying tungsten trioxide concentrations. XRD, FT-IR, and FESEM are used for physical characterisation. The optical characteristics of WO3@CMC/PVA composites were investigated using varied laser irradiation times. Similarly, the pure mix has the largest band gap (direct 5.0 eV and indirect 5.4 eV), which lowers as WO_3 inclusion increases. The decrease in bandgap also reveals an improvement in crystalline ordering, which is confirmed by the XRD diffract graph. The tungsten trioxide has a size range of 2.5 to 4.2 m, which decreases as the laser irradiation period increases. The graphs of ″ and ″″ exhibit a drop pattern when the frequency is increased, then show constant values as the frequency is increased.

Aim of the work

1-Preparing the (PVA/TiO_2/Berry dye), (PVA/TiO_2/Crocus dye) and (PVA/TiO_2/Pomegranate dye)nanocomposites films by spin coating method.

2- Studying the Structural, optical and electrical properties for (PVA/ TiO_2 /Berry, Crocus and Pomegranate dyes) nanocomposites .

3- The effect of coating (PVA/ TiO_2/Berry, Crocus and Pomegranate dyes) nanocomposites on the SnO_2/p-Si solar cell.

Chapter Two
Theoretical Part

2.1 Introduction

In this section, we will go over the study's theoretical studies, including a discussion of the nanocomposite crystal structure, the underlying physical ideas, laws, and principles employed for inference.

2.2 Optical Properties

Study of a material's optical characteristics is crucial for two reasons. Before using a material for an optical application, such as an interference filter, optical fiber, or reflective coating, It is crucial that you are well versed with its optical coefficients across a wide spectrum of wavelengths. Furthermore, the optical qualities of every material can be linked to its atomic composition, electronic band structure, and electrical characteristics [68].

2.2.1 Absorbance (A)

Absorbance (A) is defined as the amount of light that a material retains in relation to the amount of light that strikes it[69]:

$$A = \frac{I_A}{I_o} \ldots\ldots \quad (2.1)$$

2.2.2 Transmittance (T)

The exponential connection for both absorbance and transmittance may be used to calculate transmittance as a function of wavelength [70]:

$$A = \log\left(\frac{1}{T}\right) \ldots\ldots (2.2)$$

2.2.3 Absorption Coefficient (α)

Ability to soak up radiation of a specific wavelength is what we mean when we talk about a material's "absorption coefficient". Absorption coefficient is calculated in the [71]:

$$I = I_o \exp(-\alpha t) \quad \ldots. \quad (2.3)$$

$$\alpha = 2.303 \times A/t \ldots..(2.4)$$

t: the thickness of a film

2.2.4 The fundamental absorption edge

It's a key property of crystalline and amorphous materials' absorption spectra.. The increase in ray energy absorption is proportional to the energy gap of the absorbing substance. The basic absorption edge is the point where energy disproportion between the valence band's peak (V.B) and the conduction band's trough (C.B) is minimal at this point (C.B)[72].

2.2.5 Absorption regions:

There are three absorption regions

A- High Absorption Region

Figure(2.1) depicts this location. In section (A), the absorption coefficient has the value of (10^4 cm^{-1}). We can set the width of the forbidden optical energy gap($E_g^{opt.}$) [73]

B- Exponential Region

Locating this area, as shown in Figure (2.1). Parcel (B) has an absorption coefficient of ($1cm^{-1} < \alpha < 10^4$ cm^{-1}). It explains how the electron energy levels in a semiconductor move from (V.B)to (C.B) and back again[74-75].

C- Low absorption region

This area has a tiny α. It's less than 1 cm^{-1}. The transition occurs in this location due to the density of state in the mobility gap caused by structural defects, look in Fig. 2.1- C[76].

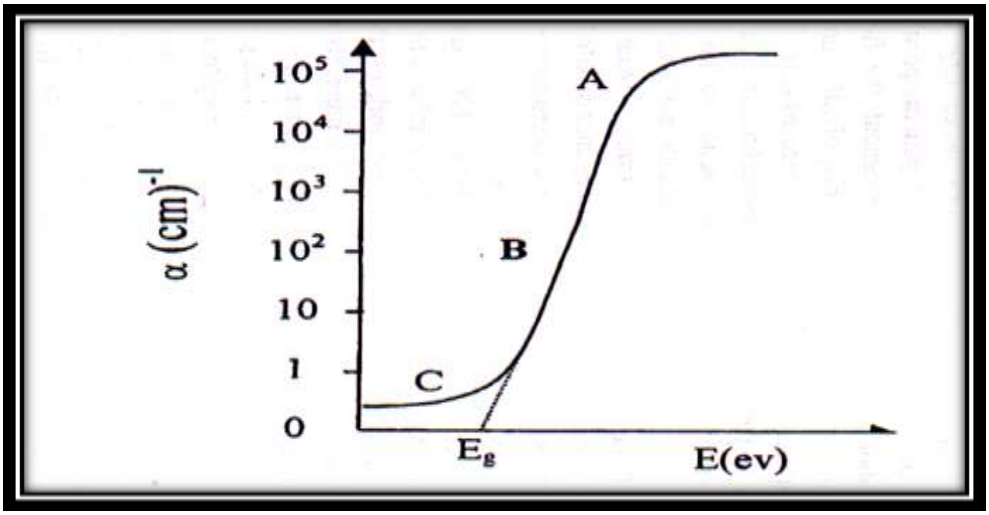

Fig. 2.1:Fundamental absorption edge of crystalline semiconductor[73]

2.2.6 Electronic transitions:

There are two types of changes in electronics: direct and indirect [77].

A) Direct transition

The energy maximum (the top of V.B) is superposed on the energy minimum (the bottom of the C.B) during this transition (the top of the V.B). It's the same wave vector value, i.e., (K=0). According to the principles of energy and momentum conservation, there must be a linear change. This shift may be divided into two categories. One type involves a smooth change from (V.B) maximum to minimum (C.B), whereas the second type is a forbidden direct transition between the extremes of (V.B) and (V.C) (C.B) as shown in Figure (2.2.a) [78]. For a straight transition (K=0) with phonon absorption, the Tauc relation provides the absorption coefficient(α) [79]:

$$\alpha h\upsilon = B(h\upsilon - E_g^{opt.})^r \quad \ldots\ldots\ldots(2.5)$$

$E_g^{opt.}$: optical energy gap,

h υ : photon energy,

A direct transition with r = 1/2 is allowed, while one with r = 3/2 is not; it specifies the kind of electronic transfer.

B)Indirect transition

Distance in the K-direction between the valence and conduction bands. is used kind($\Delta\mathbf{K} \neq 0$)[80]. The phonon and electron transition probabilities are formed by the transition probabilities. The indirect transition requires a phonon and a photon because **K**-space is very large, hence the distance between the conduction band and valence band edges is large. This shift may be divided into two categories. In the first kind, a person can make an indirect transition from the highest (V.B) to lowest (C.B), but in the second type, which occurs near to highest (V.B) and can lead to destinations other than the bottom of the (C.B), such transitions are not possible (C.B), direct transitions are not possible (C.B), is known as disallowed indirect transitions, shown figure (2.2.b) [72].

For an indirect transition ($\Delta\mathbf{K} \neq 0$) with phonon absorption, the absorption coefficient is [81].

$$\alpha h\upsilon = B(h\upsilon - E_g^{opt.} \pm E_{ph})^r \qquad \dots \quad (2.6)$$

E_{ph} : is the energy of a phonon that has been absorbed (+) or released (-)..

B: transitions are consistent based on the type of transitions.

Indirect transitions are permitted when r = 2, and prohibited when r = 3.

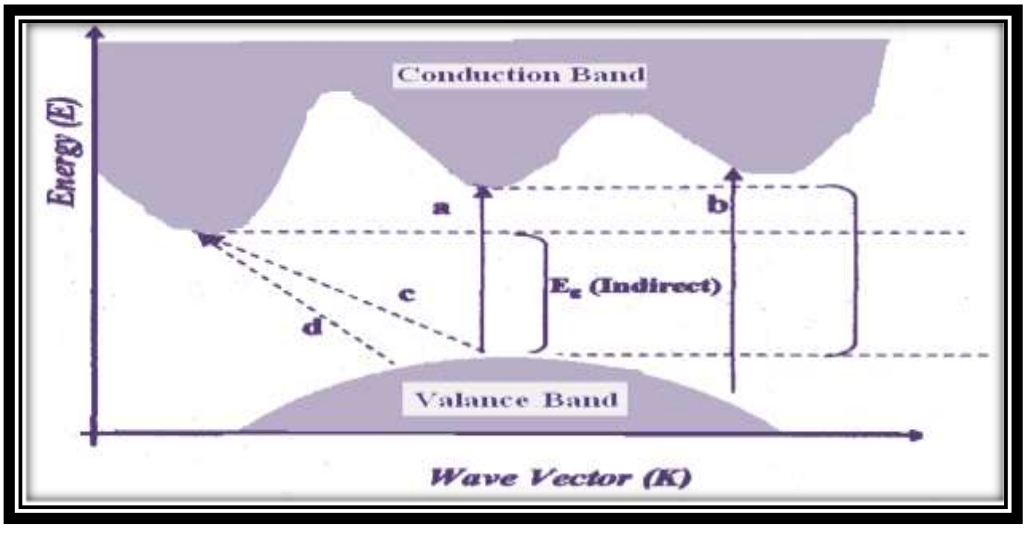

Figure (2.2) : The transition types[80]:

2.2.7 Refractive index (*n*)

According to the equation, the term "refractive index" refers to the relationship between the speed of light in a vacuum and the speed of light in a material.n =c/v …….. (2.7)

One may calculate the refractive index using the [82-83]:

$$n = \sqrt{\frac{4R - k^2}{(R-1)^2}} - \frac{(R+1)}{(R-1)} \ldots\ldots \quad (2.8)$$

2.2.8 Extinction coefficient (k_o)

A complicated refractive index with an imaginary part is known as an extinction coefficient(n*)[82,84]:

$$n^* = n - ik_\circ \quad \cdots\cdots\cdots\cdots \quad (2.9)$$

n; equivalent in terms of the real component of the refractive index (c/v).

Using the following equation below, we can determine the (k) [82]:

$$k_\circ = \frac{\alpha \lambda}{4 \pi} \quad \cdots\cdots\cdots\cdots \quad (2.10)$$

2.2.9 Dielectric constant (ε):

The dielectric constant of a matter is a scale of its capability to polarise electric field, and expression of this constant may be found in the equation below [82,85]:

$$\varepsilon = \varepsilon_1 - i\,\varepsilon_2 \quad (2.11)$$

$$\varepsilon = (n^*)^2 \quad (2.12)$$

$$(n - i\,k_o)^2 = \varepsilon_1 - i\,\varepsilon_2 \quad (2.13)$$

$$\varepsilon = (n^2 - k_o^2) - i\,(2nk_o) \quad (2.14)$$

Complex dielectric coefficients, both real and imaginary, are capable of being represented. as in equations (2-11) and (2-14)[86,87]:

$$\varepsilon_r = n^2 - k_o^2 \quad (2.15)$$

$$\varepsilon_i = 2nk_o \quad (2.16)$$

2.2.10 Optical conductivity ($\sigma_{opt.}$) :

As seen in the equation below, the constant (σ_{op}) is directly proportional to the two elements of refractive index (n) and absorption coefficient (α). [88]:

$$\sigma_{op} = \frac{\alpha n c}{4\pi} \quad \ldots\ldots\ldots \qquad (2.17)$$

2.3 Electrical Properties

Since there is such a wide range of molecular events that can occur in polymers in response to an applied electric field, the topic of electrical properties of polymers is enormous. Polymers with an electronic conduction response to an electrical stimulus, it is far fewer dramatic than when the electrical response is one of metals. However, the lack of any overwhelming conduction dosage allows for the observation of a broader range of electrical effects. Electrical characteristics research will also aid in the fundamental knowledge of polymer thermal and optical properties[89].

2.3.1 Electrical Conductivity in Direct Current ($\sigma_{d.c}$)

To determine the electrical resistance of the produced films as a function of substrate temperature, a rectangular sample was tested and its value (Rdc) was calculated [90]:

$$R_{dc} = \rho_{dc}\left(\frac{L}{bt_t}\right) \ldots\ldots(2.18)$$

The surface resistivity is denoted by ρ_{dc}. The inverse of the resistivity is the surface conductivity. Surface conductivity is so increased[90]:

$$\sigma_{dc} = \frac{1}{\rho_{dc}} = \frac{L}{R_{dc} b t_t} \ldots\ldots(2.19)$$

Where σ_{dc} is the sample's electrical conductivity and L, b, and t are the sample's length, width, and thickness, respectively. The activation energy (Ea) may be computed using the formula[89,91].

$$\sigma_{dc} = \sigma_o \exp\left(\frac{-E_a}{kBT}\right) \ldots\ldots(2.20)$$

Temperature (T), Activation Energy (E_a), and Thermal Energy (k_BT) Due to Temperature Fluctuations During the Measurement and σ_o is electrical conductivity at absolute zero of temperature[81-82].

2.3.2 Current-Voltage (I-V) characteristic

I-V measurements are used to calculate the photovoltaic efficiency for solar cell. Short-circuit current I_{sc}, open-circuit power V_{oc}, efficiency η and fill factor F.F are all photovoltaic parameters of solar cells, are described by the following equations[92]:

$$I_{sc}=I_s[\exp(qV_{oc}/ k_BT)-1]+ V_{oc}/R_{sh} \quad ....(2.21)$$

$$V_{oc}= k_BT/q \ln(I_{sc}/ I_s+1) \quad .....(2.22)$$

Where (I_s) is saturation current, (k_B) is Boltzmann constant and $k_BT/q=0.0259$ eV at ($T=25C^o$), (V_{oc}) open circuit voltage, R_{sh} is the shunt resistant.

These measurements were taken in a cell at 25 degrees Celsius, with 115 mW/cm^2 of incident solar radiation, using a degussa P25 AM1.5 photoelectrode with an active area of 0.12 cm^2 [93]. (V_{oc}) of a solar cell would be continuous since typical redox potential for an electrolyte is assumed to be fixed. Metal oxides can, however, be improved by the use of composites and dopants. and tweaking the flat band (VFB), the V_{oc} of a sollar cell may be controlled[94]. To put it another way, $J_{sc} = I_{sc}$ /A is equal to (0) when applied voltage through the solar cell is also at (0). In the best lighting circumstances as shown figure (2.3), The value of (J_{sc}) relies heavily on how well charge is injected from the excited pigment into the C.B of metallic oxide [93].

Most essential characteristic for solar cell is fill factor (F.F). It's defined as the creation of (I_{sc}) and (V_{oc}) and the highest power output (ImaxVmax). It may be deduced that for highly desired F.F, it's necessary to adopt an I-V curve with a squarer shape. Shunt resistance and fill factor can both be improved by decreasing electron loss at the FTO/electrolyte interface. Conversely, increased reverse electron transfer and charge recombination leads to poor FF. Total power output (P_{out}) relative to solar energy input can be compared to get an idea of efficiency (P_{in}),shown in fig.2.4[92]:

$F.F = V_m \times I_m / V_{oc} \times I_{sc}$…..(2.23)

$\eta = P_m / P_{in}$…….(2.24)

2.3.3 Electrical measurements for heterojunction.

A- Measure dark voltage current characteristics:

A solar cell was placed in the dark and connected to a power supply, and a simple forward bias of 0.1_0.5v was measured As well as measuring the reverse bias current for the same voltage mentioned, and drawing a relationship between the forward and reverse bias voltages, then determining the I_V characteristics in the dark state and for all solar cells manufactured under different conditions[4].

B-Measure capacity-voltage (C-V) characteristics:

The purpose of measuring the capacity-voltage characteristics is to determine the internal building voltage in addition to determining the type of hybrid junction.A reverse bias voltage (LRC) was used to determine the type of heterojunction, and with an effort ranging between (2to -2)v if the internal final effort was found [7,92].

2.3.4 Electro-optical measurements for heterojunction

1- Measurement of the current(I_{sc}) as a function of the bias voltage when illuminated by the white light from a halogen lamp of high intensity(115)mW/cm^2.

2- The current through the detector is measured in the absence of an external voltage as a function of the light intensity.

3-The open circuit voltage(V_{oc}) measurement represents the amount of voltage passing through the detector as a function of the incident light intensity

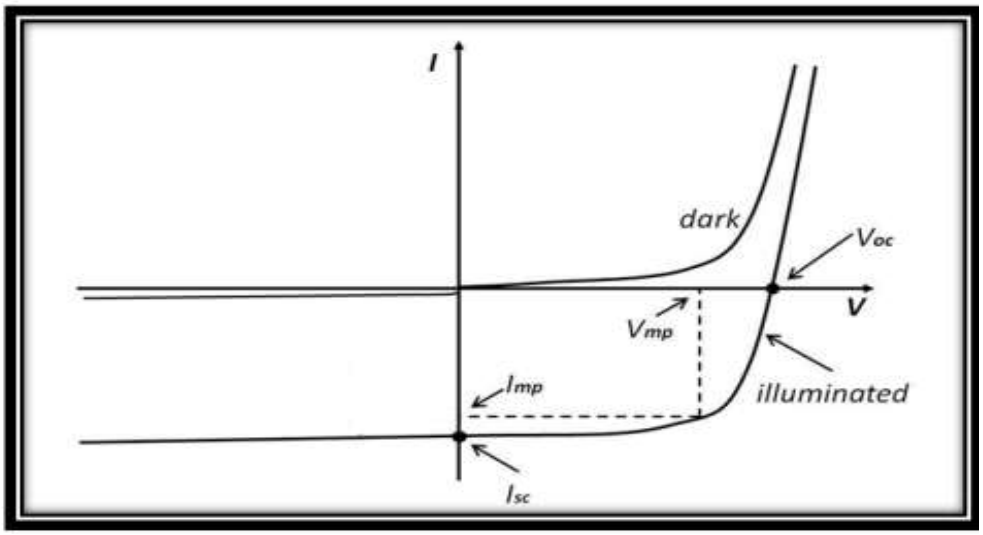

Fig.(2.3) I-V characteristics of solar cell in dark and illumination[92]

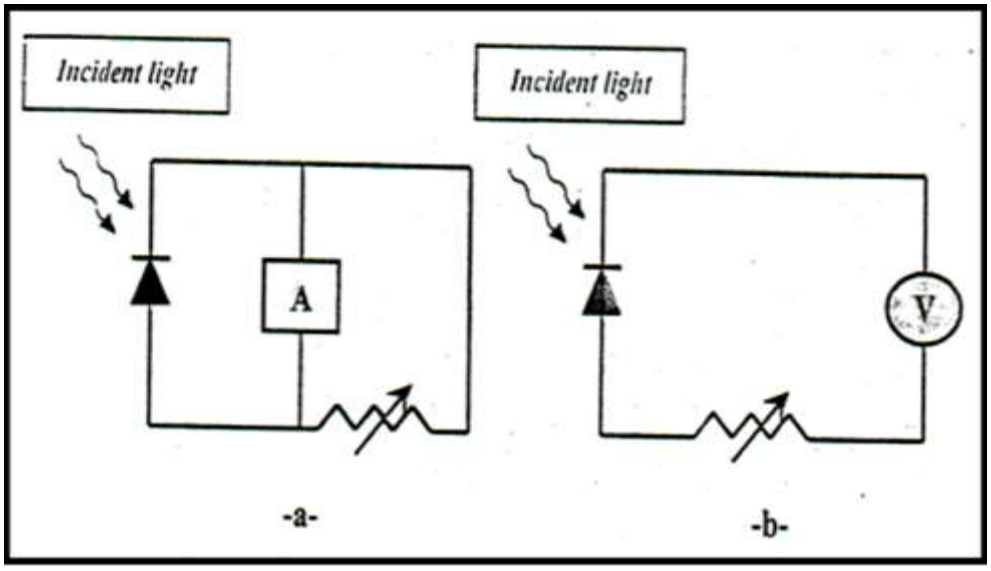

Figure (2.4) (a) Short-circuit current and (b) Open-circuit voltage Circuit Diagram

Chapter Three Experimental Work

3.1Introduction

This chapter focuses on using spin coating to prepare and handle (PVA/TiO_2) nanocomposites with various dyes. (Optical microscopy, FT-IR spectroscopy, SEM imaging, electrical characteristics) are utilized in this study, which also includes images and schematics of various electrical circuits.

3.2 Materials used

The following materials were utilized in this study:

A.Polyvinyl Alcohol (PVA)

Polyvinyl alcohol (PVA) is used as granular form, molecular weight between (26,300-30,000) g/mol. Provenance of Polyvinyl alcohol is Shanghai Kaidu Industrial development Co, Ltd, China

3.2.1 Additive nanomaterial

A. Titanium dioxide

The (Nano shel USA) corporation supplied the substance, which were discovered in powder form. TiO_2 has a small size with 20 nm and high parity of 99.9%.

3.3 Substrate Cleaning

The films were prepared on glass slides in a spin coating

3.3.1Glass substrate

Glass slides dimensions (2.5 ×7.5) cm^2 and a thickness 0.1-0.12 cm ±0.05 were utilized as substrates. The following procedures were applied on these glass slides:

1- The substrates were cleaned by alcohol.
2- The substrates were cleansed ultrasonically for 10 minutes after being submerged in a clean beaker containing distilled water.
3- Finally, the glass substrates were rubbed with soft paper and dried with an air-jet.

3.4 Preparation of natural dyes

Through Dehydration: The blackberry, pomegranate and crocus was extracted using a fruit pulper, and after being filtered, the solution was concentrated by heating it to 75°C and removing 20% of the water for the preservation of the fruit's aroma. Finally, the dehydration was done in oven at 75°C for 7 h, until a dry paste was obtained, which was then crushed to create the dye powder.

Figure(3.1) plant natural dyes

3.5 Preparation of (PVA/ TiO_2) nanocomposites

one gram of (PVA) was dissolved fully in 20ml distel water in a glass beaker for one hour under continual stirring with temperature 90°C. Then, when the pure sample has been dissolved, amount of TiO_2 NPs are added different ratios (0,1, 2 and 3) wt.%, and then putting a glass beaker into ultra-sonic device to disperse of TiO_2 for 5 min, As shown table (3.1) and (3.2).

The dye was concentrated by adding 0.01 g per 20 ml of distilled water then mixing with different ratios(1,2,3 and 4) ml of the natural dye per 100% (PVA/TiO_2) and diverse samples have been formed. Then put drops of the prepared each nanocomposites on glass substrates is used for depositing films by vacuum spin coater 700 rpm for 10 sec to 774±3nm thickness of films. The glass slides all of (2.5 × 7.5) cm^2 area are employed as substrates with thickness 0.1cm.

Table (3.1) Weight percentages of (PVA/TiO_2) nanocomposites.

PVA g	TiO_2 wt.%	PVA/TiO_2 g
1	0	1
0.99	0.01	1
0.98	0.02	1
0.97	0.03	1

Table (3.2) Mix ratio of nanocomposites with natural dyes **(PVA/TiO_2) nanocomposites.**

PVA/TiO_2 ml	Natural dyes ml	PVA/TiO_2/ natural dyes
20	1	21
20	2	22
20	3	23
20	4	24

3.6 Spin Coating

The rotation will accelerate in the second stage, and centrifugal forces will eliminate the remaining, unnecessary sol. Here, the volatile solvent evaporates to leave behind a dry, thin, metal organic coating. The viscosity, sol concentration, and angular speed all affect how thick the film is. As the angular speed increases, the film thickness falls. figure (3.2) depicts the many phases of the spin coating process schematically[53,96].

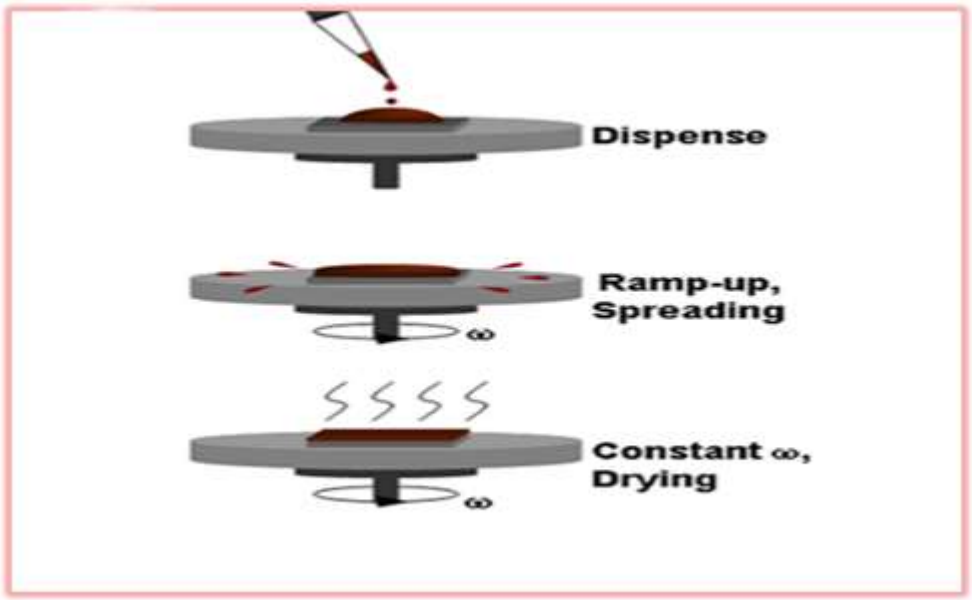

Figure (3.2): Spin coating[97].

3.7 Materials of solar cell

A. Tin Dioxide Nanoparticles (SnO_2)

Tin dioxide obtained as white or light grey powder from Sky Spring Nanomaterial. ink Company, USA, with grain size (35-55)nm and high purity (99.9%).

B. Silicon wafer (p-type)

The silicon wafer utilized in (SnO_2) is a monocrystalline p-type silicon wafer with orientation [111] and resistivity (1-10 Ω.cm) that is commercially available. Prior to film deposition, the wafer silicon was chopped into little pellets of roughly (1×1) cm in diameter and cleaned. Si wafer specimens were washed multiple times with distill water and dried with soft paper.

C. Preparation of solar cell

A solar cell was prepared in the thin-film laboratory. Where the SnO_2 material was deposited with a thermal vacuum evaporation device on p_Si junction, where we formed a SnO_2/p_Si solar cell, after which aluminum electrodes were deposited for the cell.

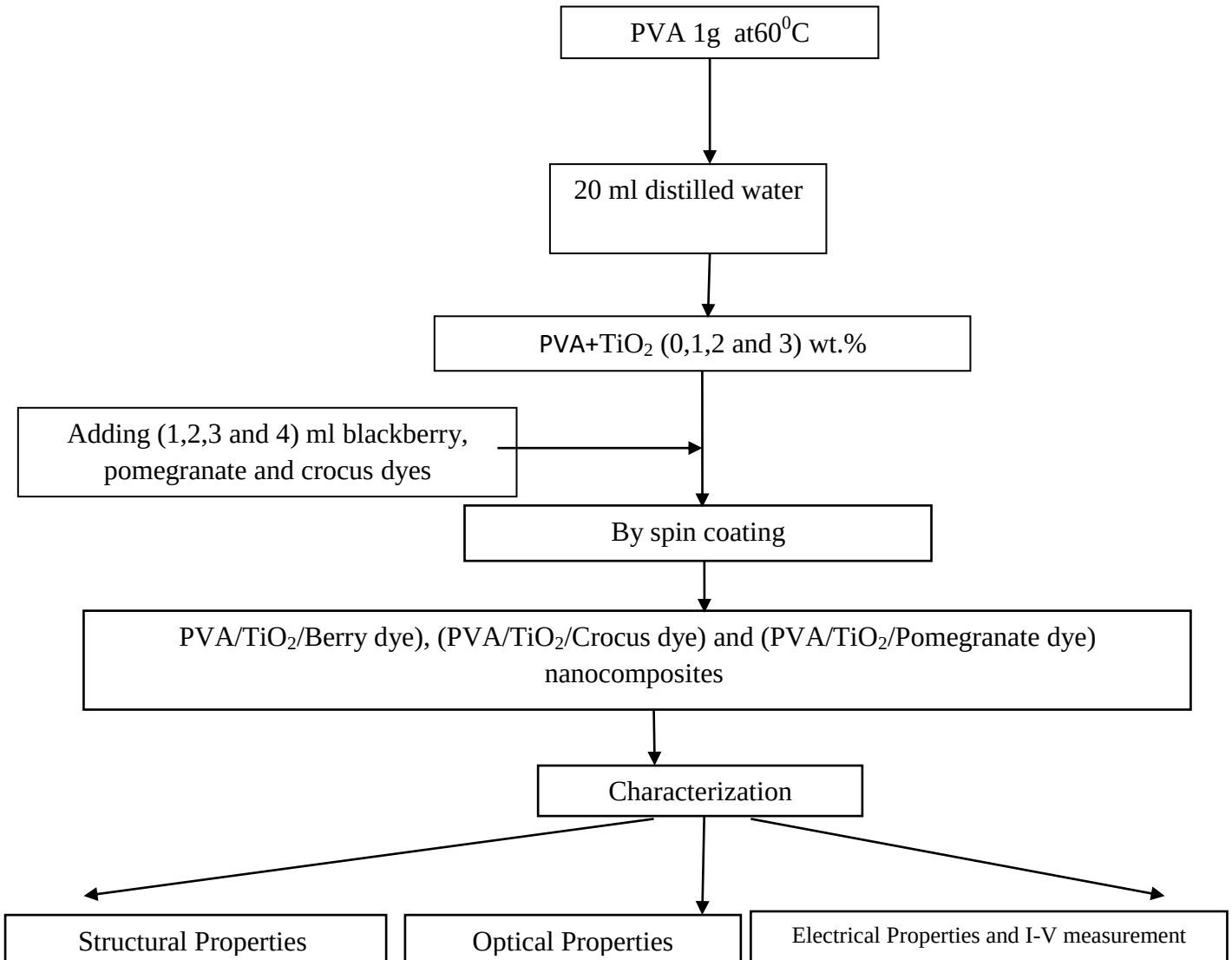

Figure (3.3): Scheme of Experimental Part.

3.8 Measurements of Structural Properties

3.8.1 Optical Microscope

Olympus Toup View (Nikon-73346) optical microscopes with built-in, light-intensity-automatically-controlled cameras are used to observe the surface morphology evolution of PVA/titanium dioxide TiO_2 and (PVA)/natural-dye nanocomposites. In closeup (10x. This instrument is present in the laboratory of advance thin films .

3.8.2 FTIR Spectral Characterization

Fourier Transform Infrared(FTIR) spectrometer spectra can be used for quantitative and identification analysis of the wave number range from 600 to 4000 cm-1 was used to record nanocomposites from the (Shimadzu firm, Japan origin, type IR Affinity-1) .

3.8.3 FE- SEM Scanning Electron Microscope

Scanning Electron Microscopy has a strong device for examining materials. It's employed in a variety of fields, including metallurgy, geology, biology, and medicine, to mention a few. The user may receive high magnification photos with a decent depth of field, allowing them to examine individual crystals or other details. In conjunction with the related technique of energy-dispersive X-ray microanalysis, a high-resolution SEM image may reveal fine features as small as 25 A°. It is possible to analyses the composition of individual crystals or other properties.

After preparation of the sample took a small part of ($1cm^2$) to examine the SEM, it provides information for dispersion of particles (TiO_2) in polymer matrix .The surface morphology of (PVA/TiO_2) and (PVA/TiO_2/Natural dyes) nanocomposites is Figured out utilising

(German-based business) Bruker Nano GmbH's (type) vertex 5600 LV SEM .

3.9 The Evaluation of Optical Characteristics

A double beam spectrophotometer (Shimadzu model UV-1800 oA (JAPAN)) was used to record the absorption spectra of (PVA/TiO_2/Natural dyes) nanocomposites films across the wavelength range (190-1100) nm. The absorption spectra were taken at ambient temperature.

A piece of software was used to determine the energy gaps, optical constants, α, k_o, and n. This piece of equipment may be found in any modern thin film research facility.

3.10 DC Voltage measurements

At different temperatures (between 30 and 70 °C), the D.C electrical resistance may be measured to provide an approximation of the material's electrical conductivity. To achieve reliable findings, after heating the sample for 10 minutes at 300 degrees, the electrical resistance was measured. The (Keithley electrometer type 2400 source matter) was used to collect the temperature readings of the Keithley electrometer, Advanced thin film research facilities. typically have access to such equipment.

3.11 The Coating Unit

The vacuum system is as follows:

Edwards Auto 306, evaporates using a tungsten or molybdenum filament, with a maximum chamber pressure of $1x10^{-7}$ mbar and a typical filament current of 100–200 A. Uses either visible or infrared light to illuminate the substrate; maximum deposit thickness is 1.5 m.

In order to remove samples from the coating unit, power was cut off and they were left in a high vacuum. The substrates are put on a spherical holder and elevated to a height of approximately 14 cm above the boat for evaporation activities to take place at room temperature (RT). When the temperature inside the boat reaches the set point, the deposition procedure begins. All the samples are prepared under

constant pressure equal 10^{-7}mbar,and rate of deposition 0.7 nm. s^{-1} with thickness 200±6 nm. After evaporating SnO_2 thin film on silicon wafer, we have formed p-n junction solar cell and Ohmic contacts for the prepared films are produced by evaporating (Al) to formed solar cell electrodes. This instrument is present in the laboratory of advance thin films .

3.12 Masking Techniques

A thick piece of (Al) foil serves as the mask. On the substrate, several forms of masks are utilized to create a suitable shape to fit the required electrode measurement. Using a thermal evaporation method using unit and electrodes (0.1×0.2) mm, ohmic connections are formed between the produced films and the electrodes.

3.13 Thickness Measurement

Film thickness is an important parameter that significantly affects film characteristics. Weighting was used as a method for measuring the thickness of thin films.

The thickness of the deposited layer may be approximated using the weighting technique. The equation below determines the film thickness (t):

$$t = \frac{m}{2\pi\rho R^2} \qquad \text{……..….} \quad (3.1)$$

m: calculates the film's actual net weight (g)

R: A space between a boat and substrate (cm). and (ρ) is the film's density (g/cm^3).

Chapter Four

Results and Discussion

4.1 Introduction

After the measurements that were reviewed in the preview

The chapter contains the consequences and discussion optical microscopy FTIR and SEM of (PVA /TiO_2), (PVA /TiO_2/Berry dye), (PVA/TiO_2/Crocus dye) and (PVA/TiO_2/Pomegranate dye) nanocomposites films which is considered as complementary results and tests of the optical characteristics and direct current electrical conductivity for (PVA /TiO_2),(PVA /TiO_2/Berry dye),(PVA/TiO_2/Crocus dye) and (PVA/TiO_2/Pomegranate dye) nanocomposites. In addition to this, it will discuss the effects of varying concentrations of additive nanoparticles (TiO_2) and various natural dyes on optical and electrical characteristics of polymers, as well as the effects of varying temperatures (30-70)^oC on the direct current electrical conductivity of nanocomposites films. Added to them, and the results of the electronic properties of SnO_2/p-Si heterojunction.

4.2 The Structural Properties

4.2.1 The Optical Microscope

Figure (4.1) shows images of (PVA/TiO_2) nanocomposites films collected at different magnification powers(10x) for samples of various concentrations. However, as seen in the images (A,B,C, and D), there is a noticeable difference between the samples. When the concentration of titanium dioxide nanoparticles in films (polyvinyl alcohol) reaches 0.3 wt.% for (PVA/TiO_2) nanocomposites, there is a continuous network of nanoparticles inside the polymers [98].

This image demonstrates homogeneous TiO_2 diffusion in the polymer, which is made possible by the presence of a network with pathways peculiar to nanocomposites that let charge transporters to traverse across them[99]. Figure (4.2) shown all samples of different concentrations(1ml, 2ml, 3ml and 4ml) of berry, crocus and pomegranate dyes gave the same images because the ratio of TiO_2 with polymer is constant(TiO_2 3wt.%+PVA97wt.%). As for the dyes, it did not show any change in the various images because the light has passed from the films and only TiO_2 particles appeared in the picture, and no various color appeared due to the low concentration of the dye.

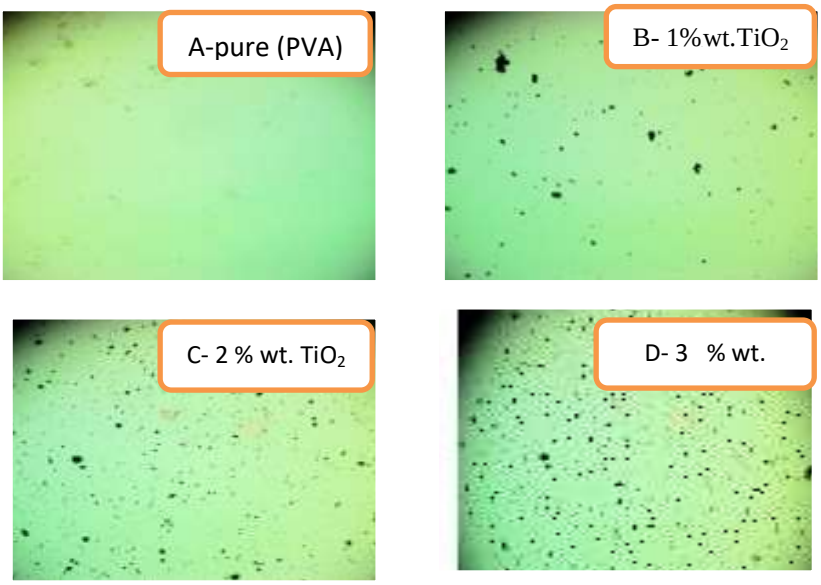

Figure (4.1) : Photomicrographs (10x) for (PVA/TiO_2) nanocomposites

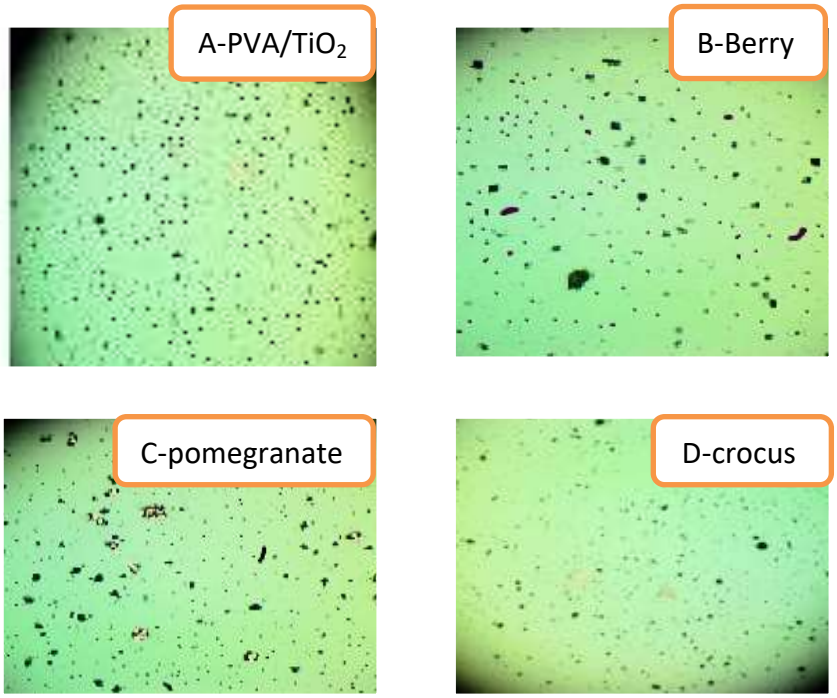

Figure (4.2) : Photomicrographs (10x) for (PVA/TiO_2 3%wt. /berry Dye), (PVA/TiO_2 3%wt. /Crocus Dye) and (PVA/TiO_2 3%wt. /pomegranate Dye) nanocomposites.

4.2.2 Infrared Spectroscopy Testing using Fourier Transforms (FT-IR)

As can be seen in figure(4.3), (FT- IR) is used to take readings of both the spectra of pure (PVA) and doped films. All of the ranges have the potential to display pure absorption bands . Observable shifts in the

samples' spectral features can be found within the range (1500–500) cm^{-1} (fingerprint area). The additional bands might be linked to flaws created on the charge transfer process between the polymer chain and nanomaterial [100].

The O-H extending sharp and broad peaks at (3352.28,3255.84) cm^{-1} and the C-H extending, C=O extending, O-H bending, C-O stretching of CH2, and CH rocking peaks at (2927.94, 1689.64, 1419.61, 1087.85, and 9.14.26) cm^{-1} can be shown in fig (4-3) for pure (PVA) and another vibrational peak for nanocomposites concentrations[101]. Furthermore, the (1000–500) cm^{-1} vibrational peaks may be ascribed to nanoparticles with polymer, indicating that nanoparticles doped in the (PVA) polymer matrix. The (O-H) stretching band is by far the most characteristic feature of alcohols, it appears in range (3000-3500) cm^{-1}.The vibrational bands of the nanocomposites, as well as the intermolecular interaction between the mix and the TiO_2 nanoparticals, are revealed using the FTIR approach [102].

The CH_2 rocking vibration is ascribed to the band at 914.26 cm^{-1}, which has been linked to syndiotactic structure. PVA crystal has a band around 1087.85 cm^{-1}, while the carbonyl group has a band around 1689.64 cm^{-1} due to absorption of leftover acetate groups during PVA manufacture from polyvinyl acetate hydrolysis. If the OH group is involved in the production of hydrogen bonds or complexes with metal particles, the group has a broad peak around 3000-3600 cm^{-1}, hence the broad peak of hydroxyl groups was seen for nanocomposites in this range[103] .

The band at 2927.94cm^{-1} was assigned to the (CH+OH) group's combination frequency. The C=O stretching mode is responsible for the peak at 1689.64 cm^{-1}[66]. Some polymer chains were disrupted when TiO_2 nanoparticles were doped, and other chains were produced in their place. In this region, nanoparticles have created new bonds. When added (TiO_2 3 wt.%) decreases the FT-IR spectra around of (3255.84) cm^{-1} for (3236.55) cm^{-1}, O-H and C-H stretching bonds are reflected in the resulting polymer networks. Also shown decreasing surrounding or pertaining to (1087.85 - 1083.99) cm^{-1}. It becomes clear when the concentration of TiO_2 increases, the FT-IR decreases. The fact that the transmitted intensity of peaks in the FT-IR spectrum decreased after

doping suggests that the number of (PVA) chains in the film structure increased. Figures (4.4), (4.5) and (4.6) show the bonds regions. For PVA/TiO_2 films, the bands at about 829 cm^{-1} and 624 cm^{-1} resemble to Ti-O widening modes. We also see a drop in the level with peaks as the concentration of TiO_2 is increased[104]

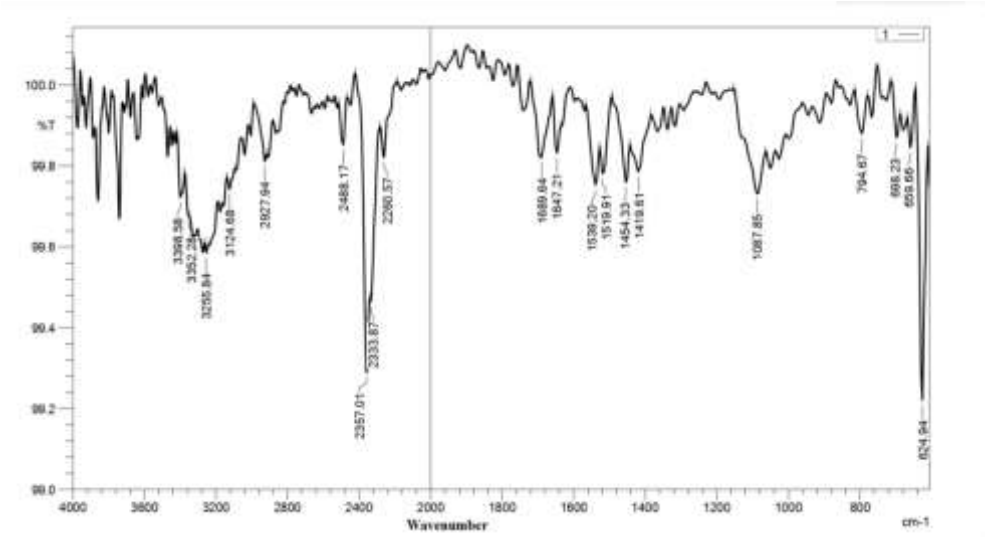

Figure(4.3): Fourier TransformInfrared Spectroscopy for pure (PVA)

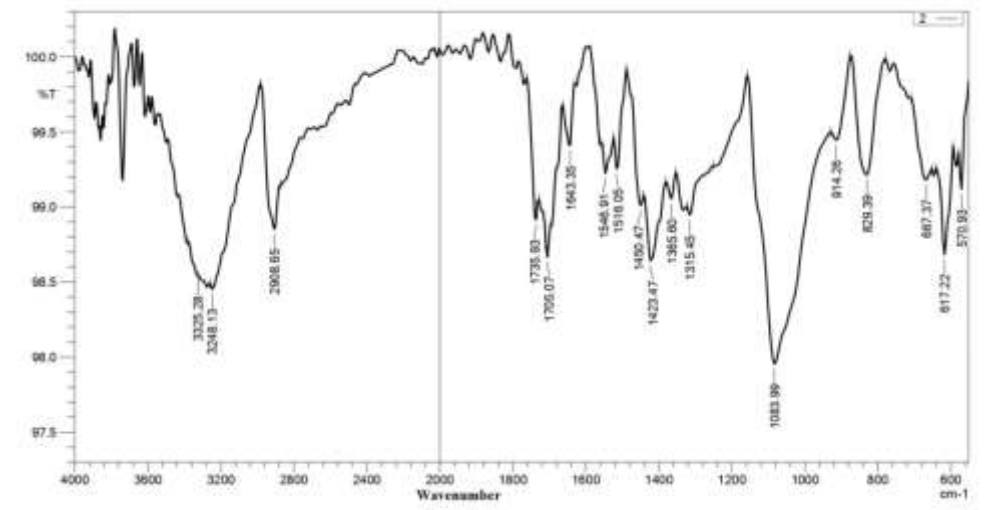

Figure(4.4): Fourier TransformInfrared Spectroscopyfor PVA/ (TiO_2) 1 wt.%

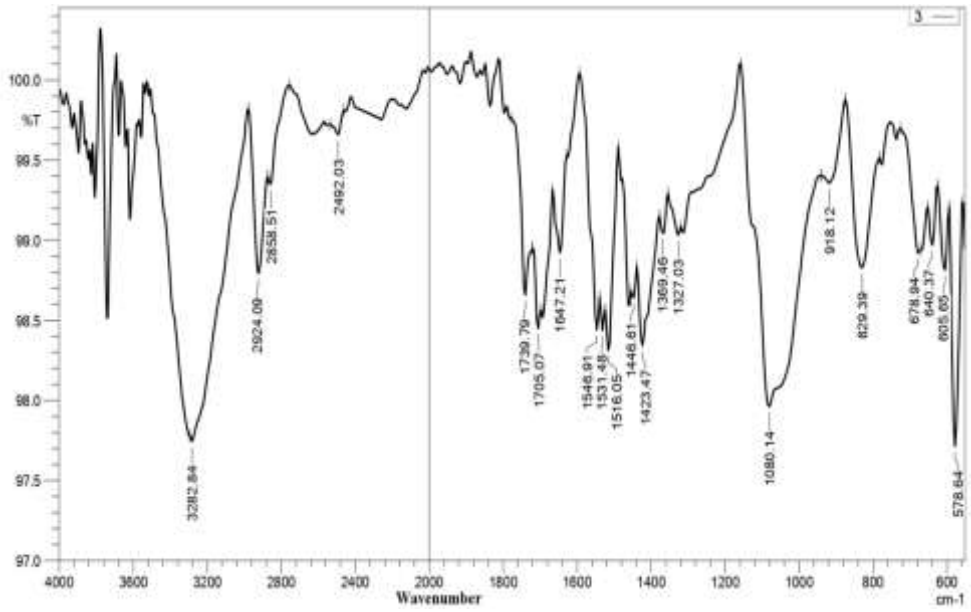

Figure(4.5): Fourier Transform Infrared Spectroscopy for PVA/ (TiO_2) 2 wt.%.

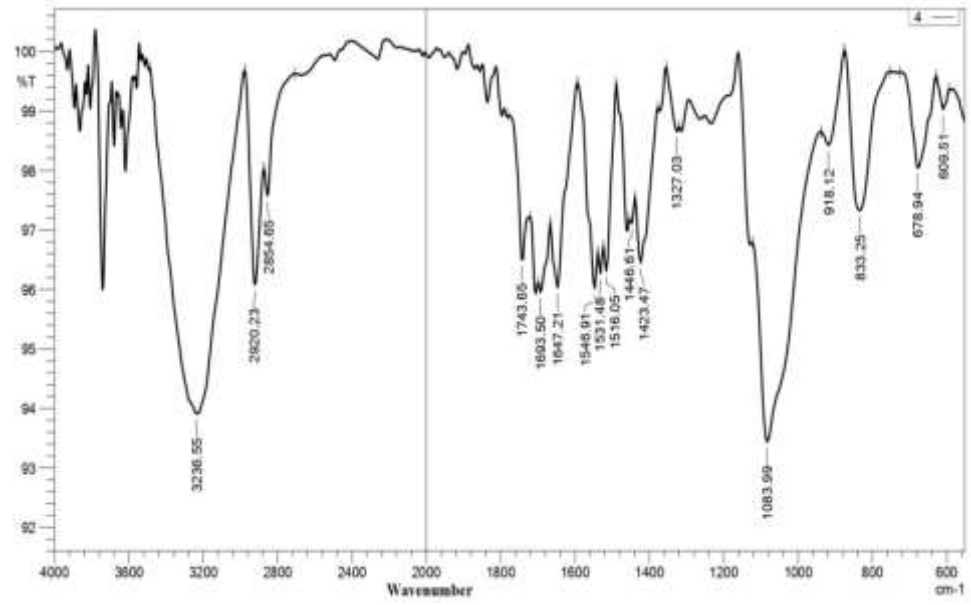

Figure(4.6): Fourier Transform Infrared Spectroscopy for PVA/ (TiO_2)3 wt.%.

Figures (4.7) and (4.8) show the FTIR analysis of (PVA/TiO_2) thin films with different concentrations of (1ml and 4ml) Berry dye concentrations respectively. The bonds between 3550 and 3200 cm^{-1} were identified and linked to the intramolecular and intermolecular hydrogen bridges' stretching O–H[63]. Stretched C–H of alkyl groups were discovered in vibrational groups between 2922 and 3000 cm^{-1}. The peak of IR-rad transmittance denotes a shift in peak locations and the creation of a new peak at 2854.23cm^{-1} ,which is due to the interaction of PVA and

dye (anthocyanin). So take note of the peak's decline from (1083.99-1080.14) cm^{-1} due that to increase concentration for berry dye [105].

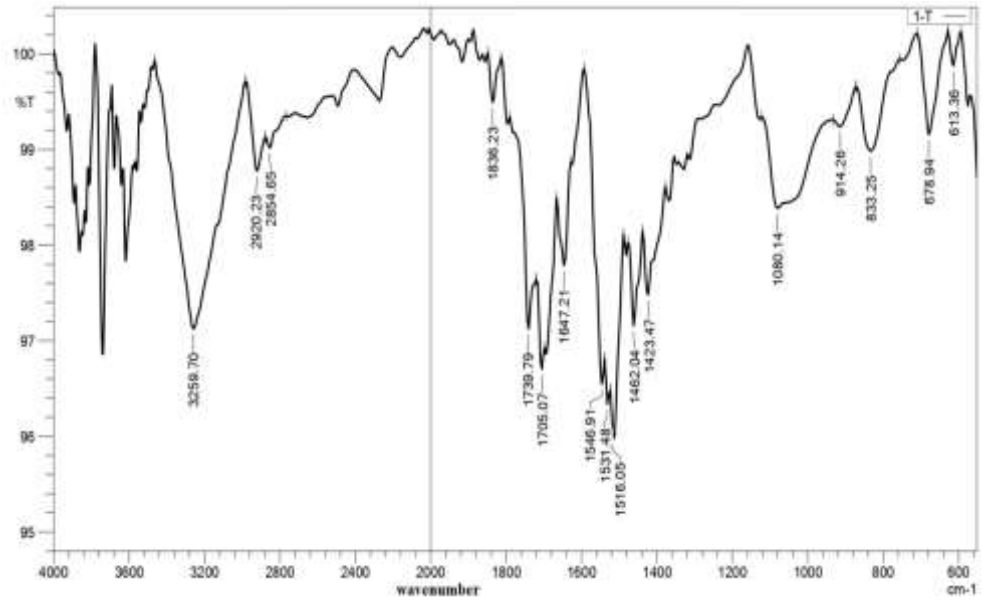

Figure(4.7): Fourier Transform Infrared Spectroscopy for (PVA/TiO_2/1ml Berry dye).

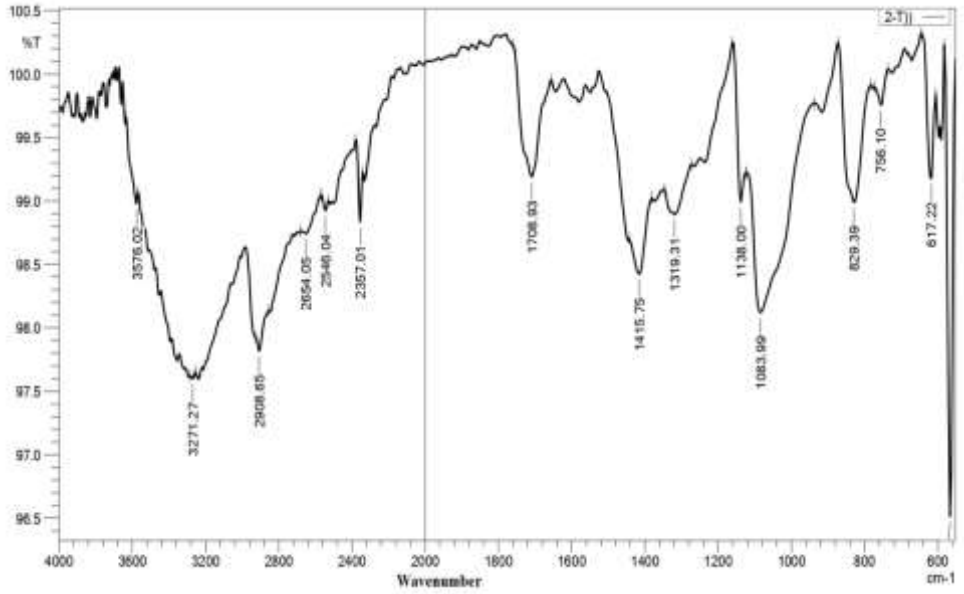

Figure(4.8): Fourier Transform Infrared Spectroscopy for (PVA/TiO_2/4ml Berry dye).

Four distinct functional groups are shown in figures (4.9), (4.10): the O-H group at 3325.28 cm^{-1}, the C - H strain(at 2908.94) cm^{-1}, the C-C strain discovered in the aromatic ring at 1423.46 cm^{-1}, also the C-O group (at 1056.) cm^{-1}. Natural dye (anthocyanin and anthocyanidin) have a benzene skelton , a conjugated double bond , a C-H carbonyl group, and a

hydroxyl (OH) bond, according to the IR spectrum , and the appearance of the peak at 2268.28cm^{-1} may indicates the presence of anthocyanide dye[106].

Figures (4.11) and (4.12) show the FTIR spectra of crocus dye. There is a band between 3344.57 and 3380 cm1 that indicates the presence of alcoholic groups due to the stretching vibration of O-H. Two peaks between 2862 and 2905 cm^{-1} are C-H stretching vibrations, which most molecules share. These two peaks may indicate the presence of an aldehyde groupin the volatile componentsof crocus dye (crocin).

Crocus was used to find the C=O stretching vibration, which was located at 1647.21 cm^{-1} in its spectrum. Stretching vibration of ester (O=C-O) groups, which are components of the crocus, is responsible for the bands that can be seen at 1319.31–1419.61 cm^{-1}. Highest peak (at 1080.14) cm^{-1} possible explanation: a mode of vibration induced by a stretching of the material of conjugatedC-O bonds of the core carotenoid chains found in crocus these results agree with Lee *et al.* [107]. the bands 829 cm^{-1} - 624 cm^{-1} correspond to Ti-O too decreases because increasing concentration of all natural dyes.

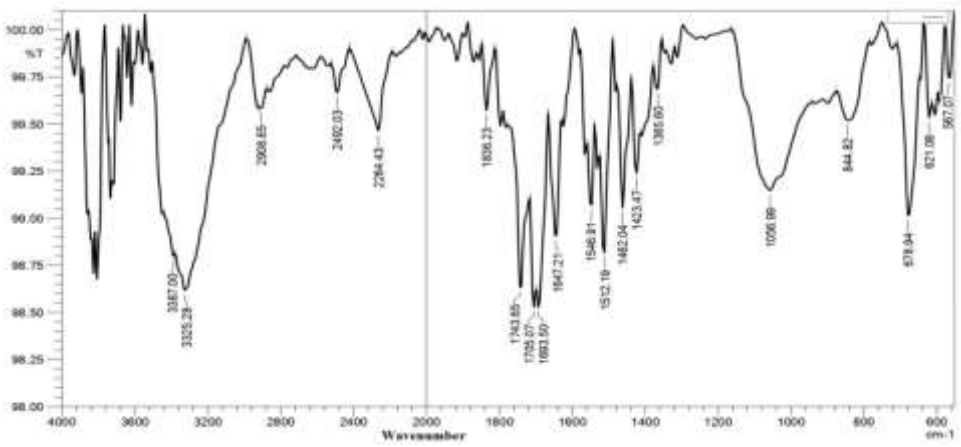

Figure(4.9): Fourier TransformInfrared Spectroscopyfor (PVA/TiO_2/1ml Pomegranate dye).

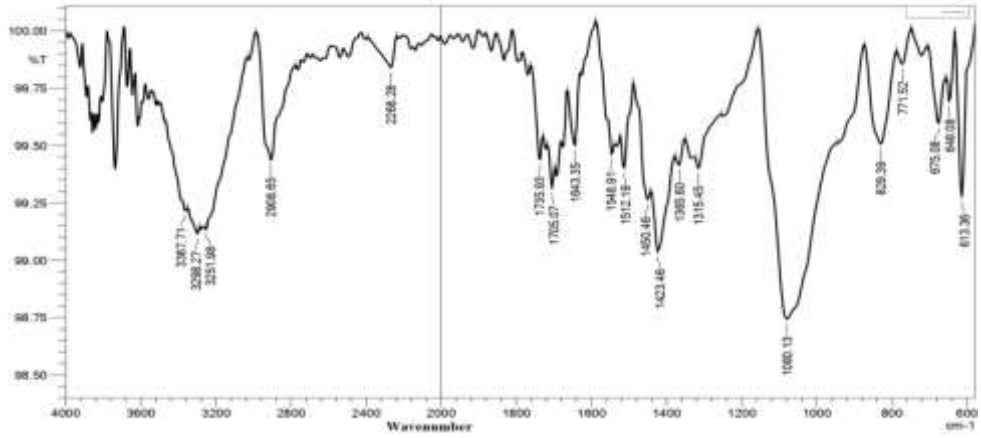

Figure(4.10): Fourier TransformInfrared Spectroscopyfor (PVA/TiO_2/4ml Pomegranate dye).

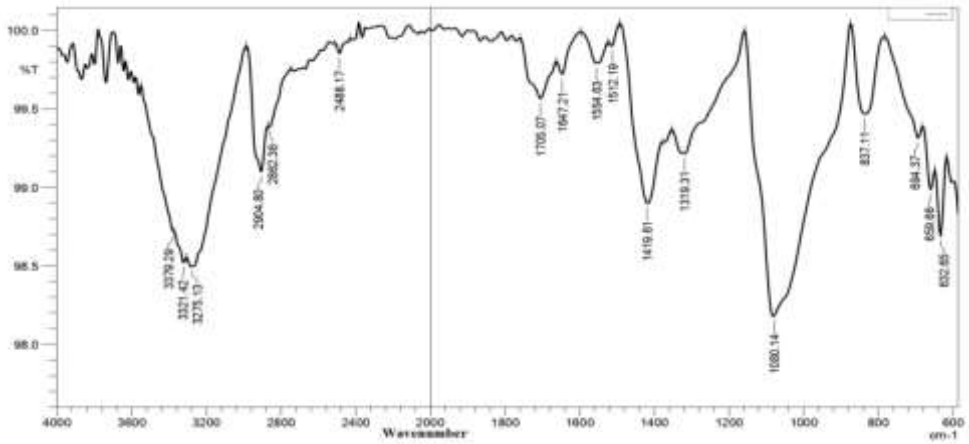

Figure(4.11): Fourier TransformInfrared Spectroscopyfor PVA/TiO_2/1ml crocus dye).

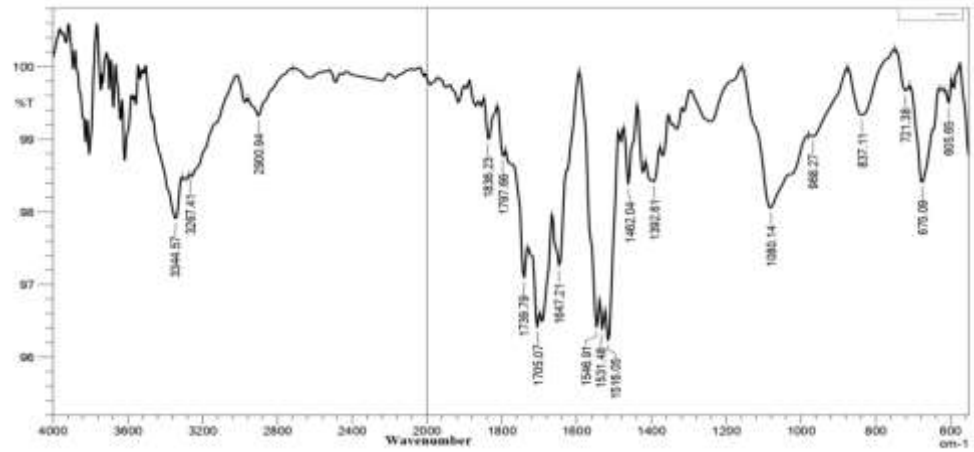

Figure(4.12): Fourier TransformInfrared Spectroscopyfor (PVA/TiO_2/4ml crocus dye).

4.2.3 (FE-SEM) Microscopy

Evaluations by scanning electron microscopy are utilized to examine the distribution and dispersion of particles TiO_2 nanoparticles in the polymers matrix. Tests also fully investigate the effect of titanium dioxide nanoparticles content. Figures (4.13) and (4.14) SEM images of characterizing the topography of (PVA) before and after a focus of TiO_2 NPs addition are exposed.

Pure polymer (PVA) is found to be softer, homogeneous, and coherent in figure (4.13). The addition of titanium dioxide nanoparticles to polyvinyl alcohol (PVA) causes alterations in the surface morphology. The grain aggregates with increasing TiO2 nanoparticles ratio, as seen in the image. On the top surface of the (PVA/TiO_2) nanocomposites films, there are numerous aggregates or pieces randomly scattered[67].

Images of TiO_2 nanostructures generated at various concentrations using FE-SEM. TiO_2 has a morphology that demonstrates the formation of minute groupings of spherical-shaped particles, and the morphology of PVA/TiO_2 agglomerates has cauliflower-like characteristics that are porous and irregular. Both of these morphologies can be seen. It was discovered that nanocomposites had spherical shape and grain sizes of 47.01nm[108] .The (TiO_2) particles were well distributed at (PVA/TiO_2) nanocomposite films, as shown in figure (4.14). From the images it can be remarked seen that the increase in particle size because increase concentration of TiO_2.

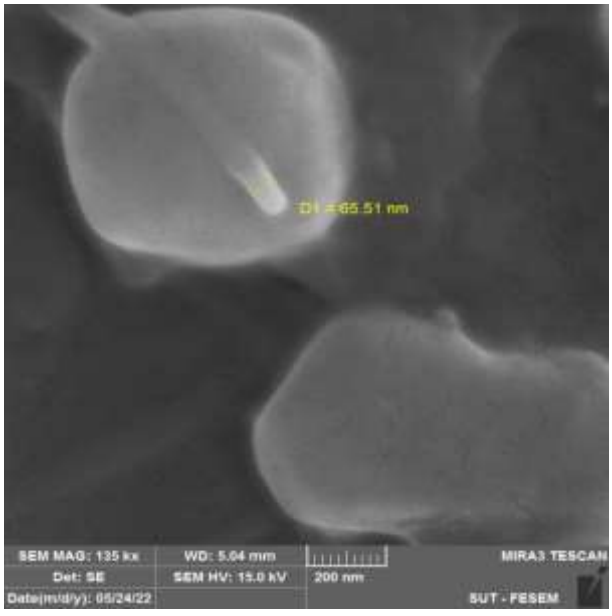

Fig (4.13): SEM measurement of (PVA) .

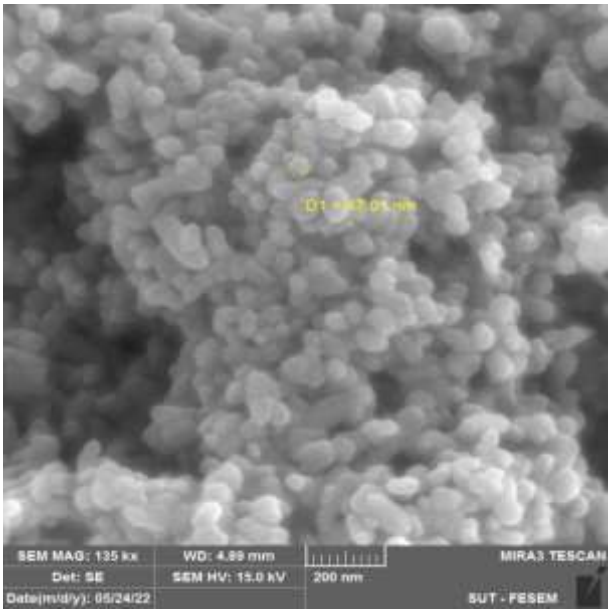

Fig (4.14): SEM measurement of (PVA/TiO_2 3 wt.%) .

In figures (4.15A,B), (4.16 A,B)and (4.17 A,B) the surface morphologies and the cluster size of (PVA/TiO_2/ berry, crocus and pomegranate dyes) films are studied. Agglomeration can be generated by Van der Waals forces, which cause filler materials to form bundles. As a result, The polymer substrate and the filler components had poor interfacial adhesion, and this figures observed. Morphological of the (PVA/TiO_2/Natural dyes) nanocomposites reveals several collection or chucks arbitrarily dispersed for (TiO_2) NPs on the films' outermost layer when the concentration is increased to 3% by weight [63].

They are showed three different one-phase composites according to the color of each dye and the grain size(47-55)nm, also no change appeared when increasing the concentration of the natural dye, and this may be due to the low concentration of the dye in relation to the polymer [109]. The granules that appear in the figures appear to be polymer-coated TiO_2 particles coated with natural dye.

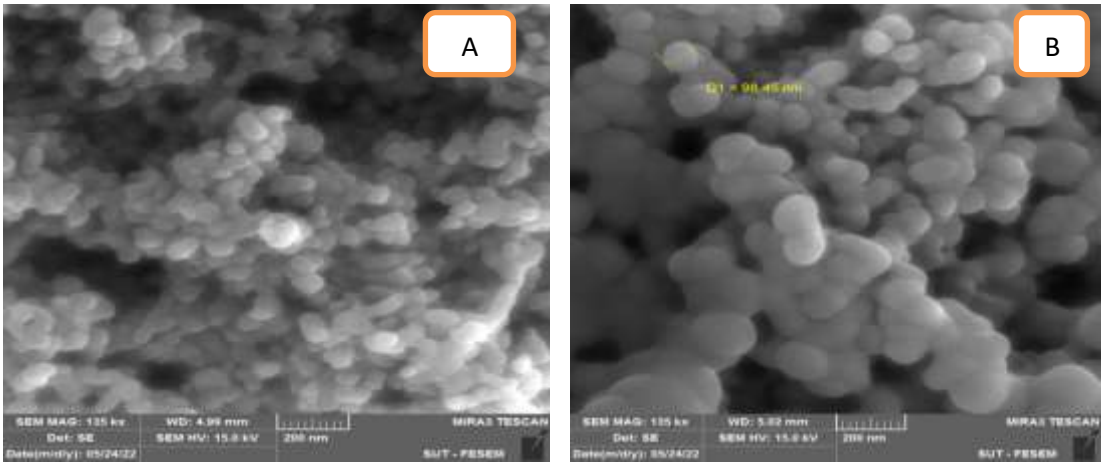

Fig(4.15): FE-SEM measurement of (PVA/TiO_2/berry dye) A) 1ml and B) 4ml.

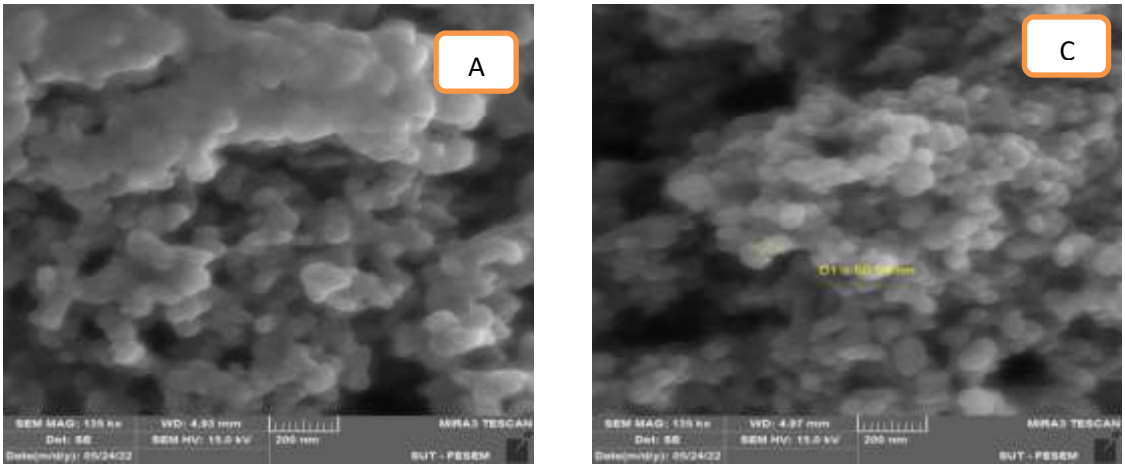

Fig(4.16): FE-SEM measurement of (PVA/TiO_2/crocus dye) A) 1ml and B)4ml.

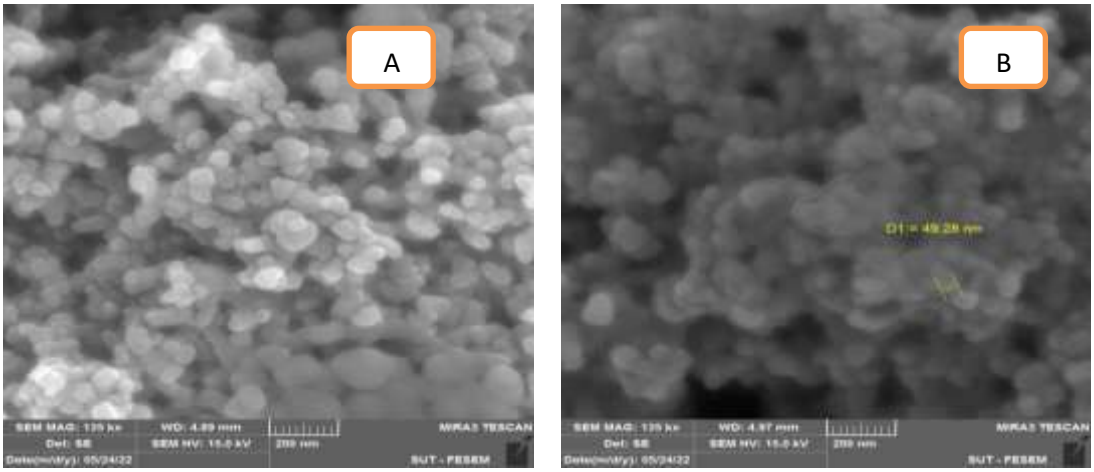

Fig(4.17): FE-SEM measurement of (PVA/TiO_2/pomegranate dye) A) 1ml and B) 4ml

4.3 Optical Properties

The primary goal of examining the optical characteristics of (PVA/TiO_2) and (PVA/TiO_2/berry dye, crocus dye, and pomegranate dye) nanocomposites is to determine the impact of titanium dioxide nanoparticles and varied concentrations of natural dyes on the optical properties of polymers. At room temperature, the research recorded the spectrum of absorbance for the (PVA/TiO_2) and (PVA/TiO_2/berry dye, crocus dye, and pomegranate dye) films, calculating transmittance, absorbance, α, k, and identifying the kinds of electronic transitions and calculating E_g, as well as other optical coefficients.

4.3.1 Absorbance (A)

At room temperature, the absorbance of (PVA) and (PVA/TiO_2) nanocomposites with unlike TiO_2 focuses (1,2, and 3)wt.% for the wavelength (320-1120) nm was measured. The fluctuation of optical absorbance with wavelength for PVA and (PVA/TiO_2) nanocomposites is displayed in figure (4.18). show the samples' optical absorbance versus wavelength prepared at thickness774±4. In regards to all tasters, in the poorer wavelength range (ultraviolet region), where nanocomposite absorbs a lot of light, and then drops as the wavelength increases (VIS & NIR regions).

The results show that the absorbance is increasing with increasing concentration of TiO_2. In all nanocomposites films, there is a red shift (greater wavelength) in the absorption edge near the lower band gap. Each nanocomposites models have a lowest at 400nm, which is attributed to the presence of (PVA) and carbonyl groups associated to ethylene unsaturation in such materials[101].

In figure (4.19) all nanocomposites samples exhibited broad absorption band in the 420-460 nm and top of peak at 440nm ,these results are caused by berry dye effect. The results show that the absorbance is increasing with increasing concentration of berry dye from(1ml-4ml) [110]. In this figure, the lines appeared almost overlapping, and this is due to the low concentration of the dye in relation to the amount of polymer, so it appeared on this figure.

Figures (4.20) and (4.21) also showed the results of the absorbance of crocus and pomegranate dyes the same responses, when focus of the dye rises, absorbance increases as well as the absorbance increases at short lengths (UV) and decreases at long wavelengths in the (VIS and NIR) regions[45]. These thin films absorb visible light according to their wavelengths and can be used as a photosensor in solar cells. The reason for this absorption is to make the natural pomegranate dye as a cover for TiO_2 nanoparticles, [57].

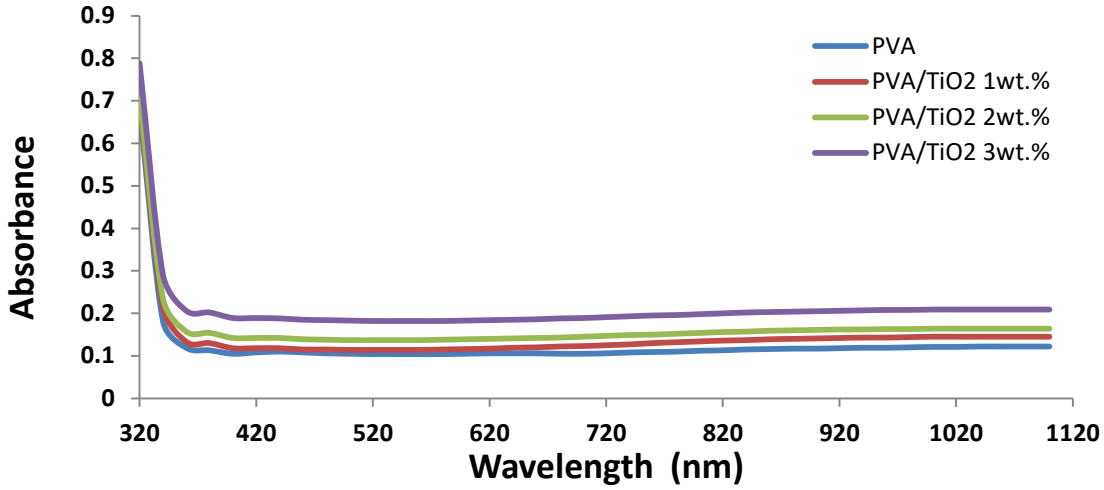

Figure (4.18): The absorbance of (PVA/TiO_2) nanocomposites

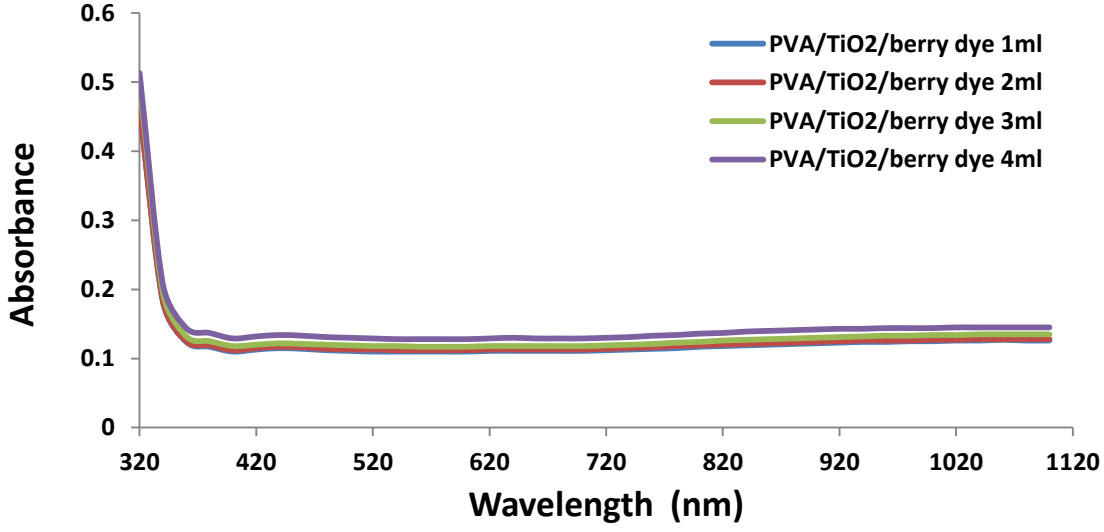

Figure (4.19): The absorbance of (PVA/TiO_2/berry dye) nanocomposites

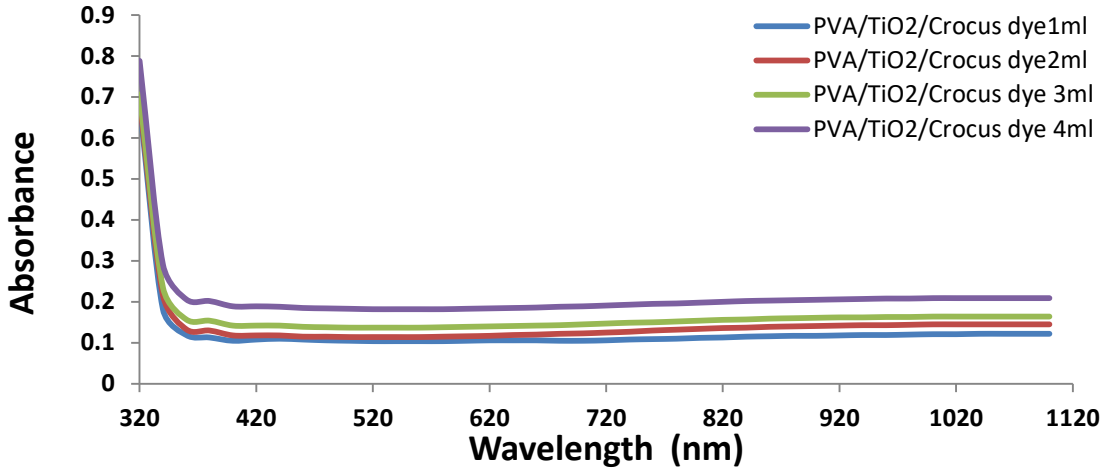

Figure (4.20): The absorbance of (PVA/TiO_2/crocus dye) nanocomposites.

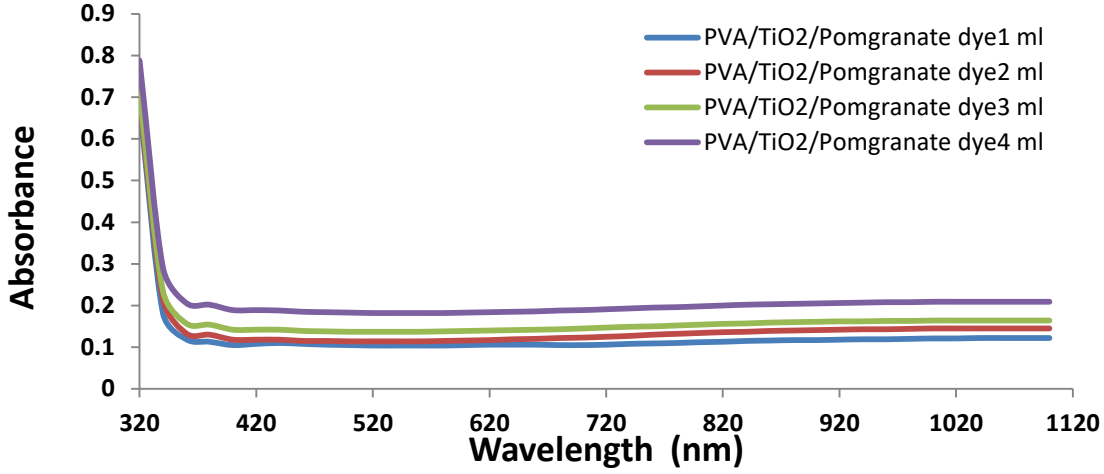

Figure (4.21): The absorbance of (PVA/TiO_2/pomegranate dye) nanocomposites.

4.3.2 The transmittance (T)

Equation(2.2) is used to compute the transmittance T. The transmittance T of polyvinyl alcohol and (polyvinyl alcohol /TiO_2) nanocomposites versus wavelength is depicted in Figure (4.22). Figure indicate that the transmittance for all samples are decreased with increasing of wavelength, like this behaviors agree with[111].The UV-Transmittance Spectrum of all the samples the logarithmic connection between absorbance and transmittance, transmittance curvature is shifted towards short wavelengths, and see the inverse pattern between absorbance and transmittance[77].

So the transmittance decrease with increase concentration of TiO_2, and recorded highest peak at 77%. Transmittance is very important for devices like solar cells [65].

The wavelength-dependent transmittance T for the (PVA/TiO_2/berry dye) system, (PVA/TiO_2/crocus dye), and (PVA/TiO_2/pomegranate dye) nanocomposites is shown with figs. 4.23, 4.24, and 4.25. The Outcomes showed that growing the concentration of the natural dye clues to a decline in transmittance, the highest peaks was recorded in berry dye, crocus dye and pomegranate dye at (77.6, 81.9, 76)% with a concentration of 1ml, respectively. Also the results observed films exhibited high transmittance color yellowish green [112]. It can be said these films can serve as a window for solar cells, because it is a material with good transmittance in the (VIS and NIR) region.

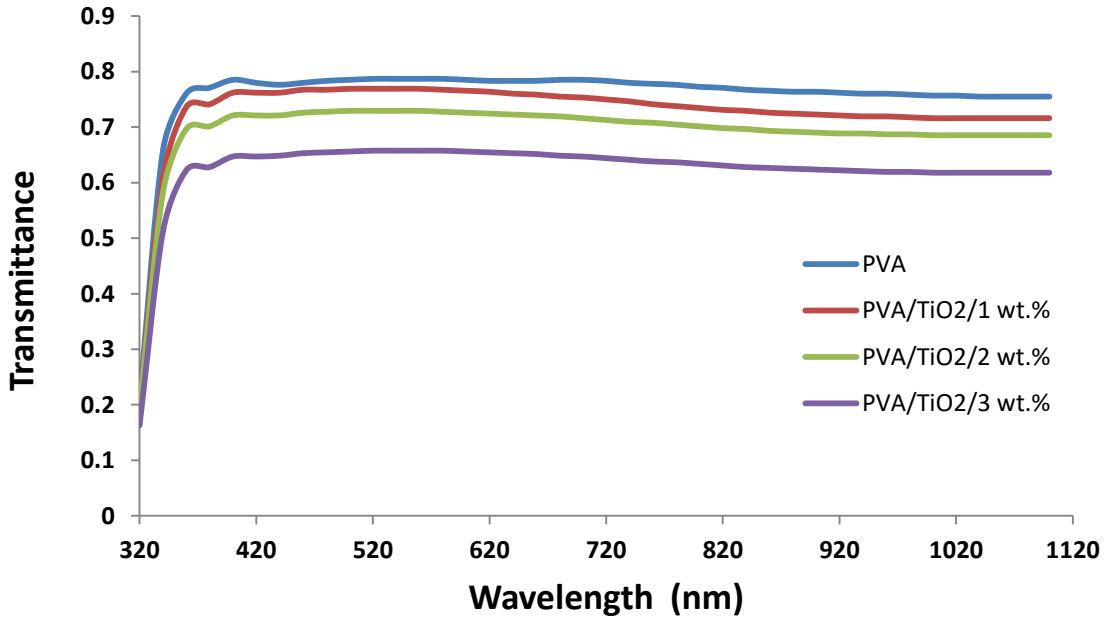

Figure (4.22): The transmittance (T) of (PVA/ TiO_2) nanocomposites

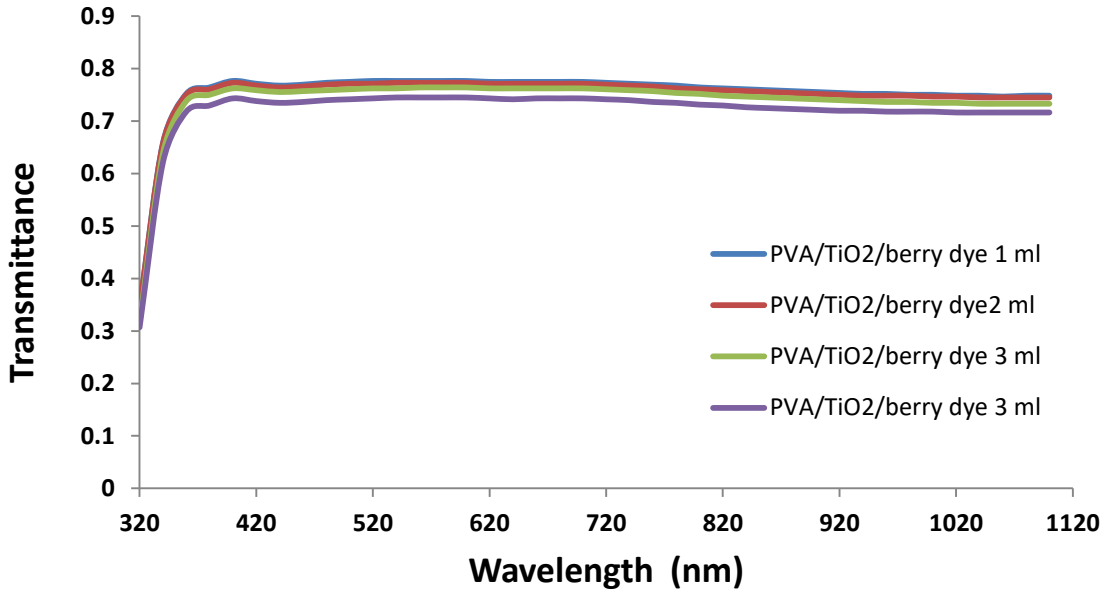

Figure (4.23): The transmittance (T) of (PVA/ TiO_2/berry dye) nanocomposites.

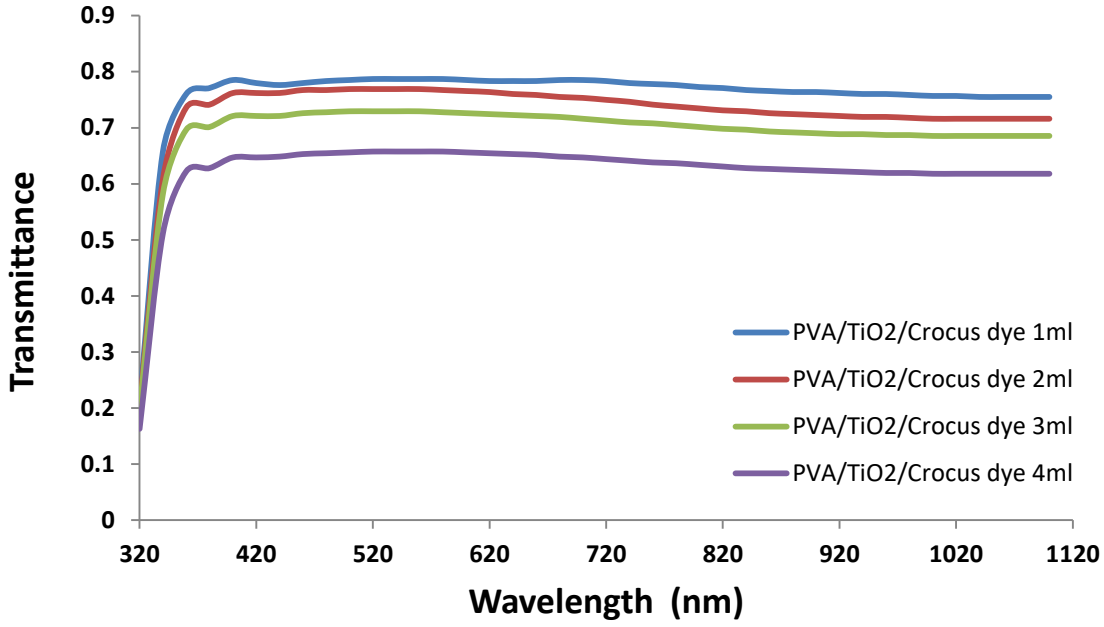

Figure (4.24): The transmittance (T) of (PVA/ TiO_2/crocus dye) nanocomposites

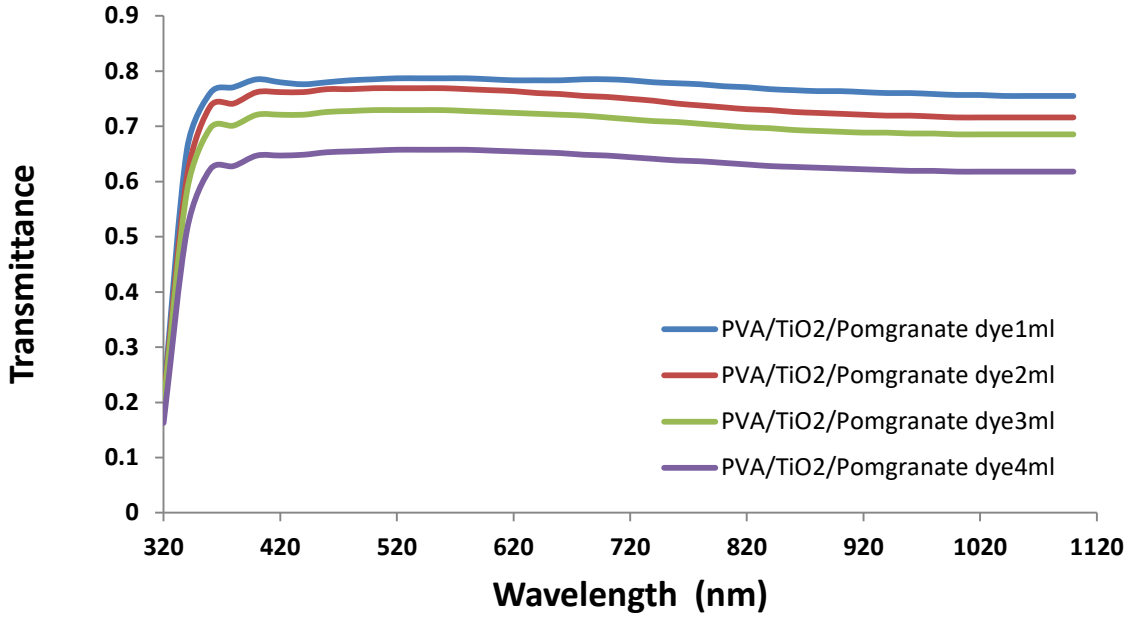

Figure (4.25): The transmittance (T) of (PVA/ TiO_2/pomegranate dye) nanocomposites

4.3.3 Absorptioncoefficient (α)

The absorption coefficient **α** is computed by using Eq. (2.4).Figure (4.26) as show (α) versus energy for (PVA) and (PVA/TiO_2) nanocomposites. The film's basic absorption edge is used to determine the absorption coefficient. With increasing concentrations of TiO_2, the modification of absorption coefficient against energy of incoming radiation (h*ν*) of (PVA)[80].It can be detected that at low energy, the absorption coefficient is the least, however, when the concentration of TiO_2 grows, so does the absorption coefficient, and so does the energy. The absorptioncoefficient has high values ($\alpha>10^4 cm^{-1}$), indicating that the direct transition has a high likelihood, hence the value of (r) in equation (2.5) is equivalent to ½[67-69].

The absorption coefficient is depicted in figures (4.27), (4.28), and (4.29) as a function of energy for (PVA/TiO_2/berry dye), (PVA/TiO_2/crocus dye) and (PVA/TiO_2/pomegranate dye) nanocomposites. The results observed the absorption coefficient increase with increase concentration of natural berry, crocus and pomegranate dyes, the highest absorption coefficient was at 4ml ml[100,108]. This might be attributed to an increase in natural dye concentration and electronic transit between the bonding and nonbonding molecular orbits.

For all testing ranges, the absorption coefficient increases as the concentration of berry dye increases. At high energies, when the absorption coefficient is great ($\alpha > 10^4$ cm^{-1}) [109].

Natural dyes in general work to increase the absorbance in addition to the absorption coefficient, according to the wavelength that is commensurate with the color of that dyes

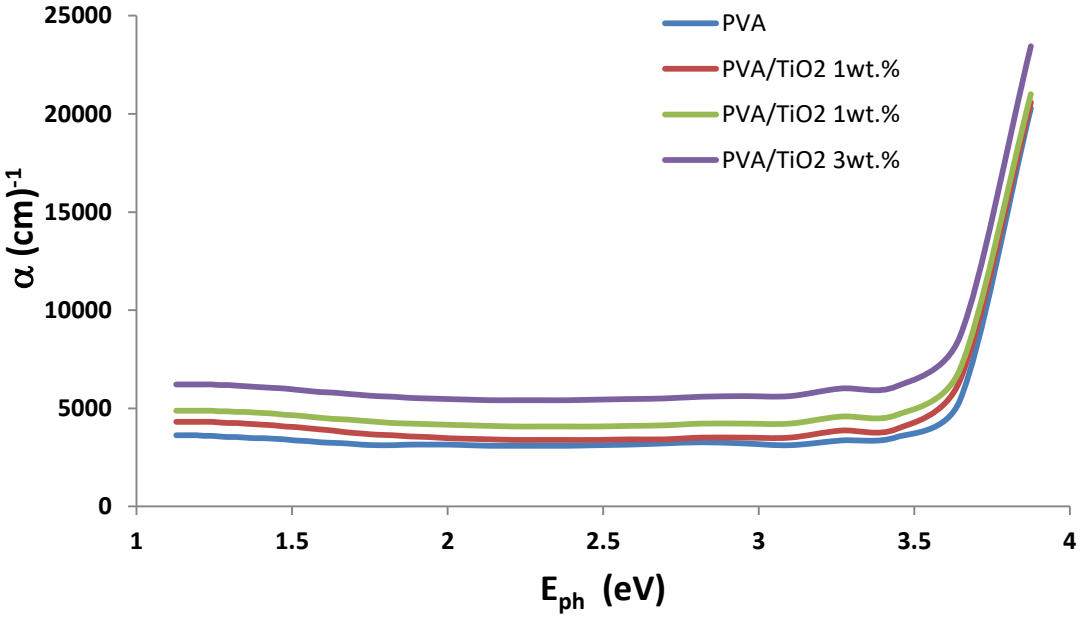

Figure- 4.26 : The absorption coefficient of (PVA/TiO_2) nanocomposites

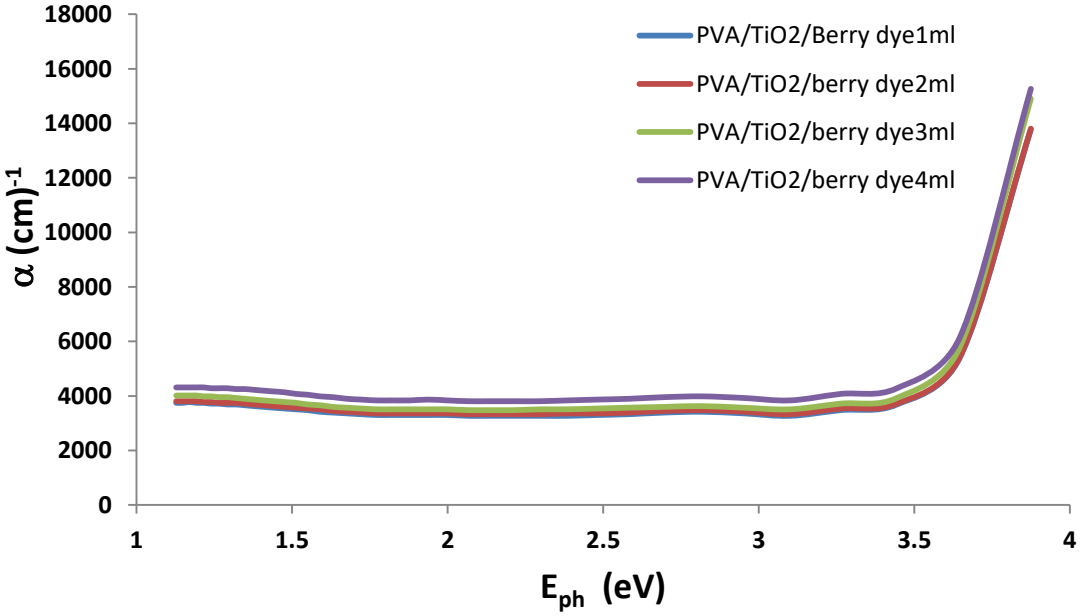

Figure- 4.27 : The absorption coefficient of (PVA/TiO_2/berry dye) nanocomposites.

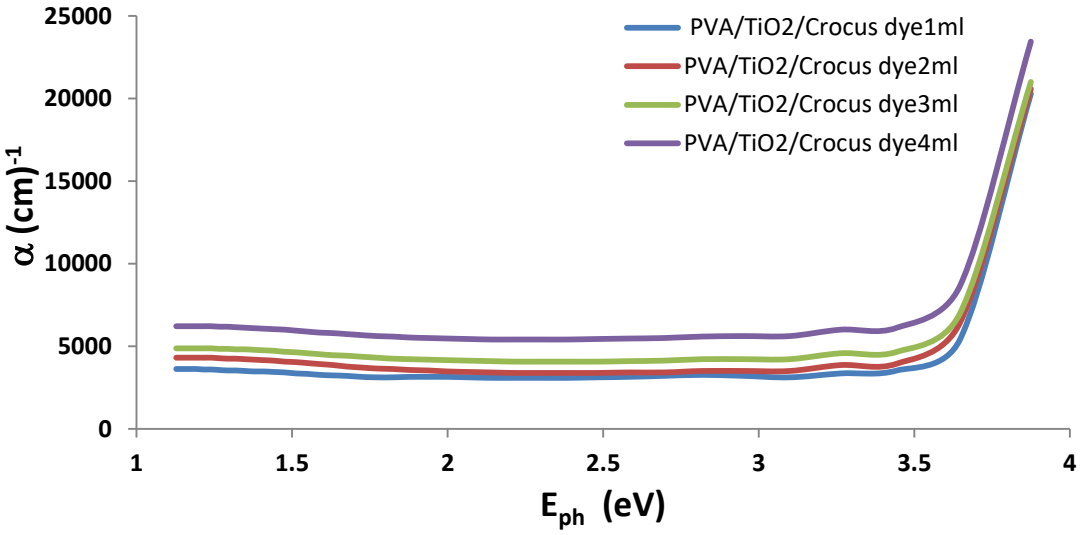

Figure- 4.28: The absorption coefficient of (PVA/TiO_2/crocus dye) nanocomposites

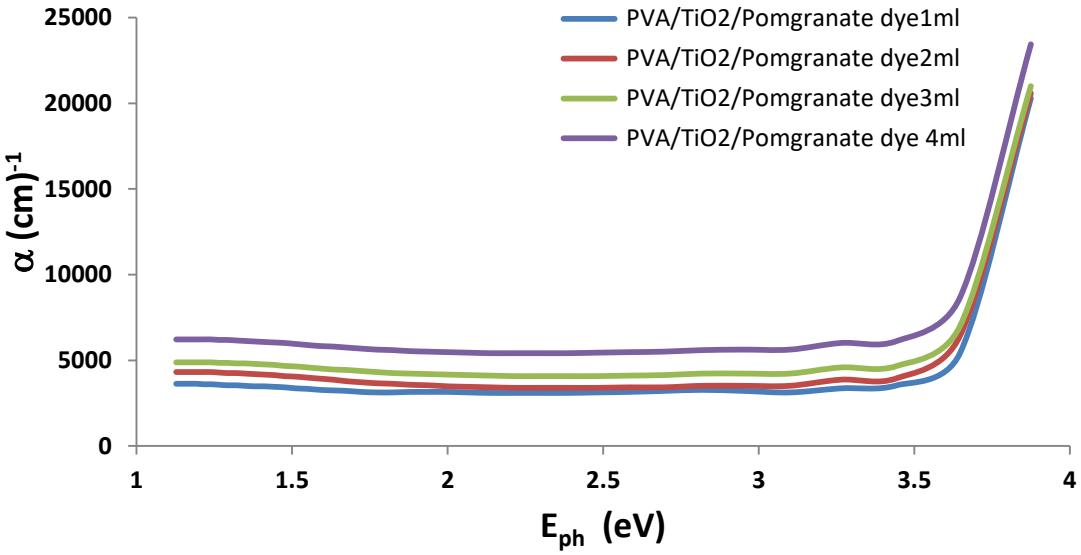

Figure- 4.29: The absorption coefficient of (PVA/TiO_2/pomegranate dye) nanocomposites

4.3.4 The Optical Energy Gap (E_g^{opt})

Optical Energy $\mathbf{E_g^{opt}}$ is calculated by using Eq. (2.5).The experimental standards of $(\alpha h\nu)^2$ plotted against photon energy ($h\nu$) of (PVA/TiO_2) nanocomposites, as expression in figure (4.30). The gap in optical energy the point when the extended linear graph intersects component line connecting the photon energy curve ($h\nu$) , $[\alpha h\nu]^2= 0$ yields the value of E_g^{opt}. indicates that (PVA/TiO_2) nanocomposites films are direct transition type[113] . This figure indicates to decrease optical energy gap (3.43- 3.37)eV. This is due to increase concentration of TiO_2. As a result,

the decline in the energy gap of (PVA/TiO_2) nanocomposites films is caused by a growth in the density of localized situations inside the band gap[114].

Adding more titanium dioxide nanoparticles to the polymer makes electrical channels there, which makes it easier for electrons to move from the (V.B) to the (C.B).This explains why the energy gap narrows as the titanium dioxide nanoparticles grow. As observed, the influence of numerous elements, including grain size, structural features, transporter concentration, the presence of impurities, and deviation from the film's stoichiometry, resulting in a narrowing of the energy gap[115].

Experimental values for $(\alpha h\nu)^2$ plotted against photon energy ($h\nu$) of (PVA/TiO_2/berry, crocus and pomegranate dyes) nanocomposites, as show in figures (4.31), (4.32) and (4.33), indicates that the energy gap decreases 3.44- 3.35 eV, 3.42- 3.31eV & 3.32-3.26 eV with the rise in the focus of the berry, crocus and pomegranate dyes, As a result, it may be concluded that they absorb a wider spectrum of visible light wavelengths[116].The energy gap varied according to the findings. The explanation for this is contaminants in natural plant extracts caused by the extraction procedure look in tables(4.2), (4.3) and (4.4) [114].

The outcome of using a natural dye with the lowest energy band gap is that it helps the eager electron from the V. B to the C. B with very little energy and in a very short period, resulting in high efficiency films that may be used in solar cells[117]. The dye operated between the valence and conduction beams to capture photons with lower energies than the concentrated dye (4ml), in addition to the intensity of the local levels created by atoms [118].

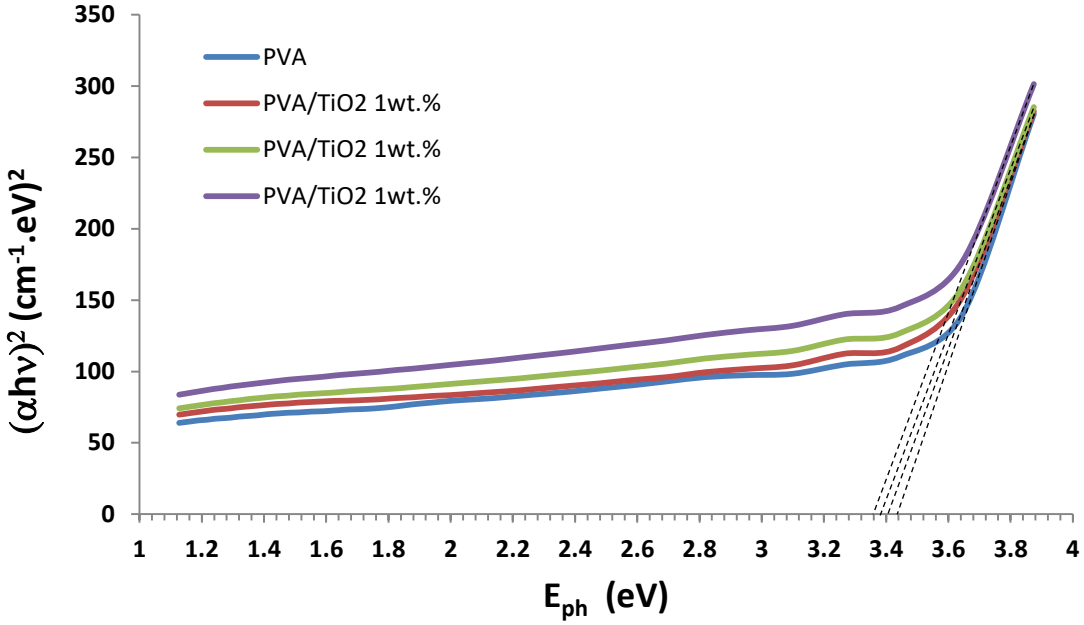

Figure (4.30): The Energy Gap (E_g^{opt}) of (PVA/TiO_2) nanocomposite

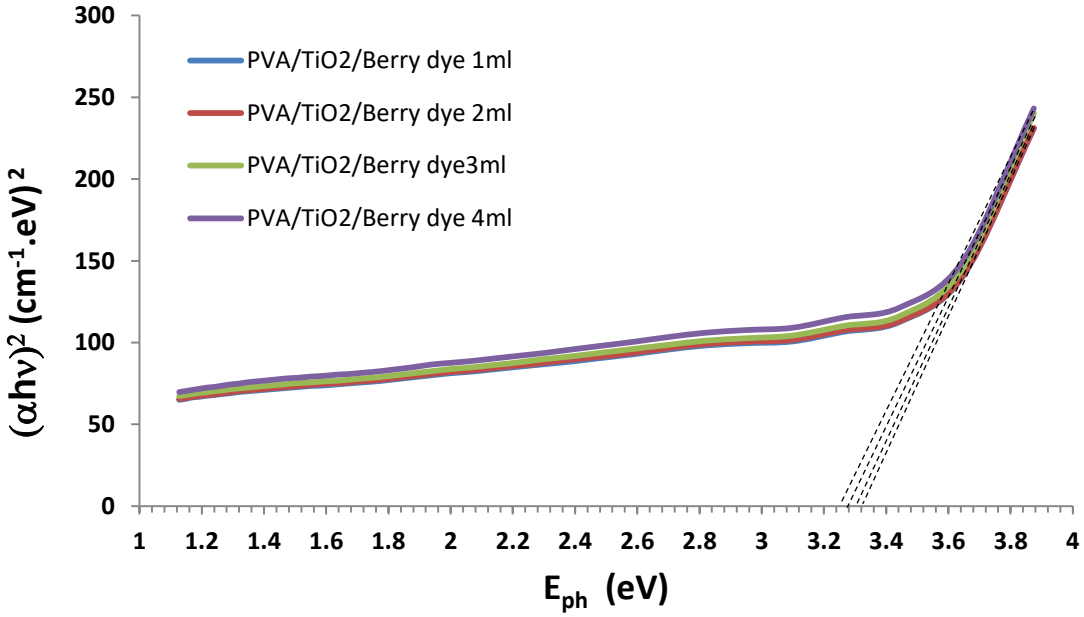

Figure (4.31): The Energy Gap (E_g^{opt}) of (PVA/TiO_2/berry dye) nanocomposites

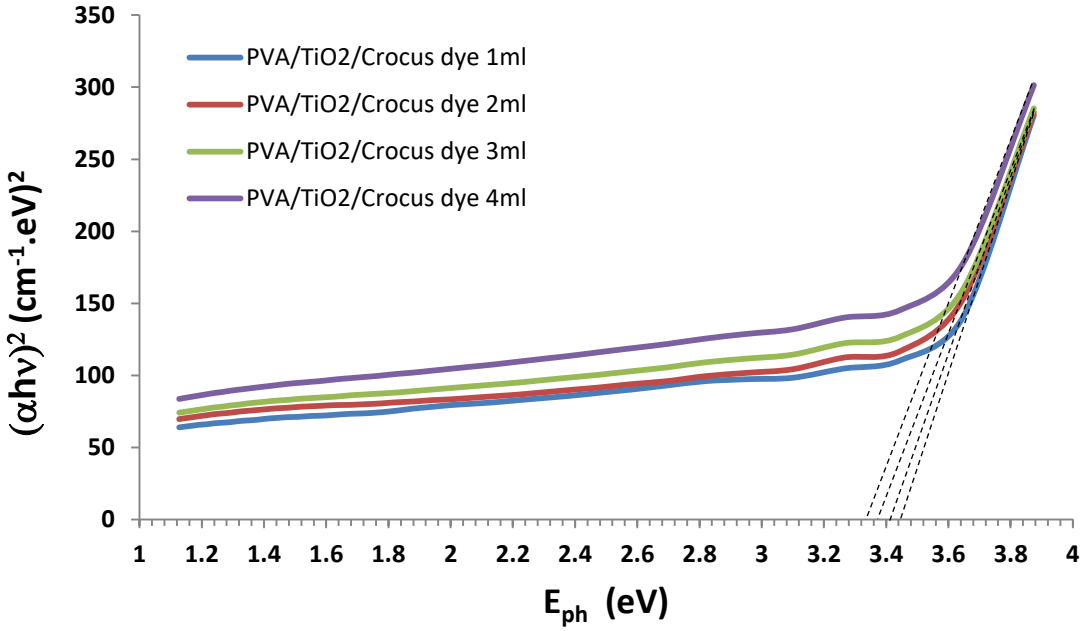

Figure (4.32): The Energy Gap (E_g^{opt}) of (PVA/TiO_2/crocus dye) nanocomposites

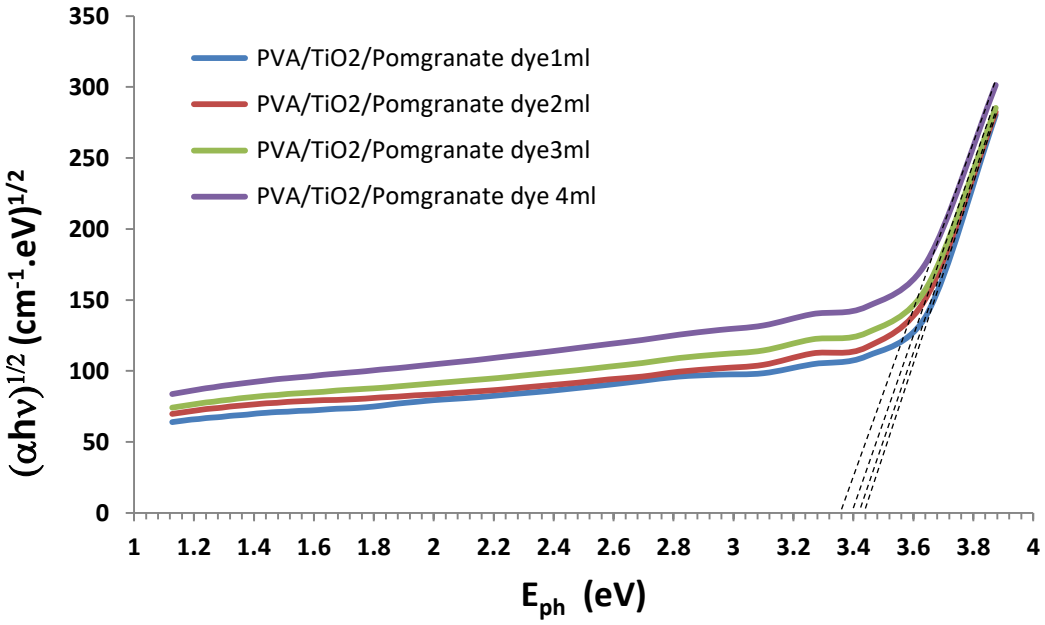

Figure (4.33): The Energy Gap (E_g^{opt}) of (PVA/TiO_2/pomegranate dye) nanocomposites.

Table-4.1 : The optical energy gap values of (PVA/TiO_2) nanocomposites.

Sample	Optical Energy Gap (eV)

PVA	3.437
PVA/TiO_2(1wt.%)	3.412
PVA/TiO_2(2wt.%)	3.382
PVA/TiO_2(3wt.%)	3.371

Table-4.2: The optical energygap valuesof (PVA/TiO_2/berry dye) nanocomposites.

Sample	Optical Energy Gap(eV)
PVA/TiO_2/Berry dye(1 ml)	3.44
PVA/TiO_2/Berry dye(2 ml)	3.42
PVA/TiO_2/Berry dye(3 ml)	3.40
PVA/TiO_2/Berry dye(4 ml)	3.35

Table-4.3: The optical energygap valuesof (PVA/TiO2/crocus dye) nanocomposites.

Sample	Optical Energy Gap(eV)
PVA/TiO_2/ Crocus dye (1 ml)	3.42
PVA/TiO_2/ Crocus dye (2ml)	3.40
PVA/TiO_2/ Crocus dye (3 ml)	3.36
PVA/TiO_2/ Crocus dye (4 ml)	3.31

Table-4.4: Values for optical energy gap for(PVA/TiO_2/ pomegranate dye) nanocomposites

Sample	Optical Energy Gap(eV)
PVA/TiO_2/ Pomegranate dye (1 ml)	3.32
PVA/TiO_2/ Pomegranate dye (2 ml)	3.30
PVA/TiO_2/ Pomegranate dye (3 ml)	3.28
PVA/TiO_2/ Pomegranate dye (4 ml)	3.26

From the (4.4) tables it appears that the energy gap of the nanocomposite to which the pomegranate dye is added is the lowest energy gap, which indicates that the electrons in this case can cross the energy gap more and this means that this dye works to increase the electronic crossing.

4.3.5 Refractive index (*n*)

The index of refraction (n) can be calculated using equation: (2.8). Nanocomposites of (PVA) & (PVA/TiO_2) are displayed Fig. 4.34, where the refractive index-n varies with wavelength. To reach its maximum values in the regain of the ultraviolet spectrum, the refractive index-n growths by wavelength . The refractive index-n increases at longer wavelengths and declines at shorter wavelengths with increasing TiO_2 content throughout the board. There was a correlation between this finding and a rise in nanocomposites density, which was caused by a rise in TiO_2 concentration[119].

Also see high refractive index values in the UV area due to the poor transmittance in this region, low values in the IR and visible ranges due to high transmittance [22,68].

(*n*) versus wavelength of (PVA/TiO_2/berry), (PVA/TiO_2/crocus), and (PVA/TiO_2/pomegranate) nanocomposites are described Figs. 4.35, 4.36, and 4.37. With increasing ultraviolet wavelength, the refractive index(n) rises, but it falls with increasing visible and infrared wavelength. Also A higher concentration of berry, crocus, or pomegranate dye results in a higher refractive index -n. This is because the material's optical density has grown, [120]. The refractive index -n is directly related to electronic

polarisation of ions and the context-specific region inside optical materials[123].

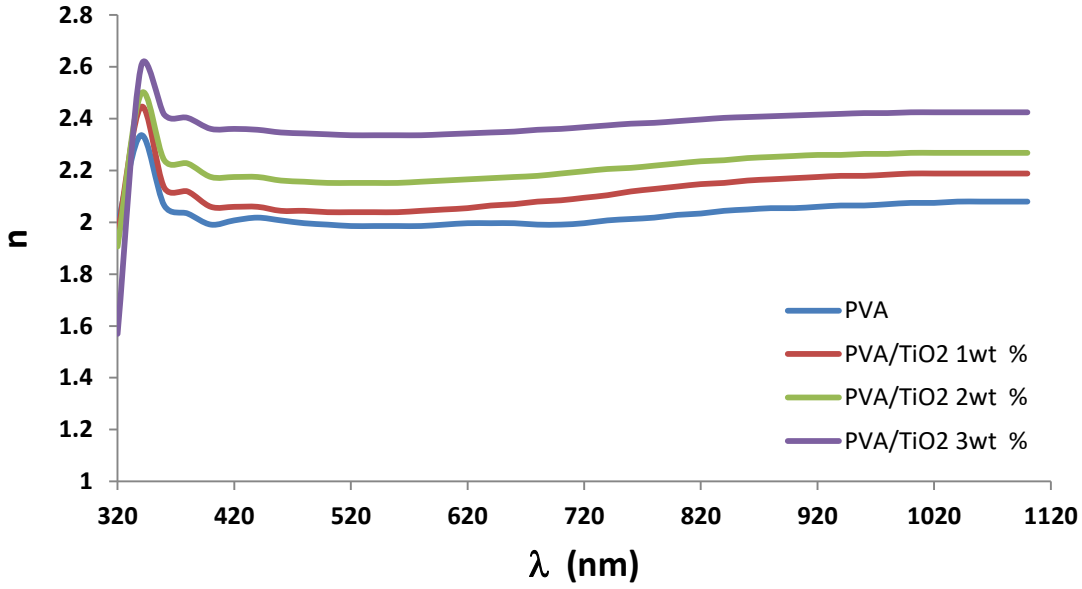

Figure (4.34): The refractive index for (PVA/ TiO_2) nanocomposites

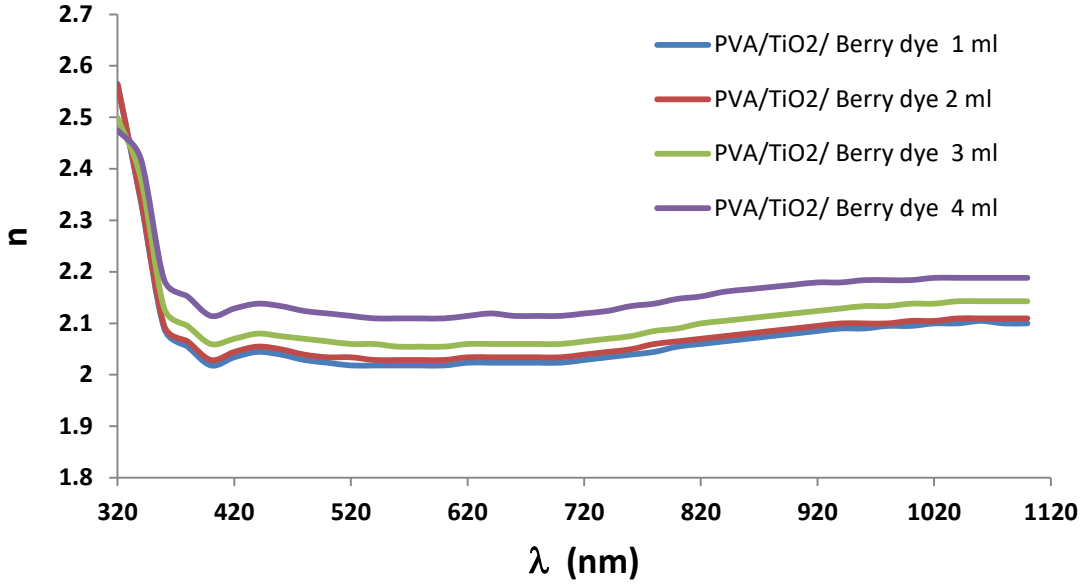

Figure (4.35): The refractive index for (PVA/ TiO_2/Berry dye) nanocomposites

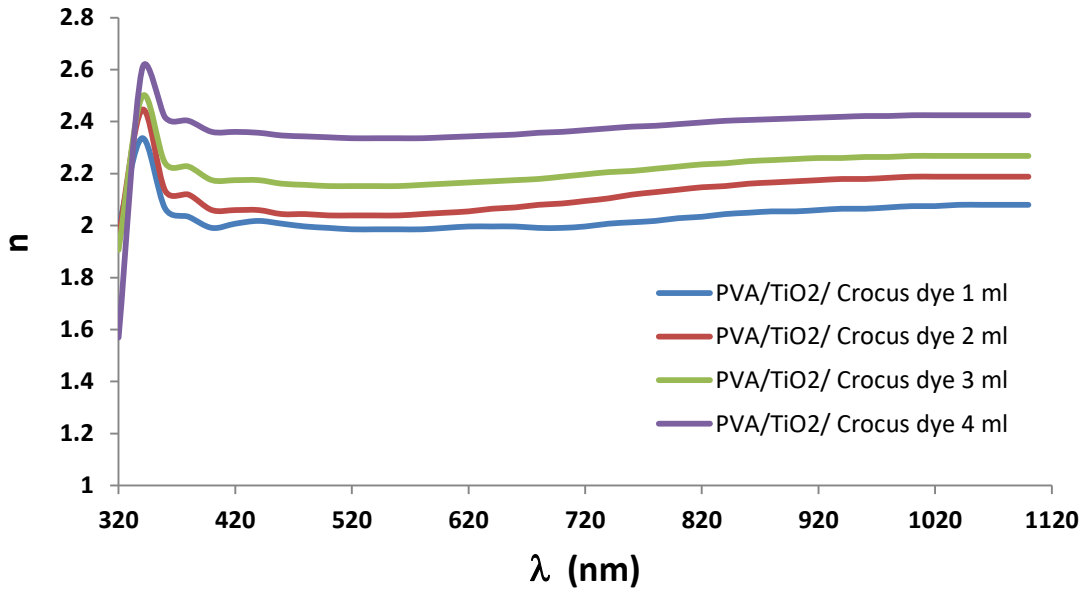

Figure (4.36): The refractive index for (PVA/ TiO_2/crocus dye) nanocomposites

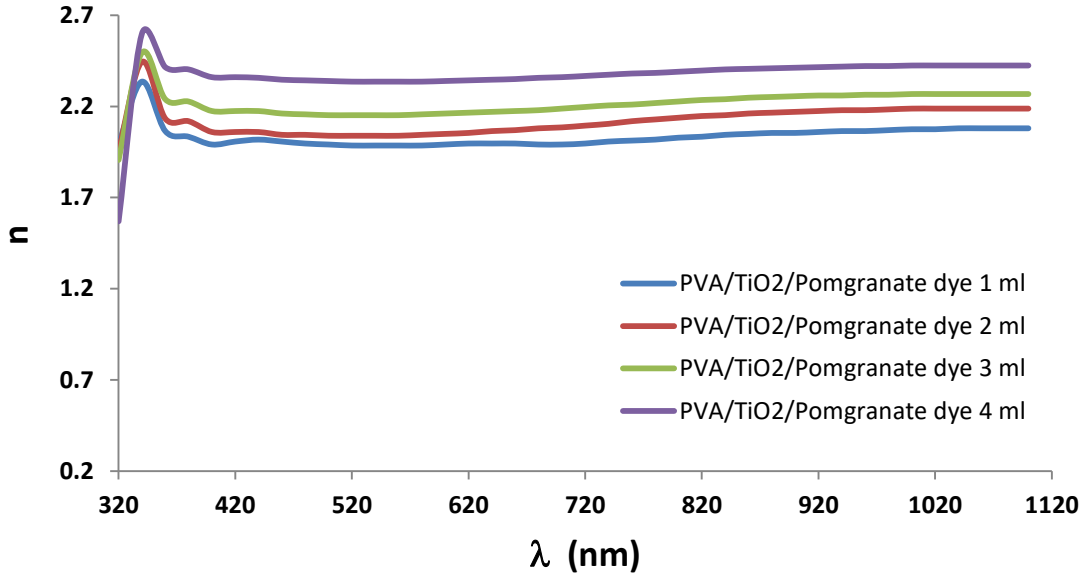

Figure(4.37):The refractive index for (PVA/TiO_2/pomegranate dye) nanocomposites

4.3.6 Extinction Coefficient -k_o

For the purpose of determining the (k_o), the following equation is used (2.10). The extinction coefficient vs. wavelength for (PVA) and (PVA/TiO2) nanocomposites is shown in Figure (4.38), and due to its relationship with the equation in the previous paragraph, its behavior is analogous to that of the absorption coefficient curve. It should be observed that (k_o) has a decreasing value at low concentrations, but grows

larger with increasing (TiO_2) nanoparticle concentration. Reason being, higher concentrations of (TiO_2) nanoparticles result in a higher absorption coefficient[66]. This shows that the atoms of (TiO_2) nanoparticles will alter the host polymer's structure[66-68].

Figure (4.39), (4.40) and (4.41) show the wavelength dependence of the extinction coefficient of (PVA/TiO_2/berry, crocus and pomegranate dyes) nanocomposites, respectively. The extinction coefficient increases in the region of short wavelengths UV and then decreases at the regions of long wavelengths VIS and IR. In addition, k_o increases with the growth in focus of natural dyes berry, crocus and pomegranate, owing to the rise in (α) as shown in equation (2.10). This is due to the same reasons that caused rise in (k_o) as crossover of the molecular orbital's electric wave function between its bonding and nonbonding states [7].

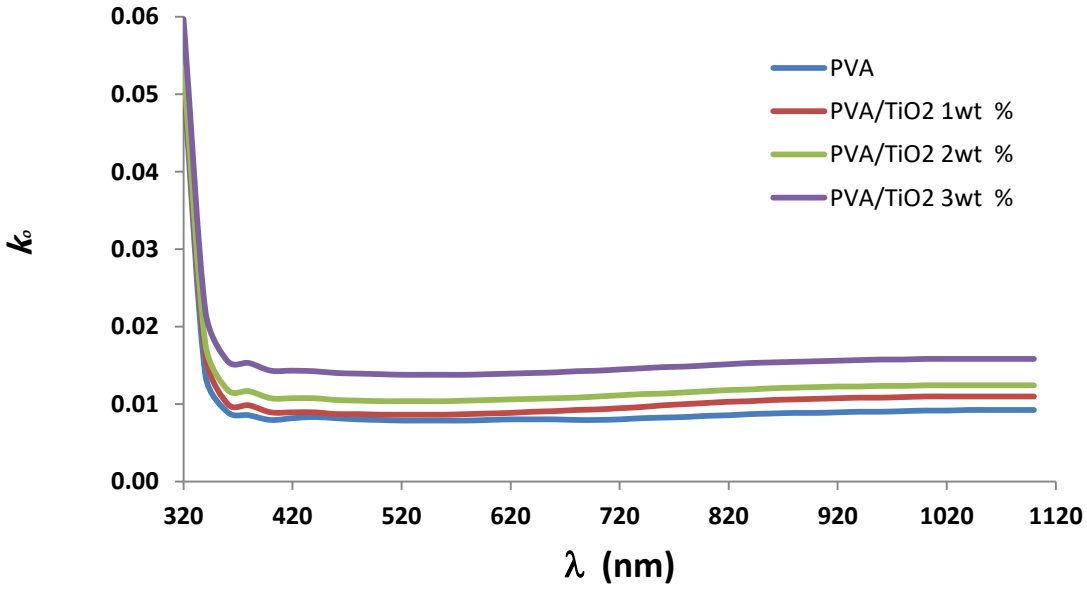

Figure(4.38):The Extinction coefficient (k_o)of (PVA/TiO_2) nanocomposites

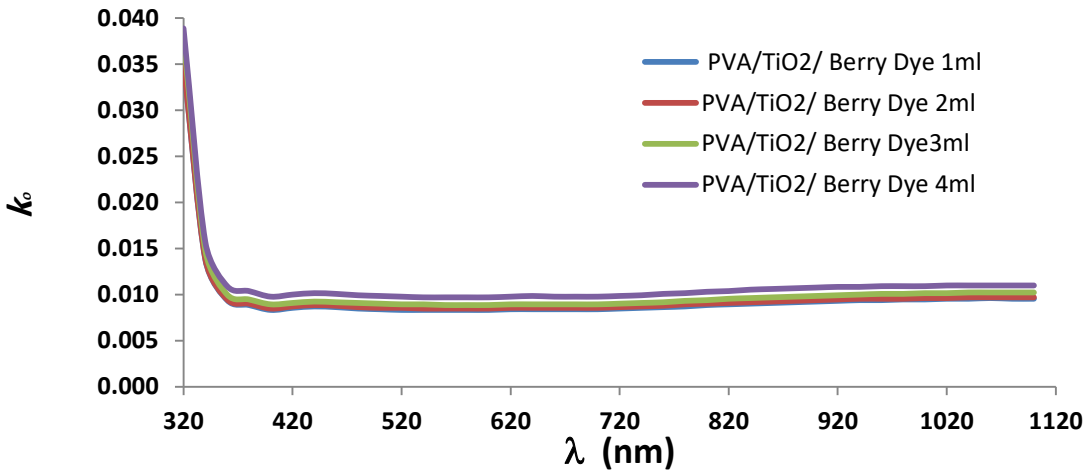

Figure(4.39):The Extinction coefficient (k_o)of (PVA/TiO_2/berry dye) nanocomposites

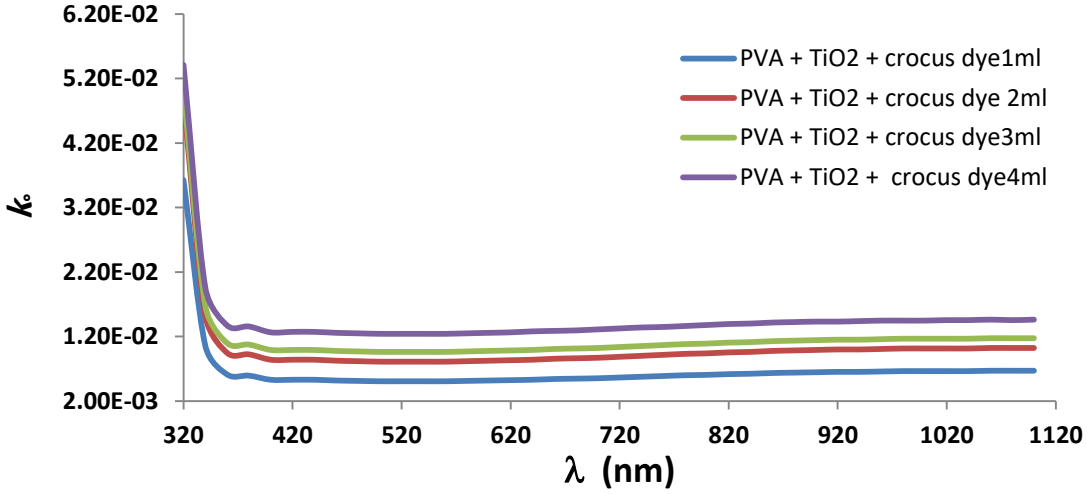

Figure(4.40):The Extinction coefficient (k_o)of (PVA/TiO_2/crocus dye) nanocomposites

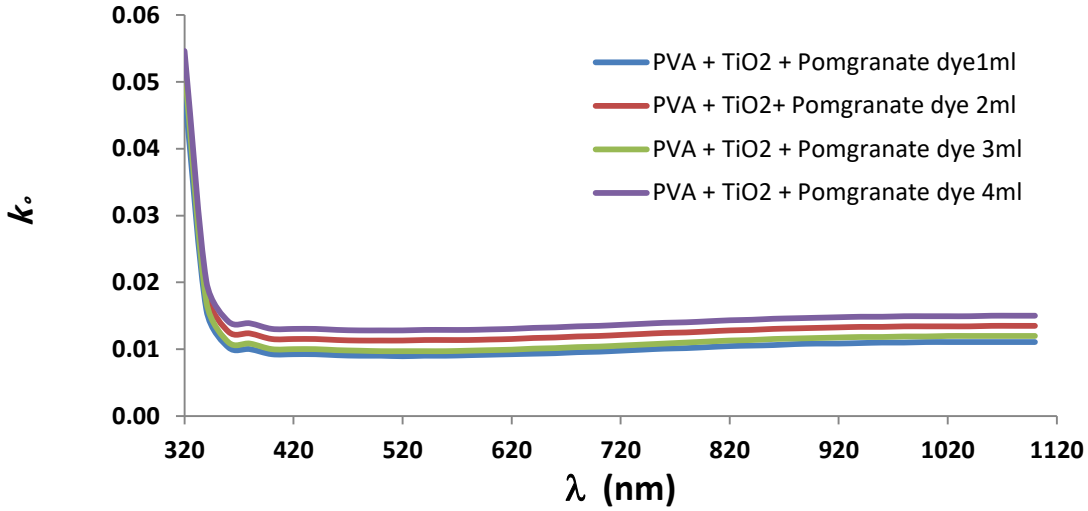

Figure(4.41):The Extinction coefficient ($k_\circ$)of (PVA/TiO_2/pomegranate dye) nanocomposites

4.3.7 Dielectric constant(real Ɛr and imaginary Ɛi)

Using equation (2.15), we can get values of the dielectric constant for both the real and imaginary portions of the equation (2.16). $Ɛ_r$ and $Ɛ_i$ (r & I as a function of wavelength are depicted) in Figures 4.42 and 4.43, respectively, for polyvinyl alcohol (PVA) and polyvinyl alcohol/titanium dioxide (PVA/TiO_2) nanocomposites. To express the extent to which an electric field can be used to increase the dielectric's absorption capacity. as a result of dipole motion, the real portion r is associated with the phrase that, and the imaginary part I shows how much the speed of light will be slowed down in the material.

The $Ɛ_r$ (the real component) signifies the absorption of radiation related with free energy (the imaginary part). Since $k_\circ^2$ is less than n^2 in equation (2.15), r behaves same to (n), while i mostly depends on the ($k_\circ$) value[122]. Values of r and i are shown to be on the rise as the concentration of (TiO_2)[123].

Figures 4.44, 4.46, and 4.48 show The $Ɛ_r$ as a function of wavelength for PVA/TiO_2/berry, crocus, and pomegranate dye nanocomposites, respectively. Figures (4.45), (4.47) and (4.49) show the $Ɛ_i$ as a function of wavelength for the same nanocomposites. Results showed that as berry, crocus, and pomegranate dyes focuses were increased, so were respective dielectric constants, both in terms of their real and imaginary parts [126].

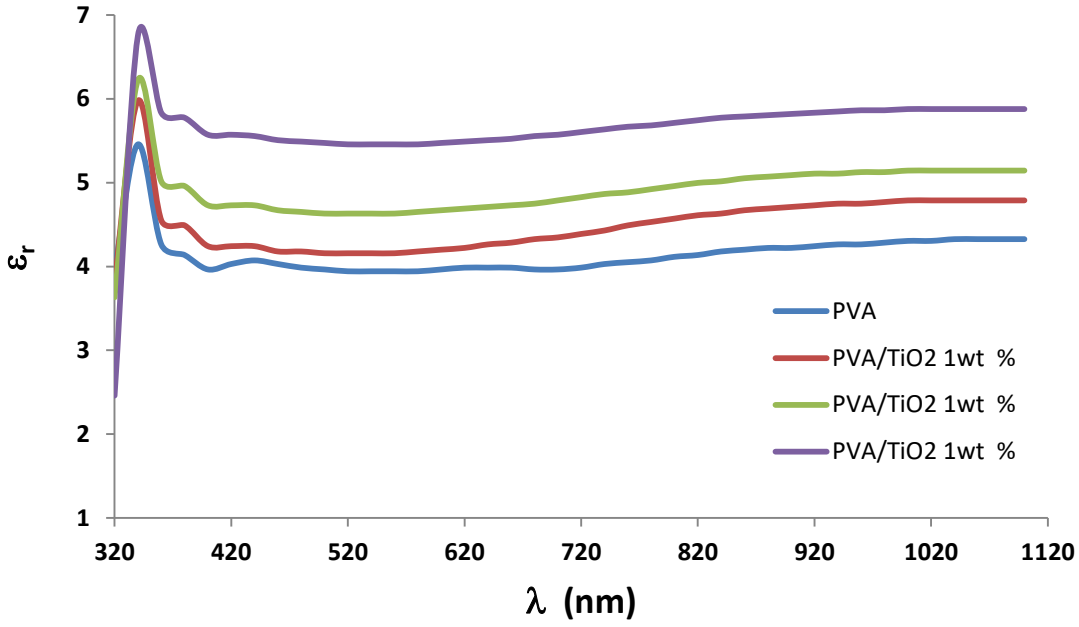

Figure(4.42): The real Dielectric Constants (ε_r)of (PVA/TiO_2) nanocomposites

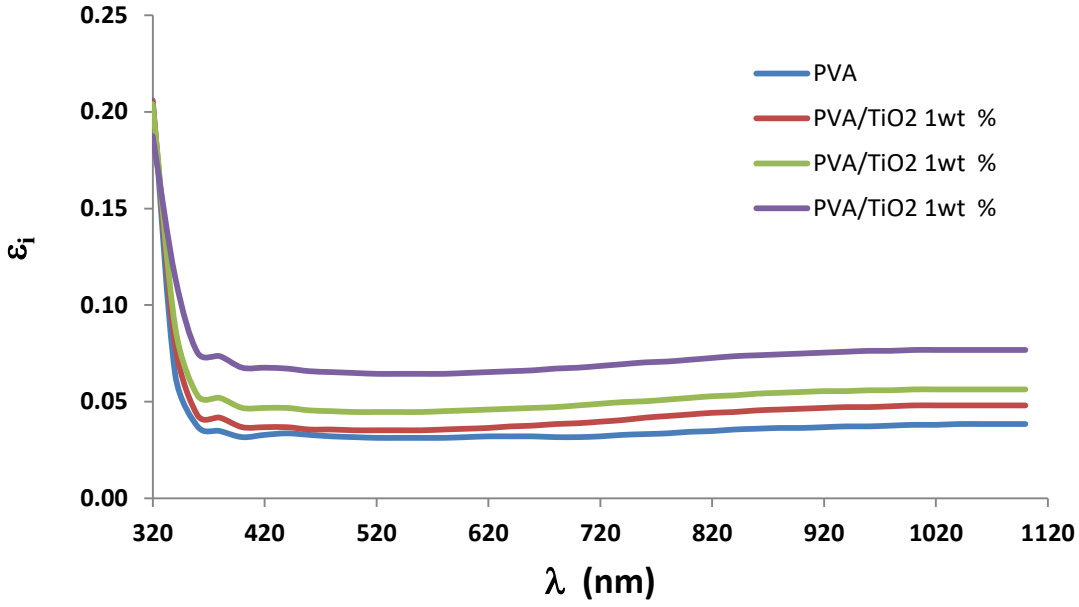

Figure(4.43): The imaginary Dielectric Constants (ε_i)of (PVA/TiO_2) nanocomposites

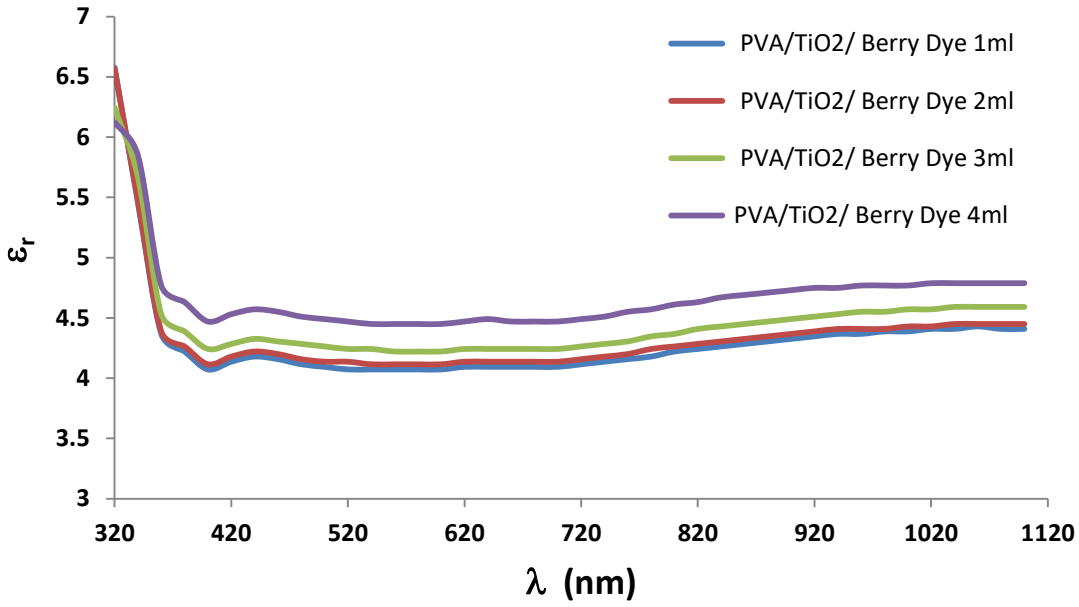

Figure(4.44): The real Dielectric Constants (ε_r)of (PVA/TiO_2/berry dye) nanocomposites

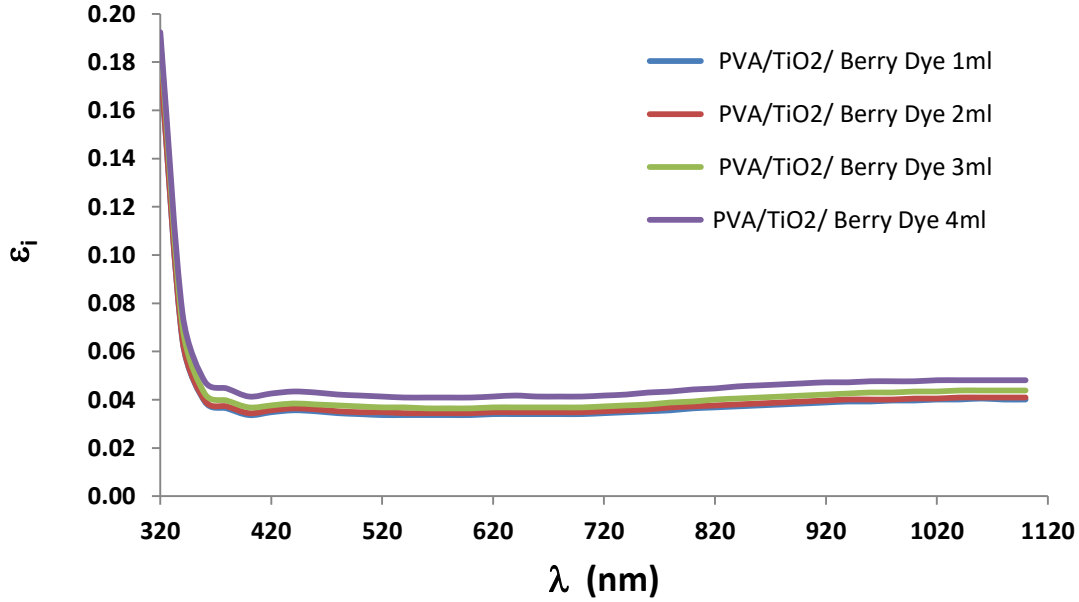

Figure(4.45): The imaginary Dielectric Constants (ε_i)of (PVA/TiO_2/berry dye) nanocomposites

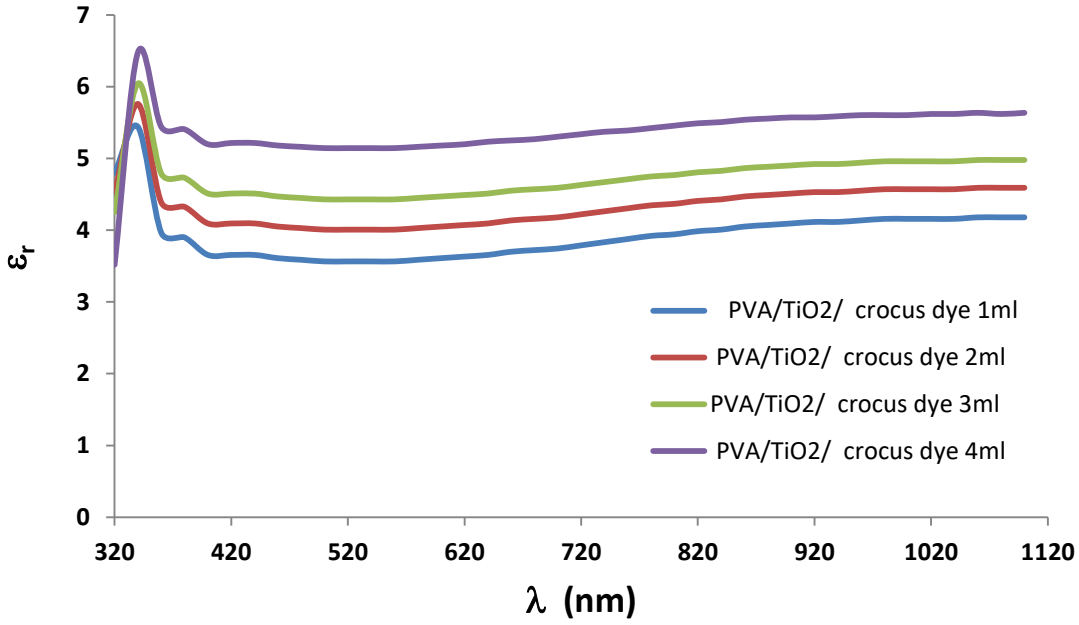

Figure(4.46): The real Dielectric Constants (ε_r)of (PVA/TiO_2/crocus dye) nanocomposites

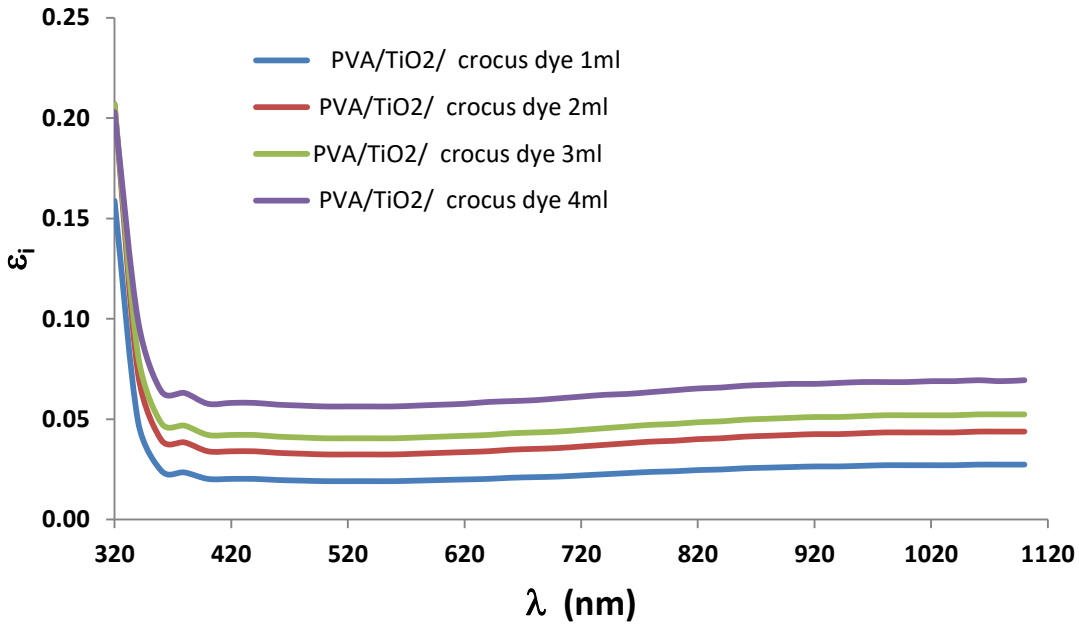

Figure(4.47): The imaginary Dielectric Constants (ε_i)of (PVA/TiO_2/crocus dye) nanocomposites

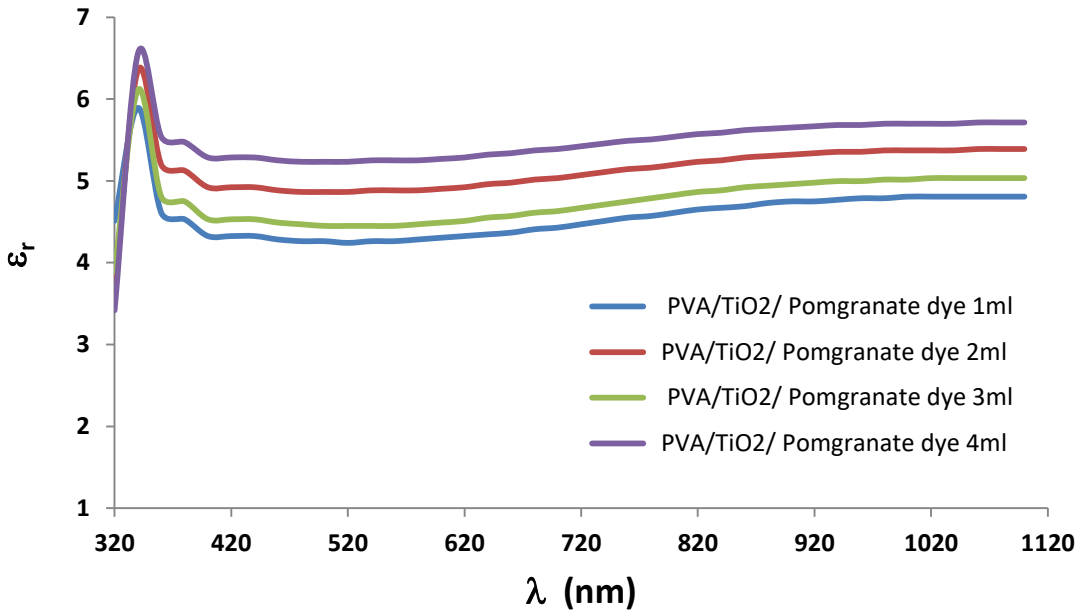

Figure(4.48): The real Dielectric Constants (ε_r)of (PVA/TiO_2/pomegranate dye) nanocomposites

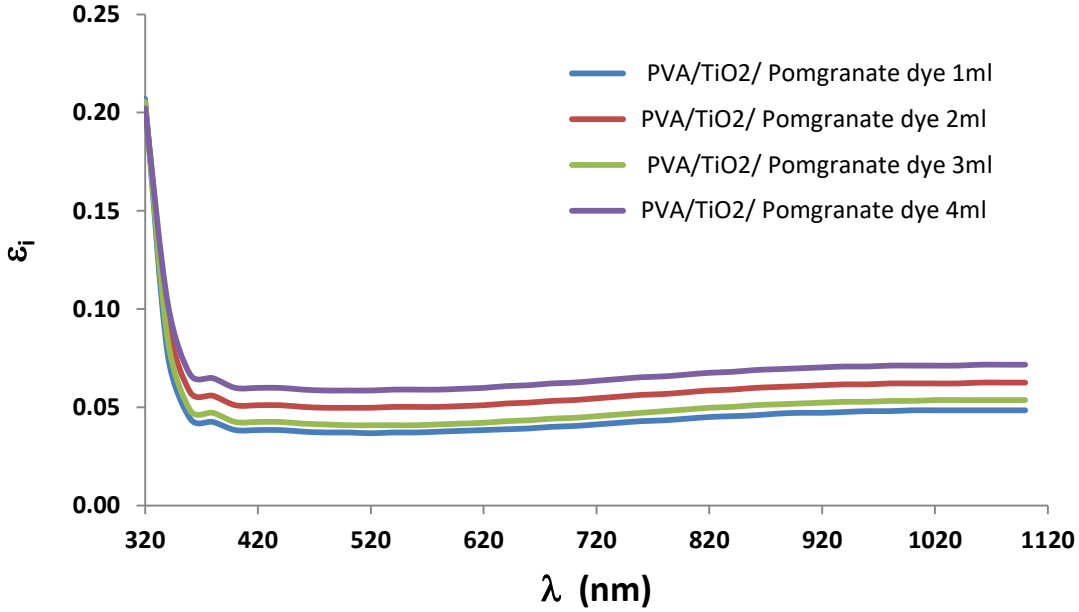

Figure(4.49): The imaginary Dielectric Constants (ε_i)of (PVA/TiO_2/pomegranate dye) nanocomposites

4. 3 .8Optical Conductivity (σ_{op})

To determine optical conductivity, used Eq.(2.17). Wavelength dependence of optical conductivity is depicted in Figure (4.50). It was discovered that when the amount of TiO_2 in the (PVA) rises, the optical conductivity increases (3 wt.%). Creating new bands within The band gap facilitates transport of electrons between the (V.B) and (C.B) at these discrete energy levels, increasing the material's conductivity. Equation (2.17), σ_{op} is dependent on the absorption coefficient, demonstrating that this decrease in band gap results in improved conductivity [71].

Figures (4.51), (4.52) and (4.53) show Optical Conductivity as a function of wavelength for (PVA/TiO_2/berry, crocus and pomegranate dyes) nanocomposites, respectively. The results showed the optical conductivity(σ_{op}) rises in proportion to the elevated concentration of berry, crocus and pomegranate dyes. This is because of the growth in absorption coefficient[123].

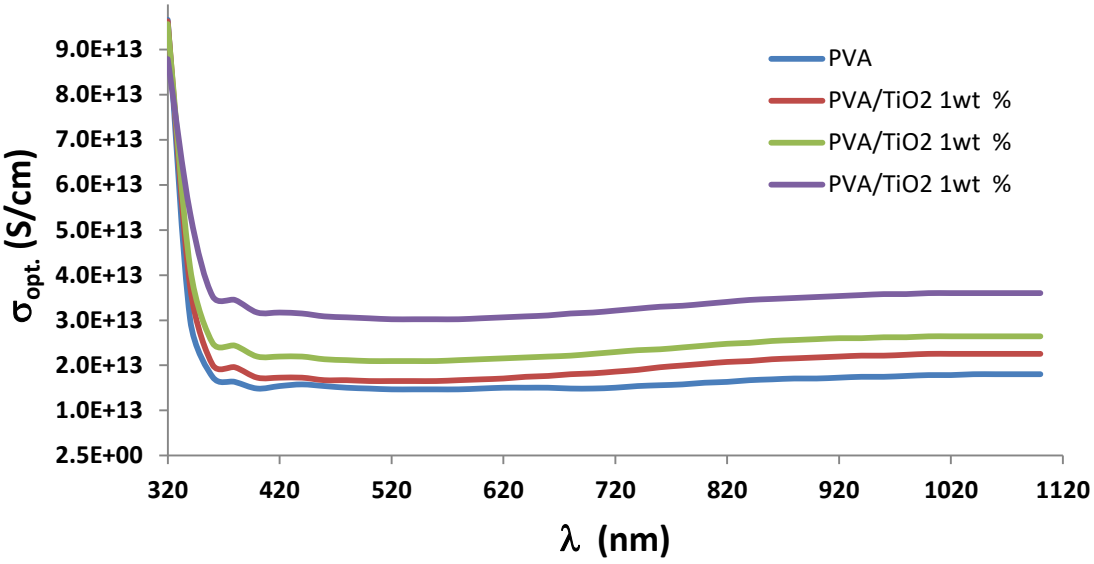

Figure(4.50): optical conductivity(σ_{op}) of (PVA/TiO_2) nanocomposites

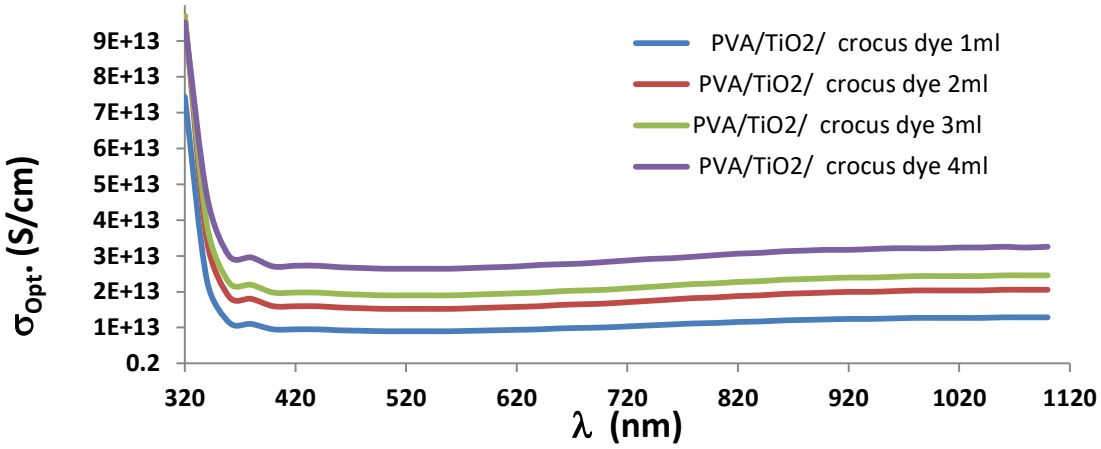

Figure(4.51): optical conductivity(σ_{op}) of (PVA/TiO_2/berry dye) nanocomposites

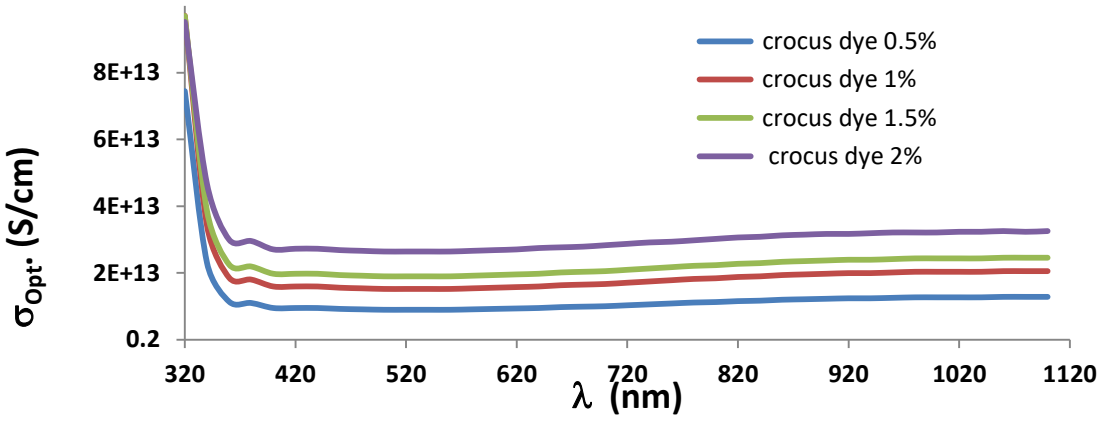

Figure(4.52): optical conductivity(σ_{op}) of (PVA/TiO_2/crocus dye) nanocomposites

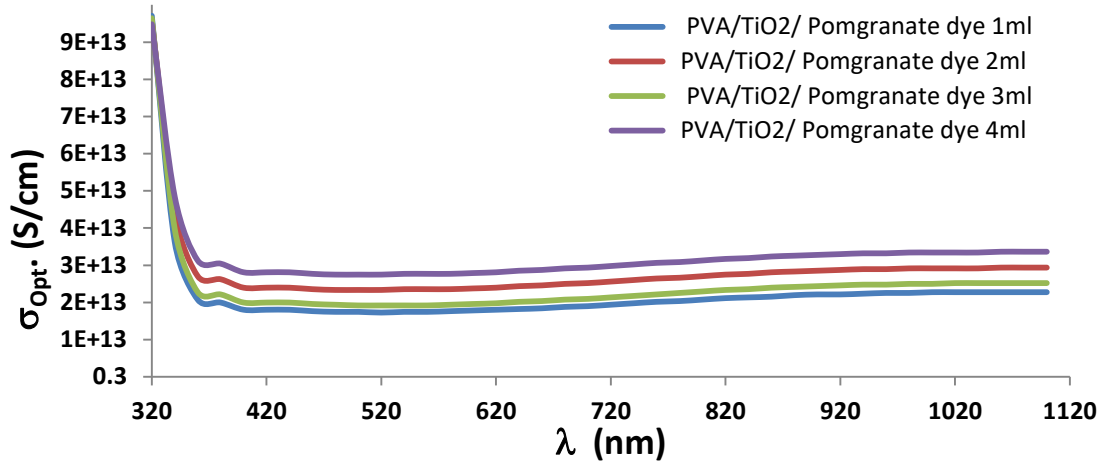

Figure(4.53): optical conductivity(σ_{op}) of (PVA/TiO_2/pomegranate dye) nanocomposites

4.4Characterization of the Direct Current Electrical Properties of the (PVA/TiO_2) Nanocomposite

Equation (2.19) is used to compute the electrical conductivity ($\sigma_{d.c}$) of the produced films. The outcomes of these properties are listed below in detail.

4.4.1 The Direct Current Electrical Conductivity of (PVA/TiO_2) and(TiO_2/Natural Dye) Nanocomposites.

The relationship between the concentration of (TiO_2) nanoparticles and their electrical conductivity, measured in $ohm.cm^{-1}$ and D.C, is depicted in fig.4.54. Given the data presented in the graph, concentration of nanoparticles of titanium dioxide has a direct correlation with the increase in($\sigma_{d.c}$). The electrical conductivity value for (PVA/TiO_2) nanocomposites is (3.5E-6) $\Omega.cm^{-1}$ at the focus (1wt.%) (TiO_2) nanoparticle, the upsurge of the concentration of (TiO_2) NPs to (3wt.%) , clues to rise of conductivity to (4.5E-6) $(\Omega.cm)^{-1}$[124].

One way to explain the increase in electrical conductivity is in continuation: at low concentrations, (TiO_2) NPs are grouped or clustered inside the polymers, as mentioned in clause (4.1). When the focus nanoparticles in (PVA/ TiO_2) nanocomposites approaches 3%. Inside the polymers, the nanoparticles connect to each other in a network. The nodes in this network will be linked together, and the paths that charge transporters take through the network will intersection. The paths taken by charge carriers will have reduced electrical resistance [125].

Figures (4.54), (4.55) and (4.56) show the electrical conductivity ($\sigma_{d.c}$) $(ohm.cm)^{-1}$ concentration dependently for berry, crocus and pomegranate dyes. It can be seen graphically that as natural dye focus rises, so does electrical conductivity. Electrical conductivity at a concentration of 4 ml was reached (4.81×10^{-6}, 4.9×10^{-6} and 6.4×10^{-6}) $(ohm.cm)^{-1}$ for berry, crocus and pomegranate dyes, respectively[126]. This might be attributed to electronic transit between the bonding.

An increase in the electrical conductivity ($\sigma_{d.c}$) is a result of an increase in the concentration of the dye. The previous paragraph, leads to a smaller energy gap since more localised states exist within it [57]. The conductivity of these composites appears to be highly stable at room temperature, but the increase appears to be high and uneven after 50C. The best conductivity value for pomegranate dye was 6.4×10^{-6} $(ohm.cm)^{-1}$.

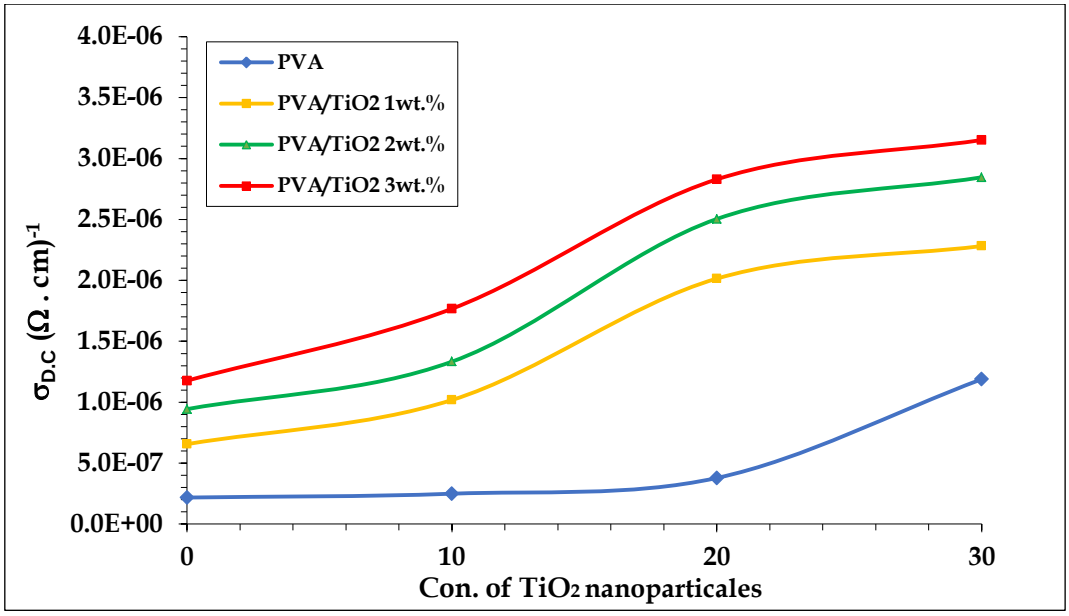

Figure- 4.54: Changes in the direct current electrical conductivity of (PVA / TiO_2) films.

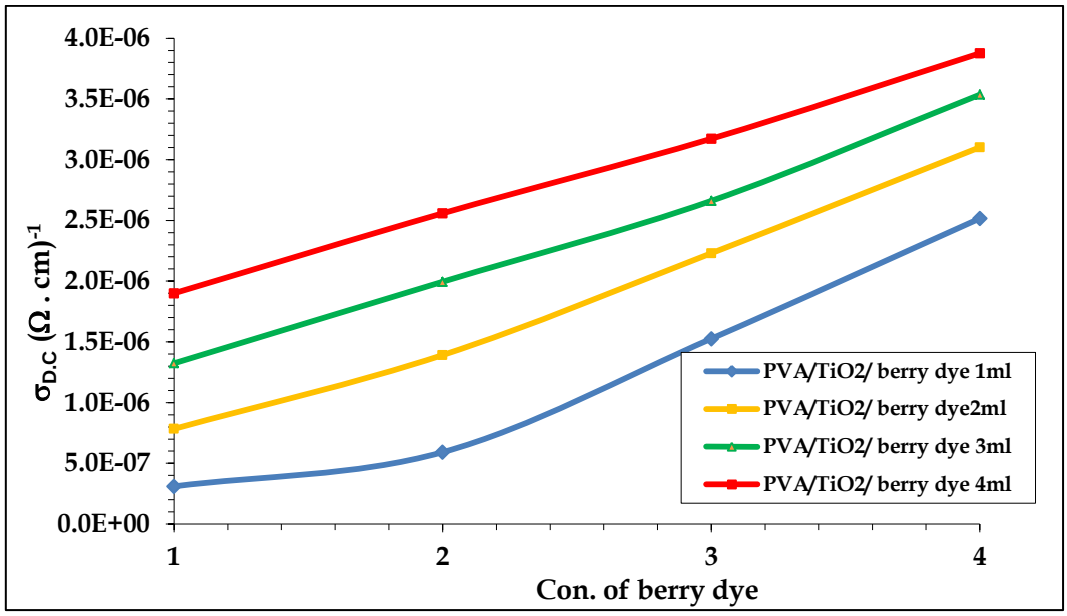

Figure -4.55: Changes in the direct current electrical conductivity of (PVA/TiO_2/berry dye) nanocomposites as a function of berry dye concentration.

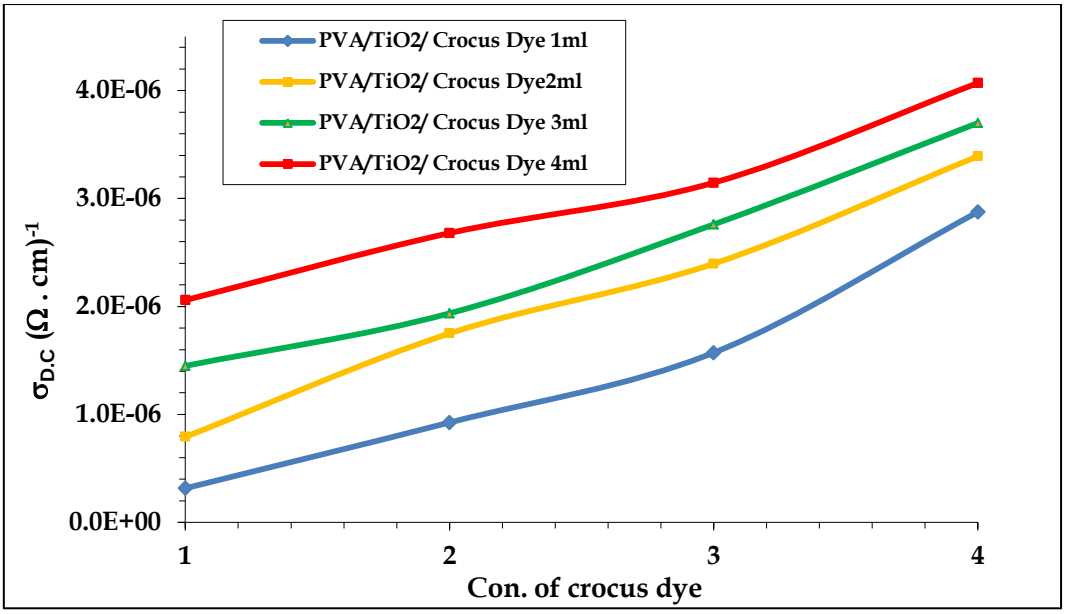

Figure-4.56: Changes in the direct current electrical conductivity of (PVA - TiO_2- Crocus Dye) nanocomposites as function of natural Crocus Dye concentration.

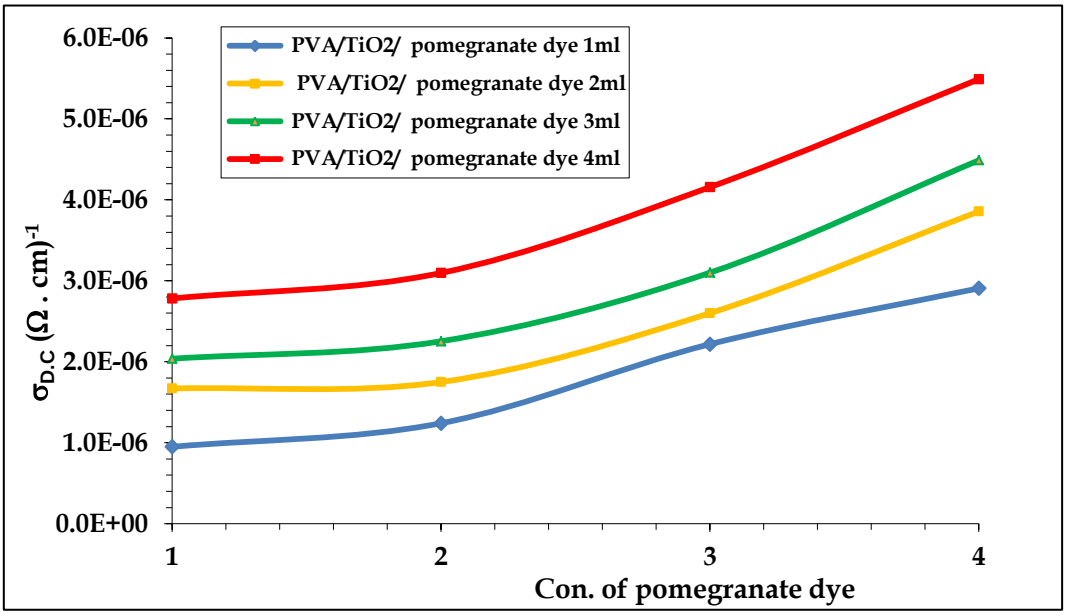

Figure -4.57: Changes in the electrical conductivity of direct current for (PVA/TiO_2) nanocomposites as a function of the concentration of pomegranate dye.

4.4.2 Temperature Effect on the Direct Current Electrical Conductivity of Polyvinyl Alcohol/Titanium Dioxide and Polyvinyl Alcohol/Natural Dye Nanocomposites.

(PVA/TiO_2) nanocomposites exhibit a temperature-dependent change in their electrical conductivity, as depicted in Figure (4.58), At low concentrations, raising temperature rises the electrical conductivity of (PVA/TiO_2) nanocomposites. For these materials, an increase in temperature results in fall in resistance, indicating that their thermal coefficient of resistance is negative. Because of the hopping mechanism, polymer chains and titanium dioxide nanoparticles operate as reservoirs for charge carriers on the move [127]. When the temperature of the polymer is raised, portions for polymer begin to migrate, freeing the imprisoned charge [98]. Molecular mobility is intricately linked to the release of trapped charges [128].

Two primary causes, charge carriers and charge mobility, may account for the temperature-dependent rise in conductivity. Carriers' mobility is determined by the structure and the temperature[86].

The temperature dependence of electrical conductivity in nanocomposites (PVA/TiO_2 berry, crocus, and pomegranate dyes) is showed in Figures 4.59, 4.60, and 4.61. Electrical conductivity of (PVA/TiO_2 berry, crocus and pomegranate dyes) nanocomposites rises with increasing temperature[129]. It also rises in correlation with the content of natural dyes. When subjected to temperatures between 30-70°C, nanocomposites coloured with PVA/TiO_2 berry, crocus, and pomegranate dyes showed optimum performance in an exponential or linear temperature response. Electrical conductivity was found to increase with temperature in PVA/TiO_2 berry, crocus, and pomegranate dye nanocomposites, according to the study's authors, suggesting that heating rates may affect the strength of the electric field or the electrical conductivity[130].

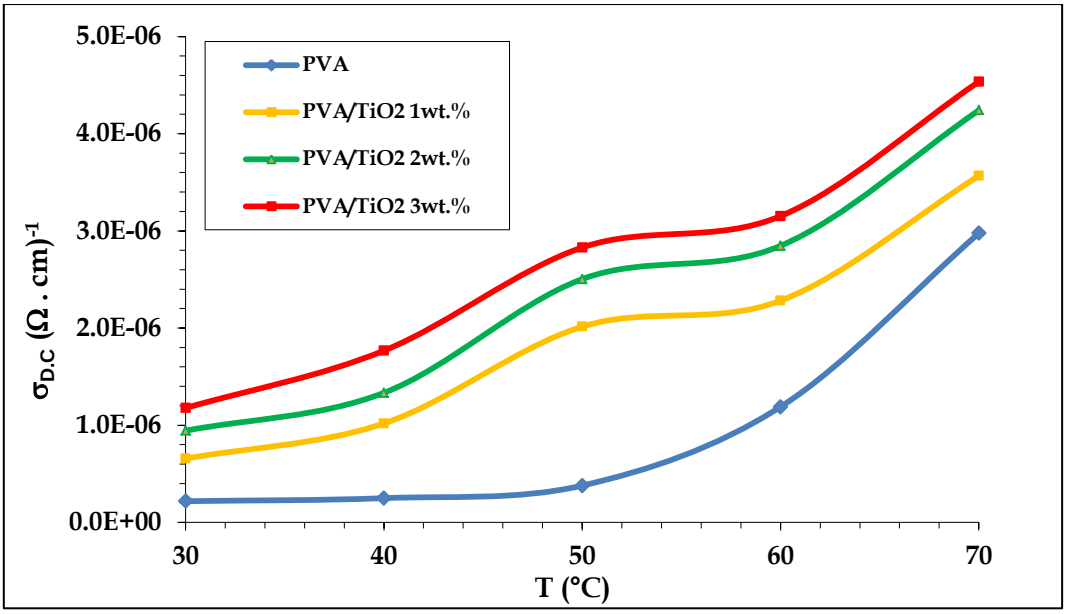

Figure -4.58 : Changes in the DC electrical conductivity of (PVA/TiO_2) nanocomposites are temperature dependent.

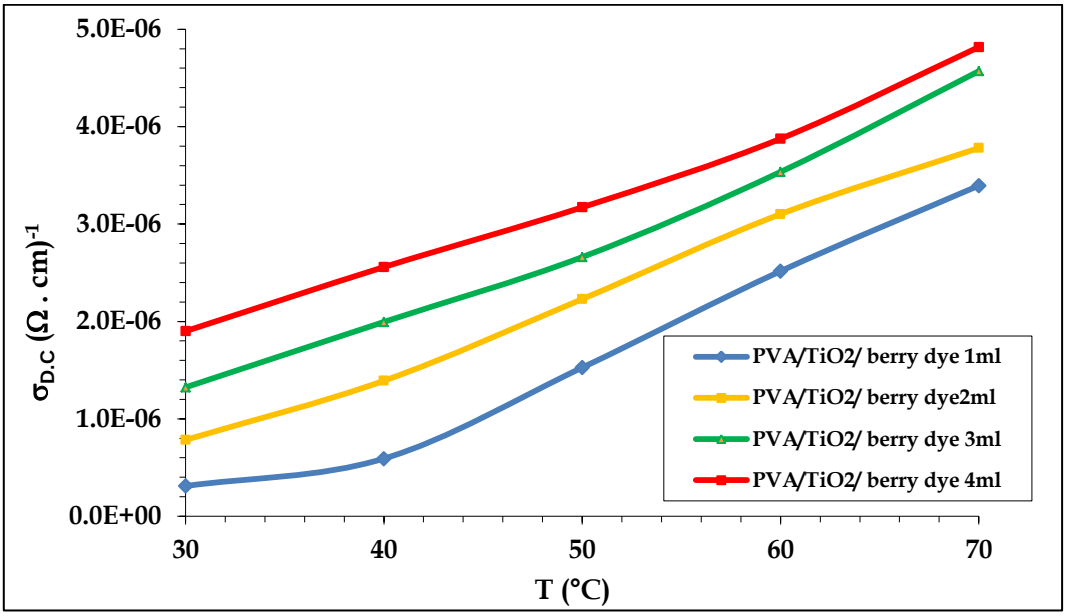

Figure -4.59 : Conductivity of (PVA/TiO_2berry dye) nanocomposites in direct current as a function of temperature

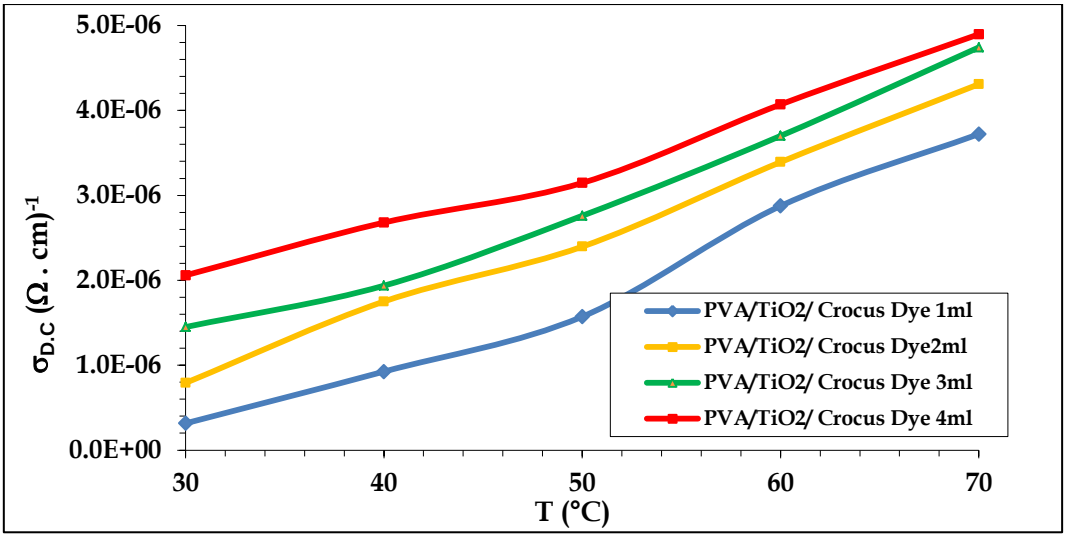

Figure -4.60 : The change in (PVA/TiO_2/crocus dye) nanocomposites' direct current electrical conductivity as a function of temperature.

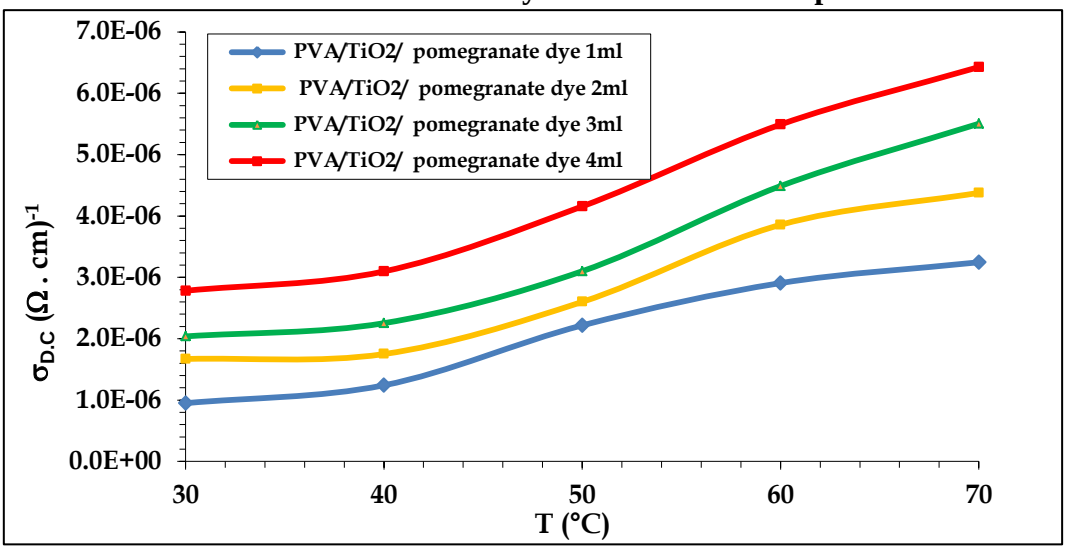

Figure -4.61 : Changes in the direct current electrical conductivity of (polyvinyl alcohol)/(titania oxide)/(pomegranate dye) nanocomposites as a function of temperature

4.4.3 The Temperature Dependence of the Direct Current Electrical Resistivity(ρ) of Polyvinyl Alcohol/Titanium Dioxide and Polyvinyl Alcohol/Natural Dye Nanocomposites.

Electrical resistivity(ρ) of (PVA/TiO_2) nanocomposites with relation to the temperature range depicted in Fig.(4.62). At low concentrations, the electrical resistivity of (PVA/TiO_2) nanocomposites drops as the temperature rises. Figure (4.62) is the reciprocal of Figure (4.58) and the reason for this is that the resistance is the reciprocal of the conductivity according to Equation (2.19). The decrease in electrical resistivity may be

attributed to the homogeneity of (PVA/TiO_2) nanocomposites (the lack of defects), and this clues to a growth in the focus of free electrons and thus a decrease in the resistance[131].

The Variation of electrical resistivity for (PVA/TiO_2/berry, crocus and pomegranate dyes) nanocomposites with temperature is shown in Figures (4.63), (4.64) and (4.65),respectively. The electrical resistivity of (PVA/TiO_2/berry, crocus and pomegranate dyes) nanocomposites decrease with increasing temperature and decrease with increase concentration of natural dyes. This can be attributed to the agglomerations that occur in the nanocomposite, as mention clause (4.2.3) as well as the synthesis of localized levels that increase the conductivity and decrease the resistance[132].

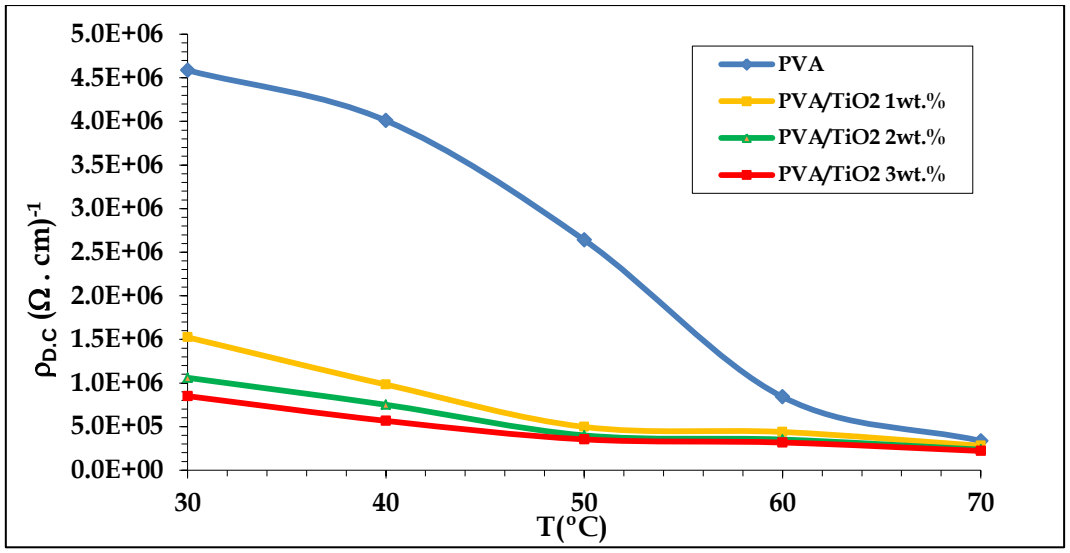

Figure -4.62 : Changing temperature effects on the direct current electrical resistivity of (poly(vinyl alcohol)/titanium dioxide) nanocomposites

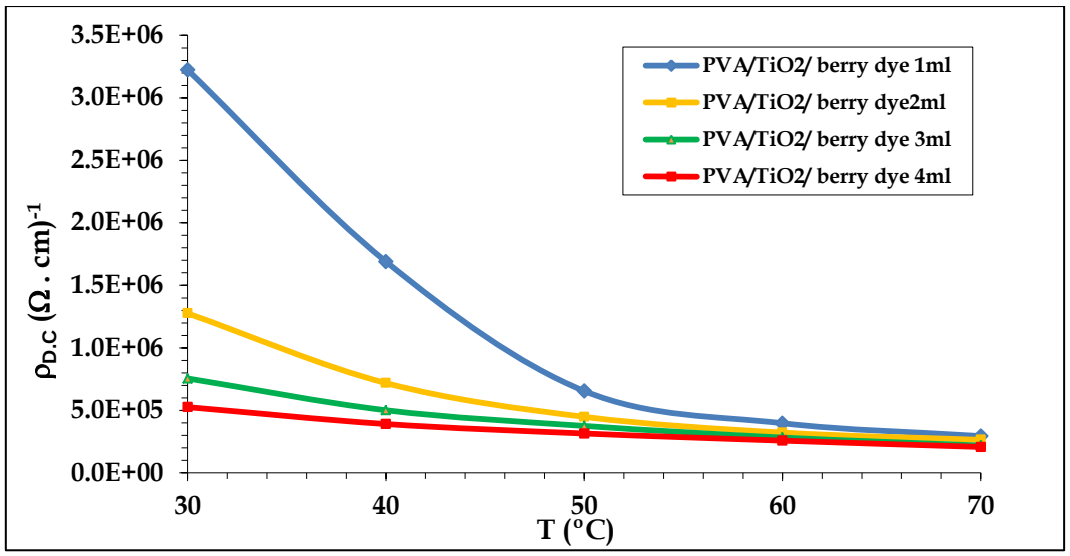

Figure -4.63 : Changes in the direct current (D.C) electrical resistivity of (PVA/TiO_2/berry dye) nanocomposites as a function of temperature

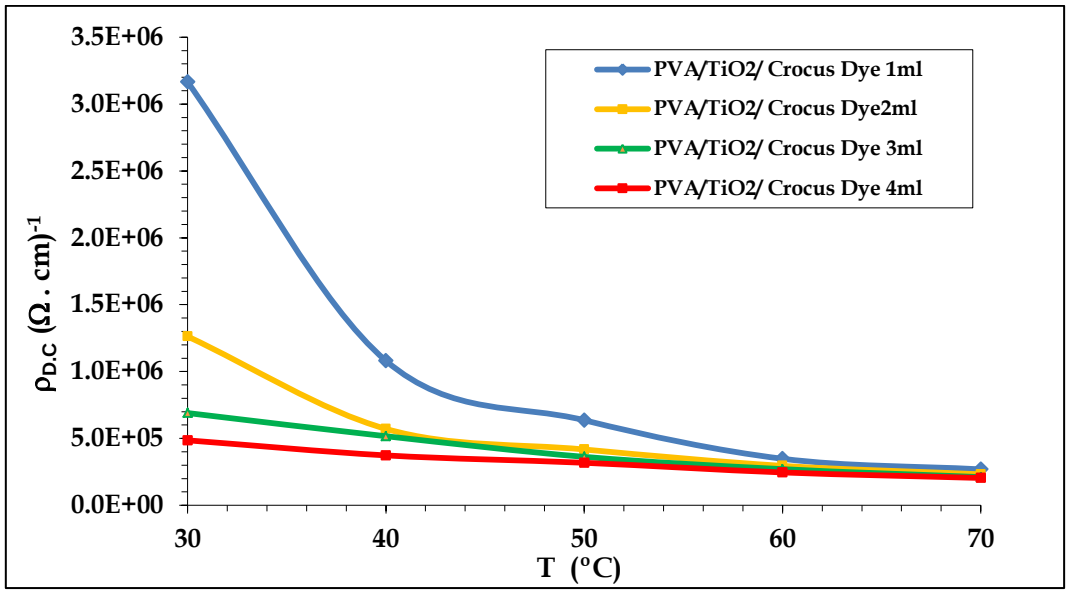

Figure -4.64 : Changes in the DC electrical resistivity of (PVA/TiO_2/crocus dye) nanocomposites as a function of temperature

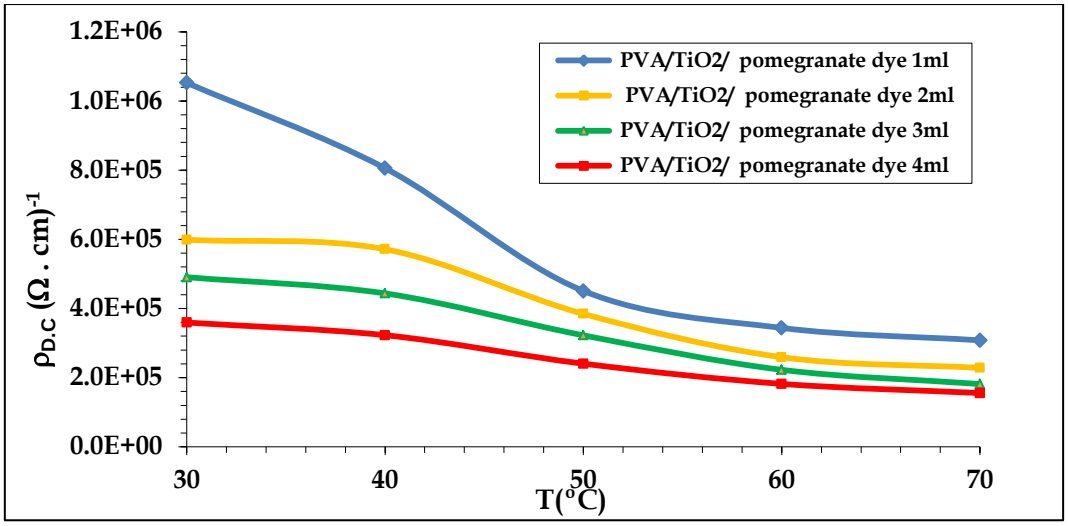

Figure -4.65 : Changes in the DC electrical resistivity of (PVA/TiO_2/pomegranate dye) nanocomposites as a function of temperature.

4.4.4 The (Polyvinyl alcohol)/Titanium dioxide) Nanocomposites Activation Energy.

An equation(2.20) is used to determine activation energy, and the findings demonstrate that (PVA/TiO_2) Nanocomposites have activation energies ranging between (0.60-0.29) eV. Fig. (4.66) shows a relationship between lnσ and the negative absolute temperature for (PVA/TiO_2). When modest quantities of titanium dioxide nanoparticles are added to all samples, levels of activation energy go down in contrast for high values found in the pure polymer state. On the other hand, the figure (4.67) show the increasing the titanium dioxide nanoparticle concentrations, with more local centers, the activation energy drops. Charge carriers, which move by hopping between energy levels, are trapped when low concentrations are added, thereby closing the forbidden energy gap [113,118].

Nanocomposites' activation energy is the labor required to create a network of titanium dioxide nanoparticles with pathways inside charge carrier conveyance polymer matrix, lowering activation energy ,as mention (4.2.1)[120].

These nanocomposites (PVA/TiO_2/berry, crocus, and pomegranate dyes) are shown in Figures (4.68), (4.69), and (4.70), which exhibit the relationship between lnσ and absolute temperature. Which shows a somewhat linear function between them .The calculations showed that the

activation energies of the(PVA/TiO_2/berry, crocus and pomegranate dyes) nanocomposites decreased with the increase in the concentration of natural dyes, table (4.5), (4.6), (4.7) and (4.8) showed variation energy activation with berry, crocus and pomegranate dyes dyes . Where the energy activation decrease (0.56-0.20) eV, (0.29-0.20) eV and (0.54-0.19) eV, when the concentration was increased from 0.5-4ml for berry, crocus and pomegranate dyes, respectively, look in figures (4.71), (4.72) and (4.73).

The natural dyes captured photons with lower energies than the concentrated dye (4ml) because they worked between the valence and conduction beams, and because atoms formed local levels. This explain the low optical energy gap, as mention paragraph(4.3.4) [117].

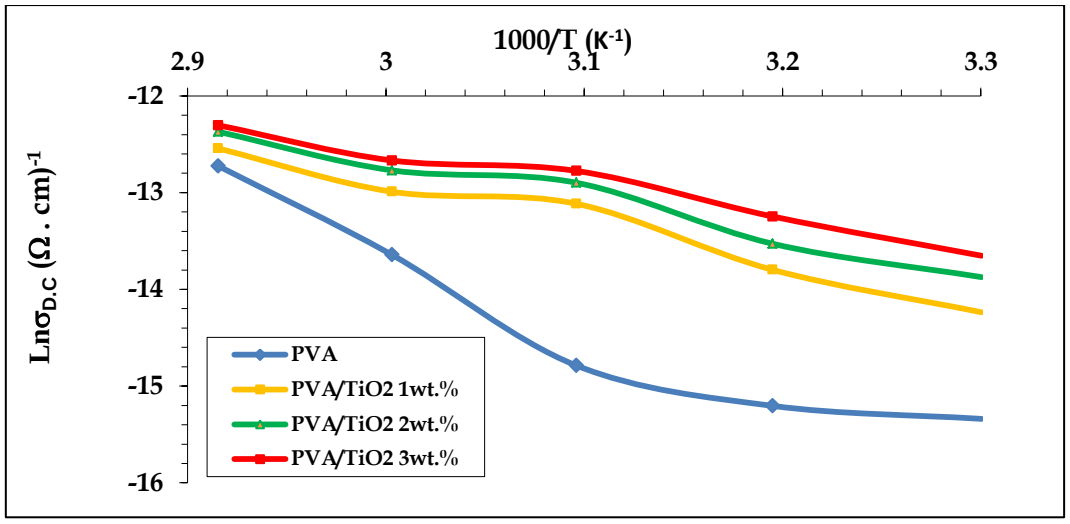

Figure -4.66: Changes in the inverse absolute temperature dependence of the Lnσ D.C electrical conductivity of (PVA/TiO_2) nanocomposites.

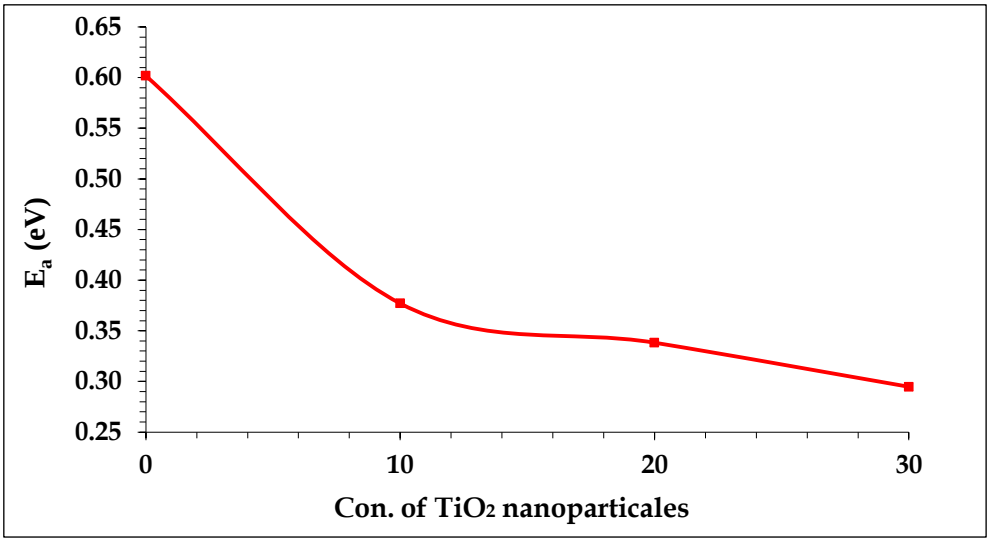

Figure -4.67: Changes in the activation energy for nanoparticle TiO_2 and its Impact on DC Electrical Conductivity 0.3 wt.% in poly(vinyl alcohol)/titania (PVA/TiO_2) nanocomposites.

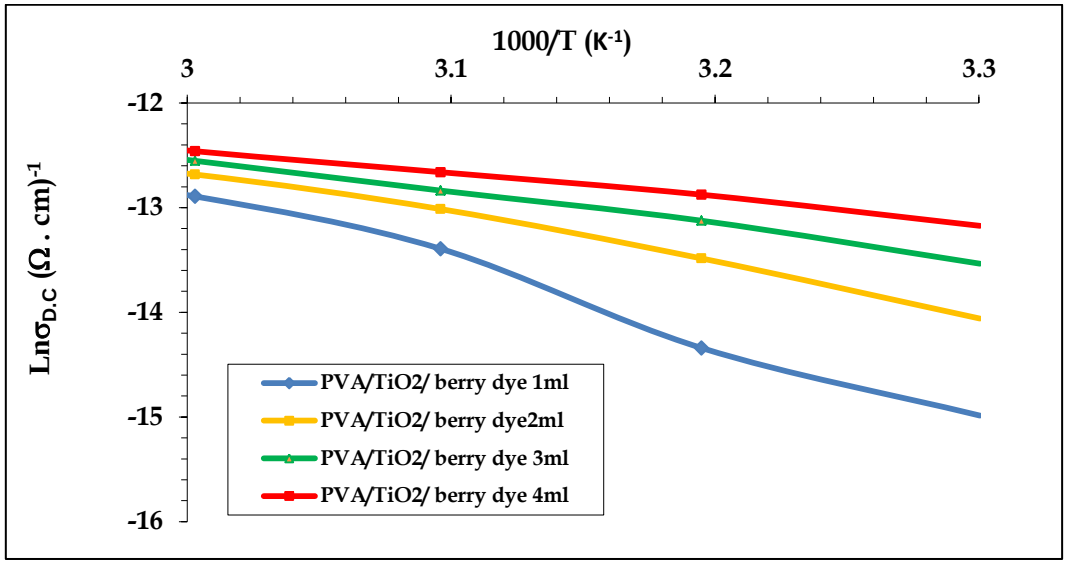

Figure -4.68: Changes in Lnσ D.C plotting electrical conductance versus inverse absolute temperature to (PVA/ TiO_2 /berry dye) nanocomposites

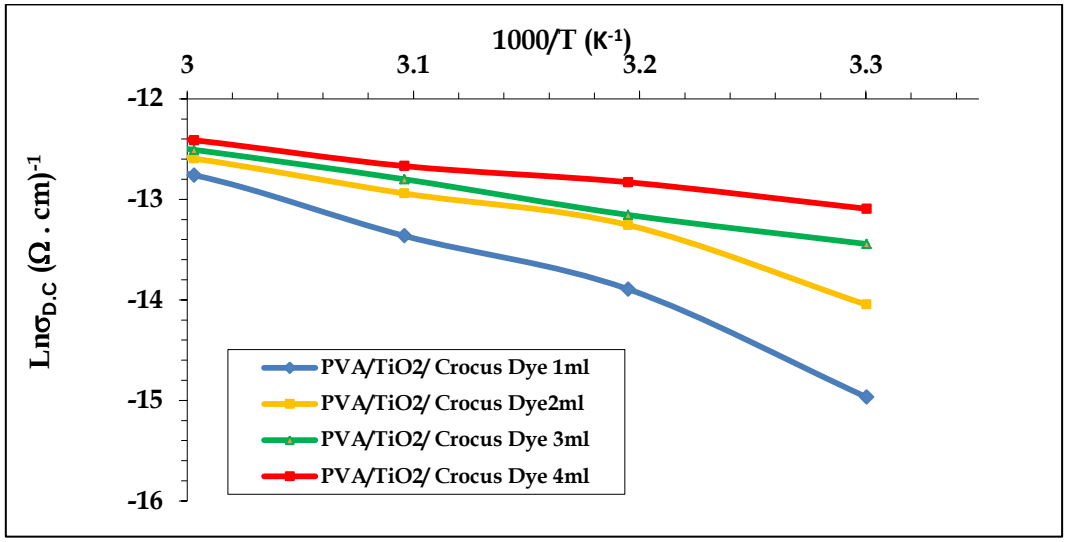

Figure -4.69: Changes in Lnσ D.C plotting electrical conductance versus inverse absolute temperature to (PVA/ TiO_2 /crocus dye) nanocomposites.

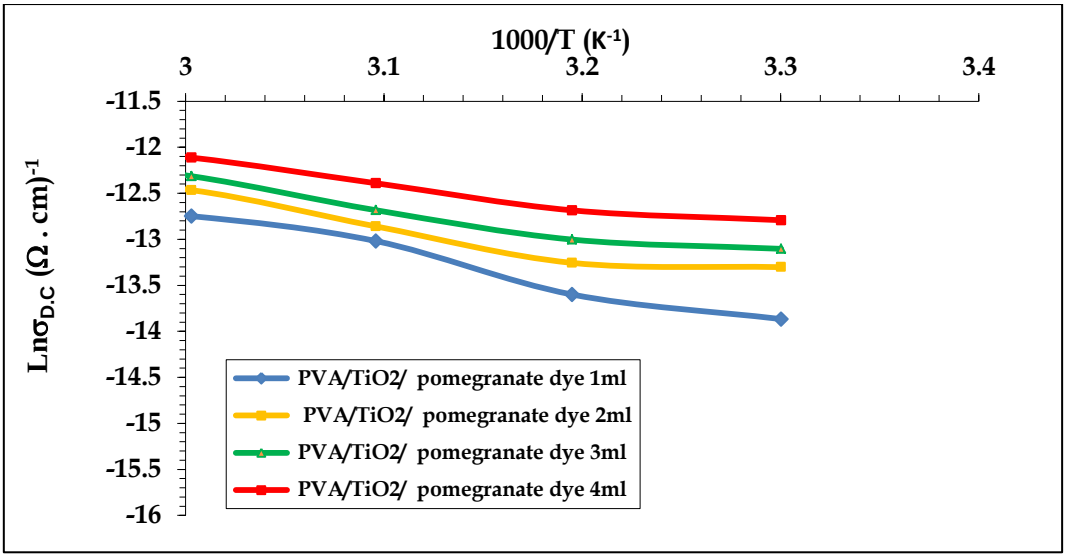

Figure -4.70: Changes in the inverse absolute temperature dependence of the Lnσ D.C electrical conductivity of (PVA/TiO_2/pomegranate dye) nanocomposites.

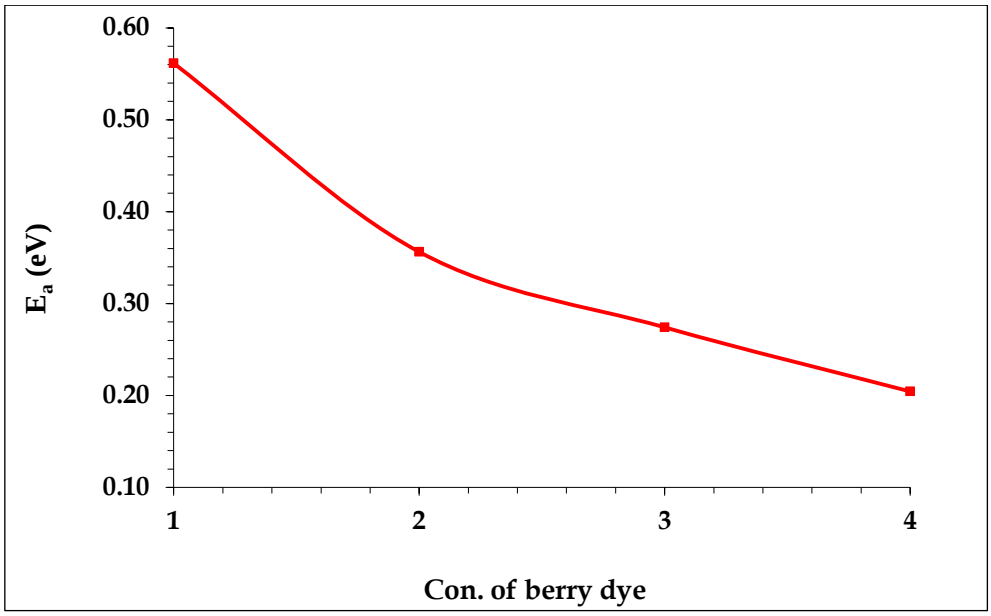

Figure -4.71: Changes in the activation energy for the direct current (DC) conductivity of (PVA/TiO_2/berry dye) nanocomposites as a function of berry dye concentration.

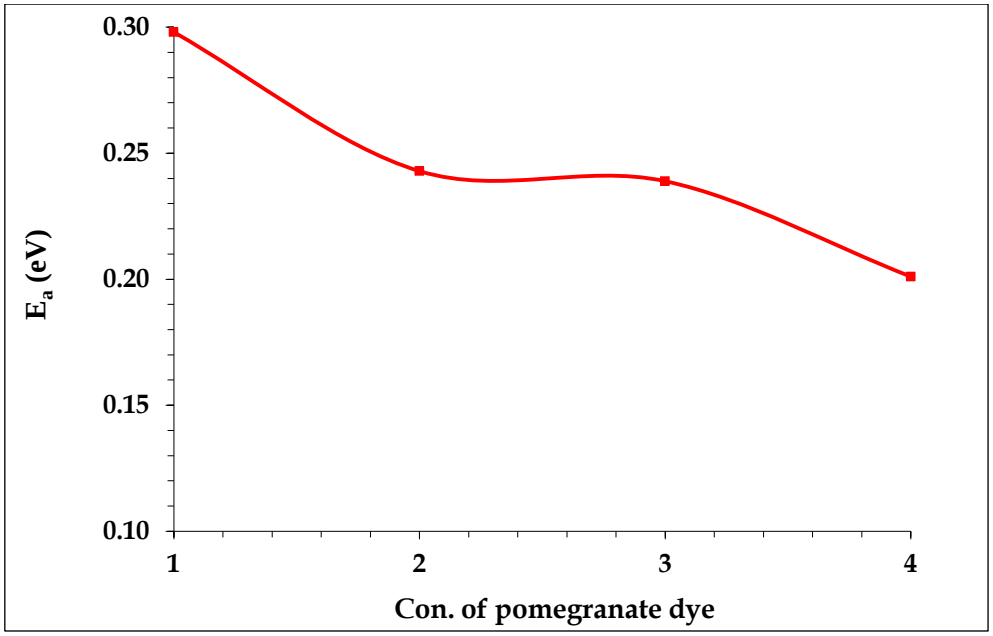

Figure -4.72: Changes in the activation energy for the direct current (DC) conductivity of (PVA/TiO_2/berry dye) nanocomposites as a function of berry dye concentration.

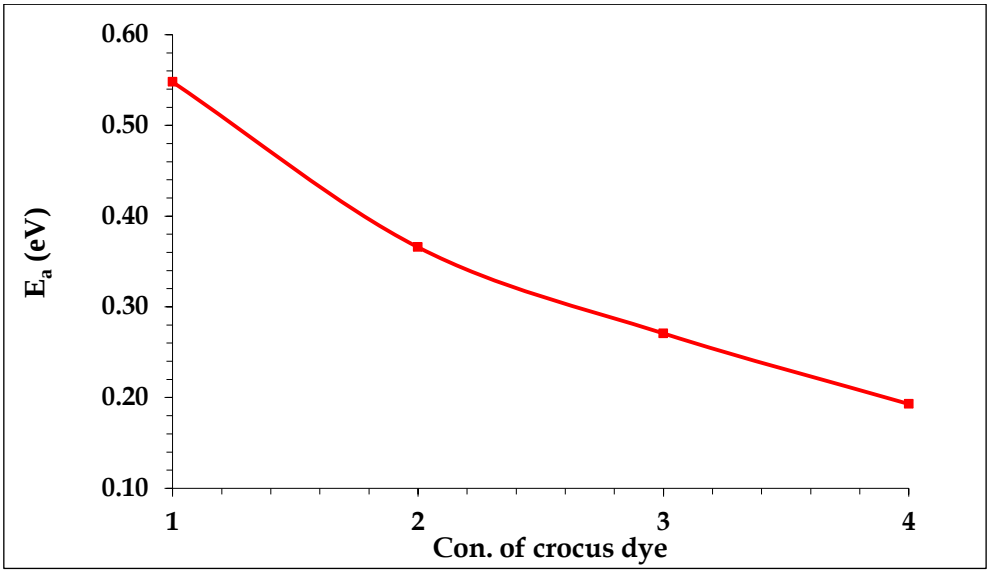

Figure -4.73: Changes in the activation energy for the DC electrical conductivity of (PVA/TiO_2/pomegranate dye) nanocomposites as a function of crocus dye concentration.

Table -4.5: Variation of activation energy proportional to the concentration of nanoparticles of TiO_2.

samples	activation energy(Eac) eV
PVA	0.60

PVA/ TiO_2 1wt.%	**0.37**
PVA/ TiO_2 2wt.%	**0.33**
PVA /TiO_2 3wt.%	**0.29**

Table (4.6): Variation of activation energy with concentration of berry dye.

samples	activation energy(Eac) eV
PVA/ TiO_2/ berry dye 1ml	**0.56**
PVA/ TiO_2/ berry dye 2ml	**0.35**
PVA/ TiO_2/ berry dye 3ml	**0.28**
PVA/ TiO_2/ berry dye 4ml	**0.20**

Table (4.7): Variation of activation energy with concentration of crocus dye.

samples	activation energy(Eac) eV
PVA/ TiO_2/ crocus dye 1ml	**0.29**
PVA/ TiO_2/ crocus dye 2ml	**0.24**
PVA/ TiO_2/ crocus dye 3ml	**0.23**
PVA/ TiO_2/ crocus dye 4ml	**0.20**

Table (4.8): Variation of activation energy with concentration of pomegranate dye.

samples	activation energy(Eac) eV
PVA/ TiO_2/ pomegranate dye 1ml	**0.54**
PVA/ TiO_2/ pomegranate dye 2ml	**0.36**
PVA/ TiO_2/ pomegranate dye 3ml	**0.27**
PVA/ TiO_2/ pomegranate dye 4ml	**0.19**

4.5 Luminous and Nonluminous I-V Behavior of a SnO_2/p-Si Heterojunction

Due to its role in solar cell technology, tin dioxide (SnO_2) is one of the semiconductors that is now being extensively researched. SnO_2 powder is used in the vacuum thermal deposition procedure to create the junction SnO_2/p-Si, which results in experimental I-V curves with a variety of behaviors depending on the environment in which the junction is being created. SnO_2/p-Si will produce anisotype n-p heterojunction (HJ) since SnO_2 is n-type with200±6 nm thickness and Si is p-type. Figures (4.74), (4.76), and (4.78) depict the I-V curves of the SnO_2/p-Si heterojunction under both dark and light circumstances. Where (I_d) represents the current in the dark, (I_t) represents the current in the lit environment, and the photocurrent is denoted by (I_{ph}) ($I_{ph}=I_t-I_d$).

To design a heterojunction, the energy gap and electronic affinity must be taken into account. It was found that the lattice constant of silicon and tin dioxide are close. The silicon lattice parameters a=4.30 Å and b=4.55Å, also for lattice parameters SnO_2 a = b = 4.738Å. In addition, the coefficient of thermal expansion of the two separator materials was found to be close, and this is important to avoid dislocations at the interface separating them.

For evaluating the importance of each component under reverse and forward bias, among other situations, The properties of the current and voltage I-V curves when the dark very important. SnO_2/p-Si HJ I-V characteristic at forward bias voltage falls within this region (-2 to 2 Volt). These charts show how the current behaves in relation to the forward and reverse bias voltage. One of the optoelectronic characteristics for HJ is the current-voltage characteristic under light. The measurements are performed with incident power densities of (115 mW/cm^2)[133].

It is clear from Figures (4.75), (4.77) and (4.79) that the photocurrent increases as the bias voltage rises. An increase in the reverse bias voltage causes electron-hole couples to split, expanding the depletion region.

After covering it with (PVA/TiO_2/berry, crocus, and pomegranate dyes) nanocomposites on the surface SnO2/p-Si, the efficiency of the solar cell increase. The efficiency(η) increase from (4.7-4.9), (5.7-6) and (4.3-4.75) was recorded after being coated with(PVA/TiO_2/berry crocus and pomegranate dyes) nanocomposites, respectively as shown in the table below(4.9). The improvement in electro-catalytic activity is what is

responsible for the performance improvement. As a result, the cell's series resistance decreases as I_{sc} grows and increase V_{oc} ,this result agree with Saad *et al.*[134].

However, it was noticeable that the dye acted as a photosensitive. This leads to more electrons being injected from natural dyes IV dye molecules to the conduction band of SnO_2 upon light illumination, resulting in an enhancement of the photovoltaic parameters of the cell such as I_{sc} and η. The reason behind the increased efficiency of the solar cell is the increased absorption of light by natural dyes, agree with Pratiwi *et al.* [135]. As a result, it has been proven that these films can be used as coverings for solar cells.

Fig.(4.74) show the dark and illuminated (I-V) characteristics for a cell. The figure reveals the effect of illumination of the (I-V) plot. The decrease in illumination forward current I_{ph} an compared with the dark forward current I_f is due to the generation of minority carriers photocurrent which are annihilated by majority carriers dark current . The forth quadrat curve in this fig. represent the photovoltaic performer in which the power can be existed from the cell. The open circuit voltage V_{oc} given from this curve.

The potential energy landscape at the contact (but inside the active layer) dominates the minority carrier current for low-voltage operation (diffusion-limited). The effect of the hole-induced space charge on the dominant electric field may be disregarded if the hole density at the anode contact is not excessive. The anode contact can be thought of as "neutral" in this situation because of the low energy level bending there. I_s(30 mA) and the short circuit current density I_{sc} is (35). A reasonable prediction may be obtained from the dark current under reverse bias I_t is a noticeable urination in dark current with reverse bias voltage ,this effect can be attributed to the carrier generation inside the depletion region.

A semi-log (I-V) plot under forward bias is represent . this figure shows that forward current consist of the region represent recombination current, while the second represents the tunneling current ,i.e SnO2/p-Si heterojunction obeys the tunneling recombination model. This results is in agreement with results obtained by Saad et al.[134],represent by spray chemical analysis.

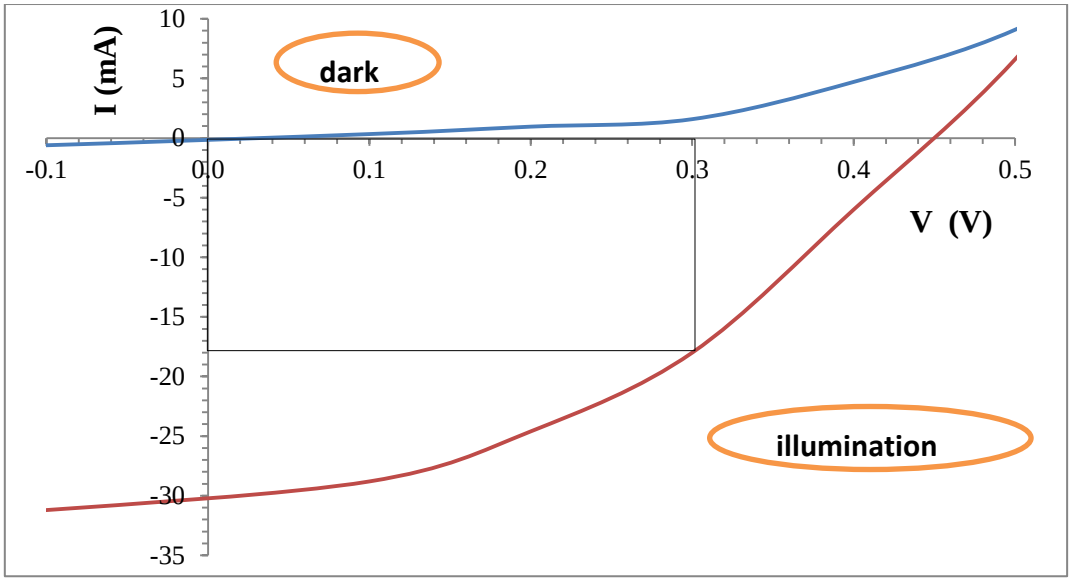

Figure (4.74) I-V behavior for SnO_2/p-Si under P=115 mW/cm^2

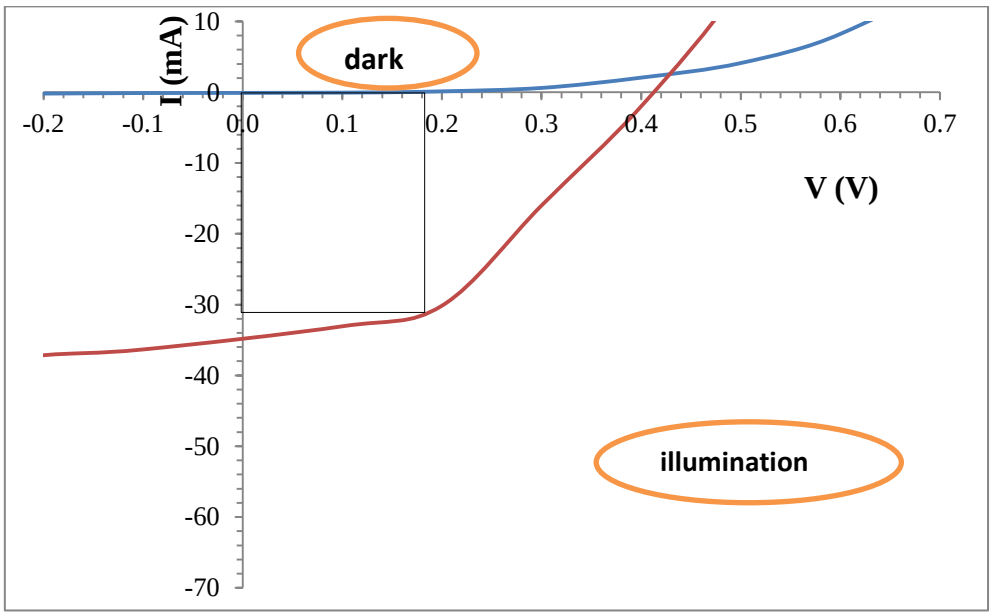

Figure (4.75) I-V behavior for SnO_2/p-Si under P=115 mW/cm^2 after being coated with PVA/TiO_2/ berry dye 4ml

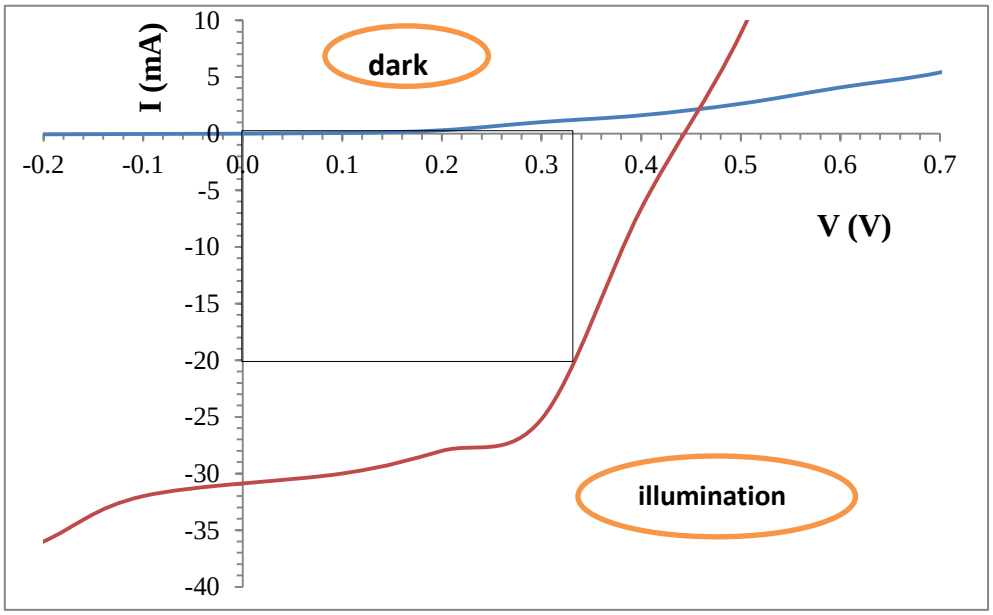

Figure (4.76) I-V behavior for SnO_2/p-Si under P=115 mW/cm^2.

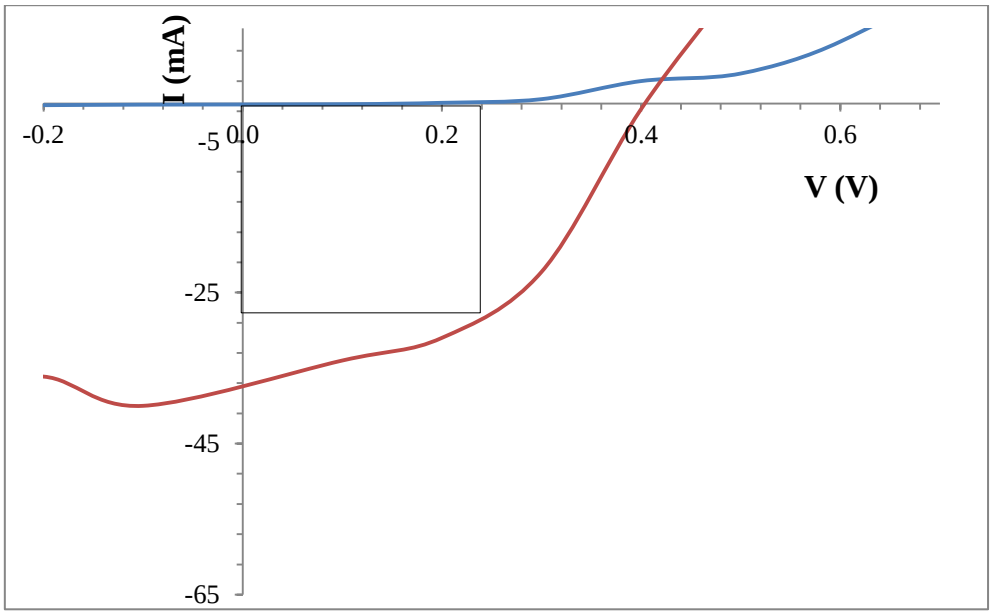

Figure (4.77) I-V behavior for SnO_2/p-Si under P=115 mW/cm^2 after coating (PVA/TiO_2/ crocus dye 4ml).

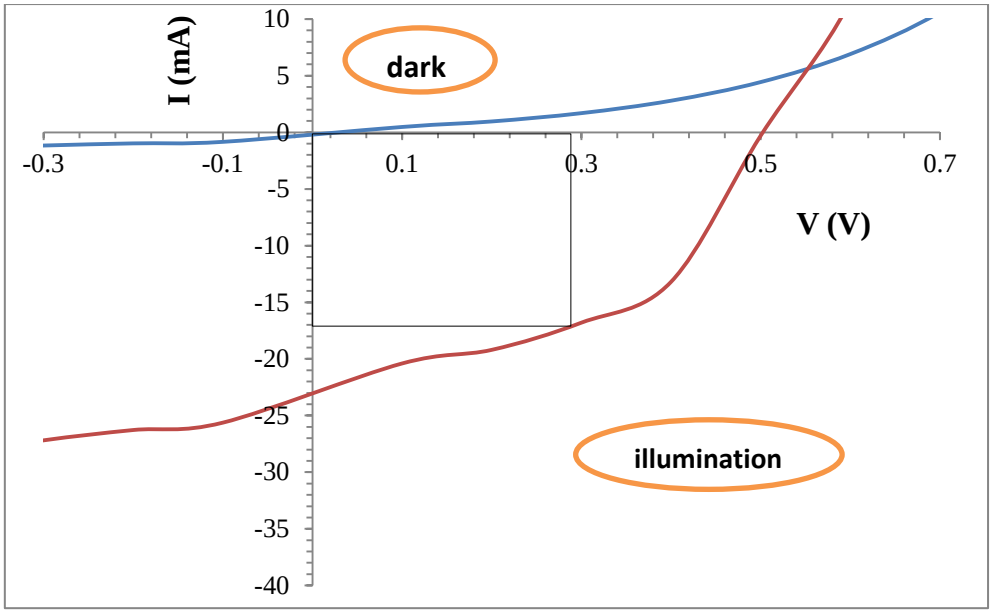

Figure (4.78) I-V behavior for SnO_2/p-Si under P=115 mW/cm^2.

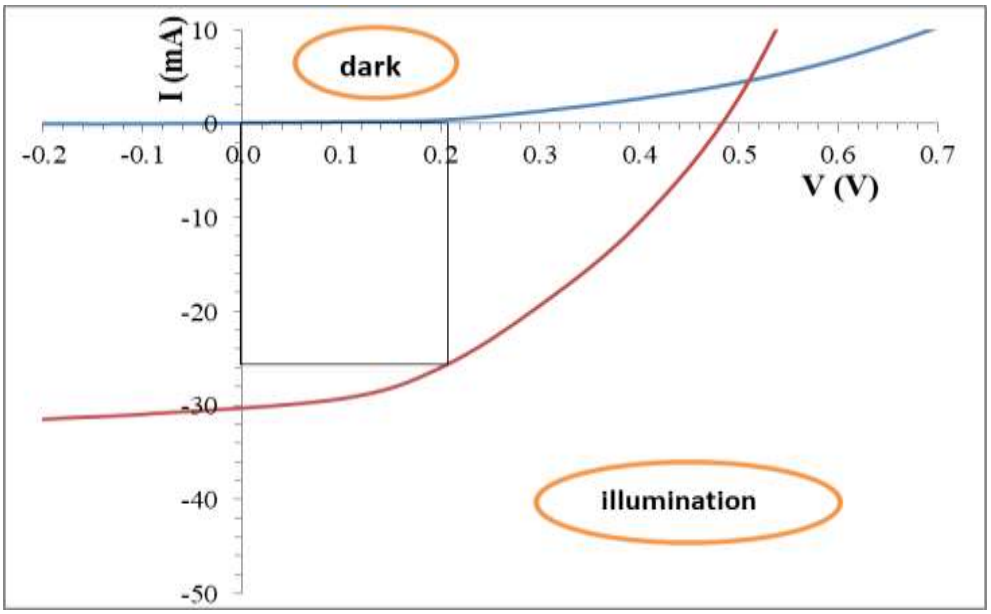

Figure (4.79) I-V behavior for SnO_2/p-Si under P=115 mW/cm^2 after coating (PVA/TiO_2/ pomegranate dye 4ml).

Table (4.9): Variation of the I-V for SnO_2/Si solar cell before and after coating by (PVA/TiO_2/ berry, crocus and pomegranate dyes) nanocomposites

Dye	I_m	V_m	I_{sc}	V_{oc}	F.F	Ƞ%

		(mA)	(v)	(mA/cm^2)	(v)		
Berry dye	before	18	0.3	30	0.45	0.40	4.7
	after	31	0.18	35	0.42	0.35	4.9
Crocus dye	before	20	0.33	32	0.44	0.46	5.7
	after	29	0.24	38	0.40	0.45	6
Pomegranate dye	before	17	0.29	23	0.50	0.42	4.3
	after	26	0.21	30	0.48	0.37	4.75

Conclusions

From the obtained results and discussions ,the following points are concluded:

1- The Fourier transformation-infrared spectroscopy(FTIR) recorded vibrational peak for nanocomposites concentrations, but when added (TiO_2 3wt.%) decreases the FT-IR spectra. The peak of IR-rad transmittance denotes a shift in peak locations and the creation of a new peak, which is due to the interaction of PVA and dye. Conjugated bonds appeared for the anthocyanin, anthocyanid and carotenoid core chains observed in berry, pomegranate and crocus respectively.

2-morphology of PVA/TiO_2 agglomerates, as seen by FE-SEM, demonstrates porous irregular cauliflower-like characteristics, while the morphology of TiO_2 shows the creation of tiny clusters of spherical shape particles. It was discovered that nanocomposites had spherical shape and grain sizes of 47.01 nm. From the images it can be remarked seen that the increase in particle size because increase concentration of TiO_2.

3-The (PVA/TiO_2/berry, crocus and pomegranate dyes) nanocomposites show that the absorbance is increasing with increasing concentration of natural dyes. Absorbance increases with increasing concentration of natural dyes from(1-4)ml. These films absorb visible light according to their wavelengths and can be used as a photosensor in solar cells. The transmittance decrease with increase concentration of TiO_2, and recorded highest peak at 81.9% in crocus dye. The absorption coefficient has high values ($\alpha>10^4 cm^{-1}$), indicating that the direct transition has a high value.

The energy gap decreases(3.64-3,58)eV with increase concentration TiO_2, also the lowest possible energy gap was recorded for Pomegranate dye (3.32-3.26)eV

4- The electrical conductivity($\sigma_{d.c}$) at a concentration of 2% was reached (4.81×10^{-6}, 4.9×10^{-6} and 6.4×10^{-6}) $(ohm.cm)^{-1}$ for berry, crocus and pomegranate dyes, respectively. The electrical conductivity of (PVA/TiO_2 berry, crocus and pomegranate dyes) nanocomposites increase with increasing temperature. It also shows a high values in correlation with the content of natural dyes. The activation energy show decrease(0.60-0.29) eV with increasing TiO_2 nanoparticle concentrations

5- An improvement of the conversion efficiency (4.3-4.75%).

6- SnO_2 films were deposited onto n-Si by thermal vacuum evaporation to introduce anisotopic heterojunction solar cell.

Future Work

1- Studying the mechanical and thermal characteristics of nanocomposites (PVA/TiO_2/chemically produced dyes).

2- Studying the PVA polymer film with natural colours and the impact of nanoparticles like ZnO on their optical and structural qualities.

3- Study of Spraying the nanocomposite along with the current investigation as a comparison.

4- Comparative study addition of natural and synthetic dyes and their effects on the (PVA/TiO_2) nanocomposite.

References

References

[1] R. Senthil, “Recent innovations in solar energy education and research towards sustainable energy development,” *Acta Innov.*, no. 42, pp. 27–49, 2022.

[2] R. Zahedi, A. Zahedi, and A. Ahmadi, “Strategic study for renewable energy policy, optimizations and sustainability in Iran,” *Sustainability*, vol. 14, no. 4, p. 2418, 2022.

[3] Elavarasan, R. M., Mudgal, V., Selvamanohar, L., Wang, K., Huang, G., Shafiullah, G. M., ... & Nadarajah, M.. Pathways toward high-efficiency solar photovoltaic thermal management for electrical, thermal and combined generation applications: A critical review. Energy Conversion and Management, 255, 115278,2022.

[4] A. Mohd Imran and A. Naushad, “Applications of Solar Cells,” *Fundam. Sol. Cell Des.*, pp. 345–369, 2021.

[5] M. Q. A. Al-Gunaid, A. Saeed, N. K. Subramani, and B. S. Madhukar, “Optical parameters, electrical permittivity and I–V characteristics of PVA/Cs2CuO2 nanocomposite films for opto-electronic applications,” *J. Mater. Sci. Mater. Electron.*, vol. 28, no. 11, pp. 8074–8086, 2017.

[6] P. S. Kanavi, S. Meti, R. H. Fattepur, and V. B. Patil, “Emphasized temperature dependent electrical properties study of fabricated ZnO/PVA/PANI nanocomposite films,” *OpenNano*, vol. 7, p. 100057, 2022.

[7] J. Salimian, S. Osfouri, R. Azin, and T. Jalali, “Efficiency improvement of crystallin silicon solar cell,” *J. Mater. Res. Technol.*, vol. 18, pp. 4816–4833, 2022.

[8] C.C.Okpala, “the benefits and applications of nanocomposites,” *Int. J. Adv. Eng. Technol.*, vol. Vol. 5, no. Issue 6, p. pp.12-18, 2014.

[9] S. Devikala, P. Kamaraj, and M. Arthanareeswari, “Synthesis, characterization and AC conductivity of PVA based composite,” *IOSR J. Appl. Chem.*, vol. 6, pp. 24–28, 2012.

[10] K. R. Nemade and S. A. Waghuley, “Gas sensing mechanism of metal oxide doped PANi composites,” *J. Mater. Sci. Eng. B*, vol. 3, no. 5B, p. 310, 2013.

[11] Zhao, C., Ren, R., Zhong, J., Goh, K. L., Zhang, K., Zhang, Z., & Le, G. (2022, July). Intralaminar crack propagation of glass fiber

reinforced composite laminate. In Structures (Vol. 41, pp. 787-803). Elsevier.

[12] F. O. Aguele, C. I. Madufor, and K. F. Adekunle, “Comparative Study of Physical Properties of Polymer Composites Reinforced with Uncarbonised and Carbonised Coir,” *Open J. Polym. Chem.*, vol. 04, no. 03, pp. 73–82, 2014, doi: 10.4236/ojpchem.2014.43009.

[13] A. K. Sharma, R. Bhandari, A. Aherwar, and R. Rimašauskiene, “Matrix materials used in composites: A comprehensive study,” *Mater. Today Proc.*, vol. 21, pp. 1559–1562, Jan. 2020, doi: 10.1016/J.MATPR.2019.11.086.

[14] B. R. N. B. and K. C. N. C. Jeevan, “Characteristic Analysis of Mechanical Properties on Carbon Fiber Reinforced Plastic,” *Int. J. Res. Eng. Adv. Technol.*, vol. 3, no. 2, 2015.

[15] Wang, J., Manolatou, C., Bai, Y., Hone, J., Rana, F., & Zhu, X. Y. Disorder of excitons and trions in monolayer MoSe2. The Journal of Chemical Physics, 157(21), 211101, 2022.

[16] Kenichi Hayashida and Yasuhiro Takatani, “Poly(methyl methacrylate)-grafted ZnO nanocomposites with variable dielectric constants by UV light irradiation,” *J. Mater. Chem. C*, vol. 4, no. 16, pp. 3640–3645, 2016, doi: 10.1039/c6tc00882h.

[17] Abu-Dalo, M. A., Al-Rosan, S. A., & Albiss, B. A. (2021). Photocatalytic degradation of methylene blue using polymeric membranes based on cellulose acetate impregnated with ZnO nanostructures. Polymers, 13(19), 3451.

[18] J. Jeevanandam, A. Barhoum, Y. S. Chan, A. Dufresne, and M. K. Danquah, “Review on nanoparticles and nanostructured materials: history, sources, toxicity and regulations,” *Beilstein J. Nanotechnol.*, vol. 9, no. 1, pp. 1050–1074, 2018.

[19] T. A. Saleh, P. Parthasarathy, and M. Irfan, “Advanced functional polymer nanocomposites and their use in water ultra-purification,” *Trends Environ. Anal. Chem.*, vol. 24, p. e00067, Oct. 2019, doi: 10.1016/J.TEAC.2019.E00067.

[20] D. Harandi, “Preparation of new polymer nanocomposites with potential use in restorative applications for the consolidation historical wooden work,” 2021.

[21] J. Moczo and B. Pukanszky, “Polymer micro and nanocomposites: Structure, interactions, properties,” *J. Ind. Eng. Chem.*, vol. 14, no.

5, pp. 535–563, 2008.

[22] A. M. Alsaad, A. R. Al Dairy, A. A. Ahmad, A. S. Al-anbar, and Q. M. Al-Bataineh, “Synthesis and characterization of as-grown doped polymerized (PMMA-PVA)/ZnO NPs hybrid thin films,” *Polym. Bull.*, vol. 79, no. 4, pp. 2019–2040, 2022.

[23] M. N. Shakhatreh, H. Chamroukhi, A. Telfah, and C. J. Tavares, “Optical, electrical and morphological properties of (PANI/CSA-PEO)/(AgNPs-AgNO3) nanocomposite films,” *Phys. B Condens. Matter*, vol. 634, p. 413636, 2022.

[24] N. N. Deshavath, V. D. Veeranki, and V. V Goud, “Lignocellulosic feedstocks for the production of bioethanol: availability, structure, and composition,” in *Sustainable Bioenergy*, Elsevier, 2019, pp. 1–19.

[25] B. Kaczmarek, K. Nadolna, and A. Owczarek, “The physical and chemical properties of hydrogels based on natural polymers,” *Hydrogels based Nat. Polym.*, pp. 151–172, 2020.

[26] S. Tabasum *et al.*, “A review on blending of corn starch with natural and synthetic polymers, and inorganic nanoparticles with mathematical modeling,” *Int. J. Biol. Macromol.*, vol. 122, pp. 969–996, 2019.

[27] A. Alsaad, A. R. Al Dairy, A. Ahmad, I. A. Qattan, S. Al Fawares, and Q. Al-Bataineh, “Synthesis and characterization of polymeric (PMMA-PVA) hybrid thin films doped with TiO2 nanoparticles using dip-coating technique,” *Crystals*, vol. 11, no. 2, pp. 1–21, 2021, doi: 10.3390/cryst11020099.

[28] M. Umesh, S. Shanmugam, T. Kikas, N. T. L. Chi, and A. Pugazhendhi, “Progress in bio-based biodegradable polymer as the effective replacement for the engineering applicators,” *J. Clean. Prod.*, p. 132267, 2022.

[29] S. J. Alsultany and A. A. Mohaimeed, “Role of Nanoparticles Synthesized from Bacteria as Antimicroorganism: A Review,” *Iraqi J. Nanotechnol.*, no. 2, pp. 44–53, 2021.

[30] A. Czupryński, “Comparison of properties of hardfaced layers made by a metal-core-covered tubular electrode with a special chemical composition,” *Materials (Basel).*, vol. 13, no. 23, p. 5445, 2020.

[31] A. B. Asha and R. Narain, “Nanomaterials properties,” in *Polymer Science and Nanotechnology*, Elsevier, 2020, pp. 343–359.

[32] D. Byrne *et al.*, “Biodegradability of Polyvinyl Alcohol Based Film Used for Liquid Detergent Capsules,” *Tenside Surfactants Deterg.*, vol. 58, no. 2, pp. 88–96, 2021.

[33] K. K. Kumar, M. Ravi, Y. Pavani, S. Bhavani, A. K. Sharma, and V. V. R. N. Rao, “Investigations on PEO/PVP/NaBr complexed polymer blend electrolytes for electrochemical cell applications,” *J. Memb. Sci.*, vol. 454, pp. 200–211, 2014.

[34] M. I. Baker, S. P. Walsh, Z. Schwartz, and B. D. Boyan, “A review of polyvinyl alcohol and its uses in cartilage and orthopedic applications,” *J. Biomed. Mater. Res. Part B Appl. Biomater.*, vol. 100, no. 5, pp. 1451–1457, 2012.

[35] A. M. Alsaad, A. A. Ahmad, I. A. Qattan, A.-R. El-Ali, S. A. Al Fawares, and Q. M. Al-Bataineh, “Synthesis of Optically Tunable and Thermally Stable PMMA–PVA/CuO NPs Hybrid Nanocomposite Thin Films,” *Polymers (Basel).*, vol. 13, no. 11, p. 1715, 2021.

[36] S. Virtanen, J. Vartianen, H. Setälä, T. Tammelin, and S. Vuoti, “Modified nanofibrillated cellulose–polyvinyl alcohol films with improved mechanical performance,” *Rsc Adv.*, vol. 4, no. 22, pp. 11343–11350, 2014.

[37] A. A. M. Shehab, E. Abid, and S. H. Salman, “tudying the Structural and Optical properties of PVA doped witSh CuO and FeCl3 composites films,” *Eng. Technol. J.*, vol. 33, no. 9 Part (B) Scientific, 2015.

[38] A. J. Haider, Z. N. Jameel, and I. H. M. Al-Hussaini, “Review on: titanium dioxide applications,” *Energy Procedia*, vol. 157, pp. 17–29, 2019.

[39] Y. Zheng and B. Nowack, “Size-specific, dynamic, probabilistic material flow analysis of titanium dioxide releases into the environment,” *Environ. Sci. Technol.*, vol. 55, no. 4, pp. 2392–2402, 2021.

[40] L. G. Bousiakou, P. J. Dobson, T. Jurkin, I. Marić, O. Aldossary, and M. Ivanda, “Optical, structural and semiconducting properties of Mn doped TiO2 nanoparticles for cosmetic applications,” *J. King Saud Univ.*, vol. 34, no. 3, p. 101818, 2022.

[41] S. Reghunath, D. Pinheiro, and S. D. KR, “A review of hierarchical nanostructures of TiO2: Advances and applications,” *Appl. Surf.*

Sci. Adv., vol. 3, p. 100063, 2021.

[42] R. A. Lance, "Optical Analysis of Titania: Band Gaps of Brookite, Rutile and Anatase," 2018.

[43] N. Patni, P. Sharma, and S. G. Pillai, "Comparison of electrolyte used in the synthesis of natural dye based dye sensitized solar cells," *Int. J. Res.*, vol. 4, no. 13, pp. 947–951, 2017.

[44] N. MZ and W. Tan, "Dye extracted from Costus woodsonii leave as a natural sensitizer for dye-sensitized solar cell/MZ Najihah and Tan Winie," *Sci. Lett.*, vol. 15, no. 1, pp. 58–68, 2021.

[45] Hosseinnezhad, M., Gharanjig, K., Yazdi, M. K., Zarrintaj, P., Moradian, S., Saeb, M. R., & Stadler, F. J. Dye-sensitized solar cells based on natural photosensitizers: A green view from Iran. *Journal of Alloys and Compounds*, *828*, 154329., 2020.

[46] M. Saltmarsh, "Food Additive Regulations in Europe," *Saltmarsh's Essent. Guid. to Food Addit. R. Soc. Chem. London, UK*, pp. 40–51, 2020.

[47] K. Hosseinpanahi, M. H. Abbaspour-Fard, J. Feizy, and M. Reza Golzarian, "Dye-sensitized solar cell using saffron petal extract as a novel natural sensitizer," *J. Sol. Energy Eng.*, vol. 139, no. 2, 2017.

[48] A. Kumari, J. Dora, and A. Kumar, "Pomegranate (Punica granatum) - Overview," *Int. J. Pharm. Chem. Sci.*, vol. 1, pp. 1218–1222, Jan. 2012.

[49] M. H. Bazargan, M. M. Byranvand, A. N. Kharat, and L. Fatholahi, "Natural pomegranate juice as photosensitizers for dye-sensitized solar cell (DSSC)," *J. Optoelectron. Adv. Mater. Commun.*, vol. 5, no. 4, pp. 360–362, 2011.

[50] Ibn-Mohammed, T., Koh, S. C. L., Reaney, I. M., Acquaye, A., Schileo, G., Mustapha, K. B., & Greenough, R. Perovskite solar cells: An integrated hybrid lifecycle assessment and review in comparison with other photovoltaic technologies. *Renewable and Sustainable Energy Reviews*, *80*, 1321-1344, 2017.

[51] T. Kong, R. Wang, D. Zheng, and J. Yu, "Modification of the SnO2 Electron Transporting Layer by Using Perylene Diimide Derivative for Efficient Organic Solar Cells," *Front. Chem.*, vol. 9, 2021.

[52] L. Xiong *et al.*, "Review on the application of SnO2 in perovskite solar cells," *Adv. Funct. Mater.*, vol. 28, no. 35, p. 1802757, 2018.

[53] Z. Hossein Esfahani, M. Ghanipour, and D. Dorranian, “Effect of dye concentration on the optical properties of red-BS dye-doped PVA film,” *J. Theor. Appl. Phys.*, vol. 8, pp. 117–121, 2014.

[54] F. M. Al-Omair, N. A., Reda, S. M., & Al-Hajri, “Effect of Organic Dye on the Photovoltaic Performance of Dye-Sensitized ZnO Solar Cell,” *Adv. Nanoparticles*, vol. 03, no. 01, pp. 31–35, 2014, doi: 10.4236/anp.2014.31005.

[55] Z. H.-M. 1 I. Vanja Gilja 1, Katarina Novakovi´c 1, Jadranka Travas-Sejdic 2 and 1 Marijana Kralji´c Rokovi´c 1 and Mark Žic 3, “Stability and synergistic effect of polyaniline/TiO2 photocatalysts in degradation of Azo dye in wastewater,” *Nanomaterials*, vol. 7, no. 12, , doi: 10.3390/nano7120412, 2017.

[56] Z. Gilja, V., Vrban, I., Mandić, V., Žic, M., & Hrnjak-Murgić, “Preparation of a PANI/ZnO composite for efficient photocatalytic degradation of acid blue,” *Polymers (Basel).*, vol. 10, no. 9, pp. 1–17, 2018, doi: 10.3390/polym10090940.

[57] M. N. Mustafa, S. Shafie, M. H. Wahid, and Y. Sulaiman, “Light scattering effect of polyvinyl-alcohol/titanium dioxide nanofibers in the dye-sensitized solar cell,” *Sci. Rep.*, vol. 9, no. 1, pp. 1–8, 2019, doi: 10.1038/s41598-019-50292-z.

[58] Anoua, R., Touhtouh, S., El Jouad, M., Hajjaji, A., Bakasse, M., Sahraoui, B., ... & Zawadzka, A. Absorbance and photoluminescence study of pomegranate for dye-sensitized solar cells. *Materials Today: Proceedings*, *66*, 109-111, 2022.

[59] W. K. Mohsen, S. H., Oneizah, L. H. A., & Alaarage, “Erythrosine and Rhodamine Dyes as a Solar Cell Concentrator,” *J. Southwest Jiaotong Univ.*, vol. 54, no. 4, 2019.

[60] O. O. Nnorom and G. C. Onuegbu, “Authentication of Rothmannia whitfieldii Dye Extract with FTIR Spectroscopy,” *J. Text. Sci. Technol.*, vol. 5, no. 02, p. 38, 2019.

[61] Y. A. T. Amogne, Negese Yazie, Delele Worku Ayele, “Recent advances in anthocyanin dyes extracted from plants for dye sensitized solar cell,” *Mater. Renew. Sustain. Energy*, vol. 9, no. 4, pp. 1–16, 2020, doi: 10.1007/s40243-020-00183-5.

[62] J. Kim, K. S. Kim, and C. W. Myung, “Efficient electron extraction of SnO2 electron transport layer for lead halide perovskite solar cell,” *NPJ Comput. Mater.*, vol. 6, no. 1, pp. 1–8, 2020.

[63] H. J. Alesa, B. M. Aldabbag, and R. M. Salih, "Natural Pigment–Poly Vinyl Alcohol Nano composites Thin Films for Solar Cell," *Baghdad Sci. J.*, vol. 17, no. 3, 2020.

[64] W. B. Chapman, N., Chapman, M., & Euler, "Modeling of poly(Methylmethacrylate) viscous thin films by spin-coating," *Coatings*, vol. 11, no. 2, pp. 1–12, 2021, doi: 10.3390/coatings11020198.

[65] M. Vishwas, "Optical Characterization of TiO2-PVA Thin Films," *Int. J. Res. Eng. Sci.*, vol. 8, no. 12, pp. 66–69, 2021.

[66] K. Khormali, Z. M. Mizwari, S. M. Ghoreishi, S. Mortazavi-Derazkola, and B. Khezri, "Novel Dy2O3/ZnO-Au ternary nanocomposites: Green synthesis using pomegranate fruit extract, characterization and their photocatalytic and antibacterial properties," *Bioorg. Chem.*, vol. 115, p. 105204, 2021.

[67] A. El Askary, N. S. Awwad, H. A. Ibrahium, M. E. Moustapha, and A. A. Menazea, "Thermal, optical and electrical properties of WO3/carboxymethyl cellulose/polyvinyl alcohol composite synthesized by laser ablation," *J. Polym. Res.*, vol. 29, no. 5, p. 155, 2022, doi: 10.1007/s10965-022-02993-9.

[68] A. Qasem, M. S. Mostafa, H. A. Yakout, M. Mahmoud, and E. R. Shaaban, "Determination of optical bandgap energy and optical characteristics of Cd30Se50S20 thin film at various thicknesses," *Opt. Laser Technol.*, vol. 148, p. 107770, 2022.

[69] J. I. Pankove, "Optical processes on semiconductors Dover publication," *Inc. New york*, 1971.

[70] H. S. Nalwa, *Handbook of thin films, Five-volume set*. Academic Press, 2001.

[71] A. F. Mansour, S. F. Mansour, and M. A. Abdo, "Improvement structural and optical properties of ZnO/PVA nanocomposites," *IOSR J. Appl. Phys.*, vol. 7, no. 2, pp. 60–69, 2015.

[72] A. S. Hassanien, "Intensive linear and nonlinear optical studies of thermally evaporated amorphous thin Cu-Ge-Se-Te films," *J. Non. Cryst. Solids*, vol. 586, p. 121563, 2022.

[73] AlAbdulaal, T. H., Almoadi, A., Yahia, I. S., Zahran, H. Y., Alqahtani, M. S., Alahmari, S., ... & Al-Assiri, M. S. Effects of potassium dichromate on the structural, linear/nonlinear optical properties of the fabricated PVA/PVP polymeric blends: For

optoelectronics. *Materials Science and Engineering: B*, *292*, 116364, 2023.

[74] W. C. Tan, “Optical properties of amorphous selenium films.” University of Saskatchewan, 2006.

[75] A. M. Mansour and A. B. A. Hammad, “Silica Zinc Titanate Wide Bandgap Semiconductor Nanocrystallites : Synthesis and Characterization,” 2022.

[76] Krbal, M., Prokop, V., Cervinka, V., Slang, S., Frumarova, B., Mistrik, J., ... & Kolobov, A. V. The structure and optical properties of amorphous thin films along the As40S60-MoS3 tie-line prepared by spin-coating. *Materials Research Bulletin*, *153*, 111871. 2022.

[77] M. M. Abdelhamied, M. M., Atta, A., Abdelreheem, A. M., Farag, A. T. M., & El Okr, “Synthesis and Optical Properties of PVA/PANI/Ag Nanocomposite films,” *J. Mater. Sci. Mater. Electron.*, vol. 31, no. 24, pp. 22629–22641, 2020, doi: 10.1007/s10854-020-04774-w.

[78] Gorelov, V., Reining, L., Feneberg, M., Goldhahn, R., Schleife, A., Lambrecht, W. R., & Gatti, M. Delocalization of dark and bright excitons in flat-band materials and the optical properties of V2O5. npj Computational Materials, 8(1), 94, 2022.

[79] J. Tauc, *Amorphous and liquid semiconductors*. Springer Science & Business Media, 2012.

[80] M. Ganaie and M. Zulfequar, “Study of morphological, electrical and optical behaviour of amorphous chalcogenide semiconductor,” in *Advances in Condensed-Matter and Materials Physics-Rudimentary Research to Topical Technology*, IntechOpen, 2020.

[81] K. A.-A. Obeid, A.-K. J. Al-Bermany, and M. A. Habeeb, “Enhancement of some mechanical properties of polyethylene glycol by adding carboxymethyl cellulose as a blends and applied in wood glue,” *World Sci. News*, vol. 21, pp. 12–23, 2015.

[82] N. Padha and S. Kumar, “A two-step method to obtain the 2D layers of SnSe2 single phase and study its physical characteristics for photovoltaic and photo-converter devices,” *Appl. Phys. A*, vol. 127, no. 11, pp. 1–13, 2021.

[83] R. J. Elliott and A. F. Gibson, *An introduction to solid state physics and its applications*. Barnes & Noble, 1974.

[84] A. H. Shukur and M. H. Tarana, “Methodology of using a computer ın teaching in compliance with the learning outcomes on the topics ‘Light refraction. The law of refraction’ in the IX grade,” 2022.

[85] R. Murata, K. Inoue, L. Wang, S. Ye, and A. Morita, “Dispersion of Complex Refractive Indices for Intense Vibrational Bands. I. Quantitative Spectra,” *J. Phys. Chem. B*, vol. 125, no. 34, pp. 9794–9803, 2021.

[86] S. L. Udachan, N. H. Ayachit, L. A. Udachan, and R. Halembre, “Impact of Thickness on the Optical Properties of Selenium Thin Films,” *Ing. y Univ.*, vol. 25, p. 2, 2021.

[87] A. Sahoo, T. Paul, S. Maiti, and R. Banerjee, “Temperature-dependent dielectric properties of CsPb2Br5: a 2D inorganic halide perovskite,” *Nanotechnology*, vol. 33, no. 19, p. 195703, 2022.

[88] O. Rejaiba, K. Khirouni, M. H. Dhaou, B. Alzahrani, M. L. Bouazizi, and J. Khelifi, “Investigation study of optical and dielectric parameters using absorption and diffuse reflectance spectroscopy method on La0. 57Nd0. 1Sr0. 13Ag0. 2 MnO3 perovskite for optoelectronic application,” *Opt. Quantum Electron.*, vol. 54, no. 5, pp. 1–34, 2022.

[89] I. B. Dimov, M. Moser, G. G. Malliaras, and I. McCulloch, “Semiconducting Polymers for Neural Applications,” *Chem. Rev.*, vol. 122, no. 4, pp. 4356–4396, 2022.

[90] N. F. Mott and E. A. Davis, *Electronic processes in non-crystalline materials*. Oxford university press, 2012.

[91] Gayner, C., Sharma, R., Malik, I., Kumar, M., Singh, S., Kumar, K., ... & Naskar, A. K. Enhanced thermoelectric performance of PbSe-graphene nanocomposite manufactured with acoustic cavitation induced defects. Nano Energy, 94, 106943, 2022.

[92] V. Viswanathan, "study of Cu free back contacts to thin film CdTe solar cell", Ph. D. thesis, University of South Florida, (1985).

[93] D. Sergeyev, K. Shunkeyev, B. Kuatov, and N. Zhanturina, “Features of model thin-film solar cells photoelectric characteristics based on a non-toxic multi-component connection CuZn 2 AlS 4,” *Eurasian J. Phys. Funct. Mater.*, vol. 5, no. 3, pp. 242–250, 2021.

[94] G. V Belessiotis, M. Antoniadou, I. Ibrahim, C. S. Karagianni, and P. Falaras, “Universal electrolyte for DSSC operation under both simulated solar and indoor fluorescent lighting,” *Mater. Chem.*

Phys., vol. 277, p. 125543, 2022.

[95] M. A. Butt, “Thin-film coating methods: a successful marriage of high-quality and cost-effectiveness—a brief exploration,” *Coatings*, vol. 12, no. 8, p. 1115, 2022.

[96] D. C. Rubio, W. Weber, and E. Klotzsch, “Maasi: A 3D printed spin coater with touchscreen,” *HardwareX*, vol. 11, p. e00316, 2022.

[97] D. Meyerhofer, “Characteristics of resist films produced by spinning,” *J. Appl. Phys.*, vol. 49, no. 7, pp. 3993–3997, 1978.

[98] A. Khalaf, D. Hassan, and M. Hasan, “Study of Electrical Properties of Poly (Vinyl Alcohol)/ Alumina (PVA / Al 2 O 3) Nanocomposites,” no. 6, pp. 95–100, 2018.

[99] Reddy, P. L., Deshmukh, K., Kovářík, T., Reiger, D., Nambiraj, N. A., Lakshmipathy, R., & SK, K. P. Enhanced dielectric properties of green synthesized Nickel Sulphide (NiS) nanoparticles integrated polyvinylalcohol nanocomposites. *Materials Research Express*, *7*(6), 064007. 2020.

[100] A. Y. Al-Mamoori, N. M. Awad, S. H. Al-Nesraway, J. M. Al-Issawe, E. R. Hamza, and M. H. Al-Maamori, “Preparation of Polymer Nano-composite Materials for Microwave Sensor Application.,” *Indian J. Forensic Med. Toxicol.*, vol. 14, no. 3, 2020.

[101] R. Ahmed, A. A Ibrahiem, and E. A El-sayd, “Effect of cobalt chloride on the optical properties of PVA/PEG blend,” *Arab J. Nucl. Sci. Appl.*, vol. 52, no. 1, pp. 22–32, 2019.

[102] Q. A. Alsulami and A. Rajeh, “Structural, thermal, optical characterizations of polyaniline/polymethyl methacrylate composite doped by titanium dioxide nanoparticles as an application in optoelectronic devices,” *Opt. Mater. (Amst).*, vol. 123, p. 111820, 2022, doi: https://doi.org/10.1016/j.optmat.2021.111820.

[103] S. Wahyuningsih *et al.*, “DEWATERING HYDROCARBON BASED ON SMART HYDROPHILIC SPONGE AND HYDROPHILIC GEL.”

[104] Prakash, P., Janarthanan, B., Ubaidullah, M., Al-Enizi, A. M., Shaikh, S. F., Alanazi, N. B., ... & Ilyas, M. Optimization, fabrication, and characterization of anthocyanin and carotenoid derivatives based dye-sensitized solar cells. Journal of King Saud

University-Science, 35(4), 102625., 2023.

[105] M. D. Sanda, M. Badu, J. Awudza, and N. Boadi, “Development of TiO 2-based dye-sensitized solar cells using natural dyes extracted from some plant-based materials,” *Chem. Int.*, vol. 7, no. 1, pp. 9–20, 2021.

[106] R. Kushwaha, P. Srivastava, and L. Bahadur, “Natural Pigments from Plants Used as Sensitizers for TiO2Based Dye-Sensitized Solar Cells,” *J. Energy*, vol. 2013, pp. 1–8, 2013.

[107] F. Y. Lee, T. T. Htar, and G. A. Akowuah, “ATR-FTIR and Spectrometric Methods for the Assay of Crocin in Commercial Saffron Spices (Crocus savitus L.),” *Int. J. Food Prop.*, vol. 18, no. 8, pp. 1773–1783, 2015, doi: 10.1080/10942912.2014.923911.

[108] S. Sharma, A. Devi, and K. G. Bhattacharyya, “Nickel-Titanium Dioxide-Fuller’s Earth Nanocomposites: Synthesis, Characterization and Application as a photocatalyst in aqueous Methylene Blue degradation under visible lightirradiation,” *Inorg. Chem. Commun.*, p. 110550, 2023.

[109] Lukhman, S., Natar, N., Ghani, N., Shukor, A., Nazeri, S., Ikhwan, S., ... & Izhan, W. (2021). Preparation of polyaniline/TiO_2 photovoltaic solar cell. *Science Letters (ScL)*, *15*(2), 102-115., 2021, doi: 10.24191/sl.v15i2.13833.

[110] R. N. Abed *et al.*, “Optical and morphological properties of poly (vinyl chloride)-nano-chitosan composites doped with TiO2 and Cr2O3 nanoparticles and their potential for solar energy applications,” *Chem. Pap.*, pp. 1–13, 2022.

[111] H. N. Najeeb, G. A. A.-W. Ali, A. K. Kodeary, and J. Ali, “Doping Effect on Optical Constants of Poly-Vinyl Chloride (PVC),” *Acad. Res. Int.*, vol. 4, no. 3, p. 56, 2013.

[112] S. H. Jang *et al.*, “Synthesis and characterisation of triphenylmethine dyes for colour conversion layer of the virtual and augmented reality display,” *Dye. Pigment.*, p. 110419, 2022.

[113] A. A. Alnoman, R. B., Nabil, E., Parveen, S., Hagar, M., Zakaria, M., & Hasanein, “Synthesis and computational characterization of organic UV-Dyes for cosensitization of transparent dye-sensitized solar cells,” *Molecules*, vol. 26, no. 23, 2021, doi: 10.3390/molecules26237336.

[114] S. Kristanti, A. N., Suwito, H., Aminah, N. S., Haq, K. U.,

Hardiyanti, H. D., Anggraeni, H., ... & Muharromah, “Dye-sensitized solar cells properties from natural dye as light-reaping materials extracted from gayo arabica coffee husks,” *Rasayan J. Chem.*, vol. 13, no. 1, pp. 38–43, 2020, doi: 10.31788/RJC.2020.1315576.

[115] C. N. Pace, F. Vajdos, L. Fee, G. Grimsley, and T. Gray, “How to measure and predict the molar absorption coefficient of a protein,” *Protein Sci.*, vol. 4, no. 11, pp. 2411–2423, 1995.

[116] G. Zhang, Q., Zhang, Y. T., & Yin, “Matrix materials used in composites: A comprehensive study,” *J. Phys. Conf. Ser.*, vol. 755, no. 1, 2016, doi: 10.1088/1742-6596/755/1/011001.

[117] I. Morad, M. Salah, H. E. Ali, and Y. Khairy, “Study the effect of mercuric ions concentration on some optical properties of Polyvinyl (alcohol/pyrrolidone) blend film,” *Phys. Scr.*, 2022.

[118] J. Orozco-Messana, “Biomimetic ZnO for dye-sensitized solar cells,” *Nanomaterials*, vol. 10, no. 10, pp. 1–8, 2020, doi: 10.3390/nano10101907.

[119] H. J. Habeeb, S. A., Birtio, N. A., & Kadhim, “Studying the effect of bio natural dye on optical properties of liquid poly vinyl alcohol,” *J Mater. Sci. Nanotechnol.*, vol. 4, no. 3, pp. 04–06, 2020.

[120] R. Syafinar, N. Gomesh, M. Irwanto, M. Fareq, and Y. M. Irwan, “Chlorophyll pigments as nature based dye for dye-sensitized solar cell (DSSC),” *Energy Procedia*, vol. 79, pp. 896–902, 2015.

[121] A. Marzuki, F. D. Ega, and A. Saraswati, “Effect of B2O3 addition on thermal and optical properties of TeO2–ZnO–Bi2O3–TiO2 glasses,” *Mater. Res. Express*, vol. 9, no. 2, p. 25203, 2022.

[122] N. Patni, P. Sharma, and S. G. Pillai, “Synthesis of dye-sensitized solar cells using polyaniline and natural dye extracted from beetroot Synthesis of dye-sensitized sensitized solar cells using polyaniline and natural dye extracted from beetroot,” *Res. J. Recent Sci.*, vol. 6, no. February, pp. 35–39, 2017.

[123] C. O. Saeed, A. A. Qader, and S. B. Aziz, “Low cost novel PEO based nano-composite for semiconductor and He–Ne lasers beam attenuation: Structural and optical properties,” *Opt. Mater. (Amst).*, vol. 129, p. 112502, 2022.

[124] Mondal, S., Ravindren, R., Shin, B., Kim, S., Lee, H., Ganguly, S., ... & Nah, C. Electrical conductivity and electromagnetic

interference shielding effectiveness of nano-structured carbon assisted poly (methyl methacrylate) nanocomposites. Polymer Engineering & Science, 60(10), 2414-2427. 2020.

[125] A. Rajeh, H. M. Ragab, and M. M. Abutalib, “Co doped ZnO reinforced PEMA/PMMA composite: structural, thermal, dielectric and electrical properties for electrochemical applications,” *J. Mol. Struct.*, vol. 1217, p. 128447, 2020.

[126] M. Hosseinnezhad, K. Gharanjig, R. Jafari, and H. Imani, “Green dyeing of woolen yarns with weld and madder natural dyes in the presences of biomordant,” *Prog. Color. Color. Coatings*, vol. 14, no. 1, pp. 35–45, 2021.

[127] L. Kushwaha, R., Srivastava, P., & Bahadur, “Erythrosine and Rhodamine Dyes as a Solar Cell Concentrator,” *J. Energy*, vol. 2013, no. Ii, pp. 1–8, 2013, doi: 10.1155/2013/654953.

[128] A. H. Hadi and M. A. Habeeb, “The dielectricpropertiesof (PVA-PVP-CdS) Nanocomposites for gamma shielding Application,” in *Journal of Physics: Conference Series*, 2021, vol. 1973, no. 1, p. 12063.

[129] D. S. Basavaraja, C., Veeranagouda, Y., Lee, K., Pierson, R., Revanasiddappa, M., & Huh, “The study of DC conductivity for polyaniline-polymannuronate nano composites,” *Bull. Korean Chem. Soc.*, vol. 29, no. 12, pp. 2423–2426, 2008, doi: 10.5012/bkcs.2008.29.12.2423.

[130] H. Darvishi, M. H. Khostaghaza, and G. Najafi, “Ohmic heating of pomegranate juice: Electrical conductivity and pH change,” *J. Saudi Soc. Agric. Sci.*, vol. 12, no. 2, pp. 101–108, 2013, doi: 10.1016/j.jssas.2012.08.003.

[131] Mondal, S., Ravindren, R., Shin, B., Kim, S., Lee, H., Ganguly, S., ... & Nah, C. Electrical conductivity and electromagnetic interference shielding effectiveness of nano-structured carbon assisted poly (methyl methacrylate) nanocomposites. Polymer Engineering & Science, 60(10), 2414-2427., 2022.

[132] A. Abbasi Moud, A. Javadi, H. Nazockdast, A. Fathi, and V. Altstaedt, “Effect of dispersion and selective localization of carbon nanotubes on rheology and electrical conductivity of polyamide 6 (PA 6), Polypropylene (PP), and PA 6/PP nanocomposites,” *J. Polym. Sci. Part B Polym. Phys.*, vol. 53, no. 5, pp. 368–378, 2015.

[133] M. A. Habeeb, “The properties of (PVA-CNTs) nanocomposites,” *Adv. Phys. Theor. Appl.*, vol. 15, pp. 61–71, 2013.

[134] T. M. Saad, L., Feteha, M. Y., Ebrahim, S., Soliman, M., & Abdel-Fattah, “Dye Sensitized Solar Cell Based on Polyaniline-Carbon Nanotubes/Graphite Composite,” *ECS J. Solid State Sci. Technol.*, vol. 3, no. 10, pp. M55–M60, 2014, doi: 10.1149/2.0051410jss.

[135] D. D. Pratiwi, F. Nurosyid, A. Supriyanto, and R. Suryana, “Efficiency enhancement of dye-sensitized solar cells (DSSC) by addition of synthetic dye into natural dye (anthocyanin),” in *IOP Conference Series: Materials Science and Engineering*, vol. 176, no. 1, p. 12012, 2017.

الخلاصة

في هذه الدراسة ، تم تحضير أغشية (PVA/ TiO_2) بتركيزات مختلفة من ثنائي أكسيد التيتانيوم (0 ، 1 ، 2 ، 3٪ بالوزن) باستخدام عملية الطلاء الدوراني. ثم تم تحضير أربعة أغشية من ٪ بالوزن PVA+ TiO_2 بأربع نسب مختلفة (1,2,3,4) مل من أصباغ التوت والزعفران والرمان ، بجهاز الدوران المغزلي 700دورة بالدقيقة لكل 10 ثانية بسمك 774 ± 3 نانومتر سمك للأفلام.

أظهرت نتائج المجهر الضوئي تكوين شبكة من جزيئات TiO_2 النانوية داخل البوليمر التي زادت من حركة الإلكترونات. سجل مطياف فوريه للأشعة تحت الحمراء (FTIR) ذروة اهتزازية لتركيزات المتراكبات النانوية ، ولكن عند إضافتها3 ٪ بالوزن TiO_2 يقلل من أطياف FT-IRتشير ذروة نفاذية الأشعة تحت الحمراء إلى تحول في مواقع الذروة وخلق ذروة جديدة ، ويرجع ذلك إلى تفاعل PVA والصبغة. ظهرت الروابط المقترنة لسلاسل الأنثوسيانين والأنثوسيانيد والكاروتينويد التي لوحظت في التوت والرمان والزعفران على التوالي. لاحظت صور FE-SEM أن الشكل السطحي ل TiO_2 تُظهر إنشاء مجموعات صغيرة من جزيئات الكروية الشكل ، بالإضافة إلى الشكل السطحي لتكتلات PVA/ TiO_2 ذات الخصائص الشبيهة بالقرنبيط المسامية. تم اكتشاف أن المتراكبات النانوية لها شكل كروي وأحجام حبيبات تبلغ 45.26 نانومتر. من الصور يمكن ملاحظة أن الزيادة في حجم الجسيمات بسبب زيادة تركيز TiO_2.

تظهر المتراكبات النانوية (التوت والزعفران والرمان /PVA/ TiO_2) أن الامتصاص يتزايد مع زيادة تركيز الأصباغ الطبيعية. أظهرت النتائج أن الامتصاص يتزايد مع زيادة تركيز الأصباغ الطبيعية من %(2-0.5). تمتص هذه الأفلام الضوء المرئي وفقًا لأطوالها الموجية ويمكن استخدامها كمستشعر ضوئي في الخلايا الشمسية. تتناقص النفاذية مع زيادة تركيز TiO_2 ، وسجلت أعلى ذروة عند 81.9٪ في صبغ الزعفران. معامل الامتصاص له قيم عالية ($\alpha >$ 10^4سم $^{-1}$) ، مما يشير إلى أن الانتقال المباشر له احتمالية عالية. تقل فجوة الطاقة (3.58-3.64) مع زيادة تركيز TiO_2 ، كما تم تسجيل أدنى فجوة طاقة ممكنة لصبغة الرمان (3.56 - 3.66) الكترون فولت. تزداد الثوابت الضوئية بزيادة تركيز TiO_2 ، كما تزداد بزيادة تركيز صبغة الزعفران والتوت وصبغات الرمان.

تم الوصول إلى الموصلية الكهربائية ($\sigma_{d.c}$) بتركيز 2% (4.81×10^{-6} و 4.9×10^{-6} و6.4×10^{-6})(أوم.سم) $^{-1}$ لأصباغ التوت والزعفران والرمان على التوالي. ترتفع الموصلية الكهربائية لمركبات النانو (التوت والزعفران والرمان/ TiO_2 / PVA)) مع زيادة درجة الحرارة. كما أنه يرتبط ارتباطًا وثيقًا بمحتوى الأصباغ الطبيعية. يمكن أن يُعزى الانخفاض في المقاومة الكهربائية إلى تجانس المركبات النانوية) (PVA / TiO_2) (وجود عيوب قليلة) ، وهذا يؤدي إلى زيادة تركيز الإلكترونات الحرة وبالتالي انخفاض المقاومة. تظهر طاقة التنشيط انخفاضًا (0.29 -0.60)الكترون فولت مع زيادة تراكيز جزيئات TiO_2 النانوية. كما تم تسجيل أقل طاقة تنشيط ممكنة لصبغة الرمان (0.19-0.54)الكترون فولت عند زيادة التركيز من (1 – 4) مل.

تم عرض منحنيات I-V للوصلة المتغايرة SnO_2 /p-Si في ظل ظروف الظلام والضوء. يزداد التيار الضوئي مع ارتفاع جهد التحيز. بعد إضافة طبقة من(التوت ، الزعفران ، وأصباغ الرمان / TiO_2 / PVA) على سطح SnO_2 /p-Si، تزداد كفاءة الخلية الشمسية. تم تسجيل زيادة الكفاءة (η) من (٪4.75-٪ 4.3) بعد الطلاء بالمتراكب النانوي (صبغة الرمان / PVA / TiO_2). لذلك ، يمكن استخدام هذا الفيلم كغطاء للخلايا الشمسية.

جمهورية العراق
وزارة التعليم العالي والبحث العلمي
جامعة بابل
كلية التربية للعلوم الصرفة
قسم الفيزياء

دراسة تغيرات كفاءة الخلايا الشمسية عند طلائها بمخاليط بوليمرية مع صبغات نباتية

اطروحة مقدمة
الى مجلس كلية التربية للعلوم الصرفة في جامعة بابل
وهي جزء من متطلبات نيل درجة الدكتوراه فلسفة
في التربية/ الفيزياء

من قبل الطالب

أمين علوان محيميد ملوح
بكالوريوس في التربية/ الفيزياء
جامعة بابل 2004 م
ماجستير في التربية/ الفيزياء
جامعة بابل 2017م

بأشراف

أ. د. بهاء حسين ربيع

1444هـ **2023م**